Development of a Finite Element Matrix (FEM)Three-Phase Three-Limb Transformer Model for Geomagnetically Induced Currents (GIC) Experiments

Prepared by:

Sizwe Mkhonta

MKHSIZ010

Submitted to the Department of Electrical Engineering at the University of Cape Town in partial fulfilment of the academic requirements for a Master of Science in Electrical Engineering.

Supervisor: Dr. David Oyedokun

Co-Supervisor: Prof. Komla Folly

February 2020

Key Words: Transformer modelling; Finite Element Matrix (FEM); Transformer saturation; Harmonics; Flux density distribution; Laboratory testing

Acknowledgements

"*If I have seen further, it is by standing on the shoulders of giants" – Bernard of Chartres, 12th Century*

For work put into this project, for the hard work and resilience, for the motivation and encouragement, for the wisdom, guidance and mentorship, and for the general support given, I am deeply indebted to the following giants:

- Em Prof. CT Gaunt, for initiating this work and for taking me under his wings. For allowing me to learn under his guidance and expertise. I also appreciate him for the financial support given to me to embark on this journey.
- Dr. David T. Oyedokun and Prof. Komla Folly, for supervision and guidance through my academic journey.
- Hilary K. Chisepo and Dr. Leslie D. Borrill, for mentorship and words of advice.
- Talent T. Murwira, for a great partnership and support throughout the journey.
- Mrs. Tebello Mahlaba and Eskom Distribution at Eskom Brackenfell, South Africa, for providing a transformer testing space in their workshop.
- Kingley Akpeji for reviewing and proofreading my work.
- Chris Wosniak, Philip Titus, Maysam Soltanian, Hoosain Salie, Bonginkosi Hadebe, Tasrique and Riyaad at the University of Cape Town (UCT) Machines lab, for laboratory assistance.
- The UCT Power systems research group, for insightful feedback and contributions at our weekly seminars.
- My family and friends, for their constant support through the journey.

I am grateful to the Open Philanthropy Project, the National Research Foundation (NRF) of South Africa, and the John Davidson Educational Trust for the scholarships provided for my degree. I am also grateful to UCT's high performance computing team for providing the facilities used for the FEM computations.

Abstract

Geomagnetically Induced Currents (GIC) have been a growing concern within power system operators and researchers as they have been widely reported to lead to power system related issues and material damage to system components like power transformers. In power transformers, GIC impacts are evidenced by part-wave saturation, resulting in transformers experiencing increased presence of odd and even harmonics. The three-phase three-limb (3p3L) transformer has been found to be the most tolerant to high dc values compared to other core types.

The research was based on a hypothesis which reads "transformer laboratory testing results can be used as a guide towards developing suitable Finite Element Matrix (FEM) models to be used for conducting GIC/DC experiments". This study thus investigates the response of a 15 kVA 3p3L laboratory transformer to dc current, emulating the effects of GICs. GIC and dc current are the same under steady state conditions, and hence mentioned interchangeably. Laboratory tests conducted identified two critical saturation points when the transformer is exposed to dc. The early saturation point was identified to be at around 1.8 A/phase of dc (18% of rated current), while the deep saturation point was at around 15 to 20 A/phase of dc (about 72% of rated current). Further analysis showed that holes drilled on the transformer can lower the transformer knee-point by about 26%, depending on the size and location of the holes. The holes hence end up affecting the operating point of the transformer due to losses occurring around the holes.

A transformer FEM model was developed following the laboratory exercise, where it was concluded that a 2D model leads to grossly erroneous results, distorting the magnetizing current by about 60% compared to the laboratory results. A solid 3D model improved performance by about 30% as it took the transformer's topological structure into consideration. The 3D model was then refined further to include joints and laminations. It was discovered that laminations on the transformer need to be introduced as stacks of the core, with each core step split into two, allocating a 4% air gap space between stacks. Refinement of the T-joints proved that the joints have a relatively high influence on the transformer behaviour, with their detailed refinement improving the transformer behaviour by about 60%. The final FEM model was used for dc experiments. The results of such experiments showed close resemblance to the laboratory results, with saturation points identified in FEM lying within 10% of the laboratory identified saturation points. Overall, the various investigation methods explored showed that the hypothesis was satisfactorily proven true. Laboratory results functioned as a guide in developing the model, offering a reference case.

Research outputs

The following papers were published during this research:

1. S. Mkhonta., T. T. Murwira,, D. T. O. Oyedokun, K. A. Folly, C. T. Gaunt, “Investigation of transformer reactive power and temperature increases under dc” in 2018 IEEE PES/IAS Power Africa, Cape Town, South Africa, 2018.
2. T. T. Murwira, S. Mkhonta, D. T. O. Oyedokun, K. A. Folly, C. T. Gaunt, “Three-Phase Five-Limb Transformer Harmonic Analysis under DC-bias." in Southern African Universities Power Engineering Conference/Robotics and Mechatronics/Pattern Recognition Association of South Africa (SAUPEC/RobMech/PRASA), Bloemfontein, South Africa, 2019.

Declaration

I know the meaning of plagiarism and declare that all the work in this dissertation, save for that which is properly acknowledged, is my own. This dissertation has been submitted to the Turnitin module to validate its originality. Furthermore, I confirm that my supervisors have seen and read this dissertation and any concerns related to my work have been resolved with my supervisors.

Signed by: Sizwe Mkhonta (MKHSIZ010)

Signature: Signed by candidate

Date: 09/02/2020

Table of Contents

List of Figures

List of Tables

1. Introduction

1.1 Background and motivation

Over the past century, space weather has been found to have a significant impact on ground-based technological systems such as pipelines, telecoms, and power systems, [1, 2]. This impact is through solar storms; coronal mass ejections (CMEs) from the sun reaching the earth. The interaction between CMEs and the earth's magnetosphere is called a geomagnetic disturbance (GMD). GMDs induce electric fields that cause the flow of geomagnetically induced currents (GICs) in ground-based systems which may lead to a range of disturbances. GICs flow into power systems through grounded transformer neutrals. These currents have been found to be the cause of major power system events, including system-wide blackouts in Quebec in 1989 [3-5].

Historically, GICs were recorded at regions of higher latitudes. After further studies, it has been proven that even regions of lower latitudes could experience GICs. Gaunt et al [6] showed that GICs were the most probable cause of transformer damages reported in South Africa after the 2003 Halloween storm [7]. This event shifted the focus of the study of GICs from the western world to the global power systems community, including South Africa [6].

GICs are characterized by very low frequencies of about 0.001 to 0.01 Hz (quasi-dc) with an average magnitude of 10 – 15 A and peaks of 100 A for about 1 to 2 minutes [8]. This frequency range is very low compared to the frequency (50/60 Hz) at which most power system components are designed to operate. Hence, the flow of GICs in power systems leads to a simultaneous presence of ac and dc components which may lead to a wide range of issues.

One of such issues is associated with the flow of GICs through extra high and high voltage transformers. Transformers are a significant part of the power system, and their reliable and continued operation is of utmost importance for power delivery. To enhance the understanding of the effects of GICs on power transformers, different transformer models have been developed for computer simulations through various studies [9-12]. Such studies have explored the different aspects of the transformer that influence its behaviour under GIC. This work aims to improve a three-phase three-limb (3p3L) transformer Finite Element Matrix (FEM) model used for studying the impacts of GIC. The FEM model development is based on laboratory experimentally measured results of the physical transformer. The research undertaken builds on previous works by Chisepo and

Borrill [13, 14] which studied single-phase four-limb transformers. These studies identified the influence of the joints in the magnetic flux distribution which affects the saturation patterns of transformers. The authors showed that careful representation of the joints in simulated models is very important.

To improve the transformer FEM model used for the study of GICs in transformers, it is imperative that the behaviour of these FEM models closely resemble that of real power transformers. The information obtained from laboratory tests can be used to obtain design rules and validate mathematical models [8]. The design rules can be eventually optimized considering GIC cases. Accordingly, FEM models will be developed from a laboratory scale transformer designed to resemble large scale power transformers. Subsequently, the simulated FEM models will be refined for the alignment of their results with laboratory results.

1.2 Objectives of the study

The objectives of this research are to:

- Improve the understanding of the various ways in which transformers are affected by the flow of GICs.
- Design and validate a laboratory scale 3p3L power transformer to be used as a basis for developing a FEM model.
- Propose and run a base testing system to be used for running GIC/dc through the 3p3L transformer.
- Identify critical saturation points for the transformer
- Develop a base solid 3p3L transformer FEM model based on the transformer physical dimensional data and parameters.
- Develop and test a refined 3p3L transformer FEM model with improved resemblance to the physical transformer behaviour, with and without GIC/dc flow.

1.3 Hypothesis

The hypothesis which is foundational to this study is:

Transformer laboratory test results can be used as a guide for developing suitable Finite Element Matrix (FEM) models for conducting GIC/dc experiments.

1.4 Research questions

The following research questions were formulated to test the hypothesis above:

RQ1: What laboratory testing methods exist for measuring transformer response to GICs and how do current FEM models in literature accommodate for the study of transformer response to dc/GIC?

RQ2: How does the transformer FEM model behaviour differ from its actual physical behaviour?

RQ3: What kind of structural detail needs to be incorporated in FEM models for improved resemblance to the laboratory transformer?

RQ4: How can a balance between the amount of detail applied to a transformer FEM model and computational restrictions be achieved without losing the accuracy of the FEM model?

1.5 Scope of work

The scope of this work is guided by the hypothesis outlined in section 1.3. The main requirement is the development of a 3p3L transformer FEM model based on laboratory results. There will thus be laboratory tests conducted to provide suitable data for the FEM model development. The FEM model will be developed and refined based on the laboratory data. The work will end with a comparative analysis of the FEM model and physical transformer behavior under dc.

The 3p3L transformer (transformer under test) was tested in parallel to a similarly sized three-phase five-limb (3p5L) transformer. Although the 3p5L transformer is not the focus of this study, reference to its laboratory results will be made whenever it is necessary to enhance the understanding of the 3p3L behaviour in comparison to other transformer designs. Furthermore, transformer response to dc/GIC was analysed using its saturation as a baseline. Drawing from this, laboratory experiments were focused on identifying critical dc levels associated with the different levels of transformer saturation.

2. Literature Review

2.1 GIC and Power Systems

2.1.1 Background

The ground-based impacts of the sun's coronal mass ejections (CMEs) are increasingly becoming of concern to power system operators. This concern follows recorded evidence of GIC-related power system impacts. Due to the historic severity of its consequences, GIC have gained traction at a global scale, earning inclusion in international bodies, gazettes and standards. Table 2.1 highlights some of the key documents that are addressing GMDs and GIC as part of their disaster monitoring programs.

Table 2.1: Global inclusion of geomagnetic disturbances in national risk registers

Country	**Document**	**Highlight**	**Reference**
United Kingdom	London Risk Register	Labelled GIC as a very high risk, with emphasis on the electricity industry monitoring and analysing GIC.	[15]
	2015 National risk register for civil emergencies	Acknowledged *the influence of space weather as a threat to essential services* due to potential electricity blackouts.	[16]
USA	Risk Management Issue brief	This brief outlined the *need for the development of geomagnetic storm risk management assessments and strategies* by the Federal government, owning to the amount of economic threats posed (particularly towards high voltage transformers).	[17]
	Technology Assessment: protecting the electric grid from geomagnetic disturbances	Called for the *advancement in transformer designs and research that has led to the mitigation of the effects of GICs on power transformers*, while maintaining *that further mitigation strategies are an urgent need*.	[18]
Finland	2018 National Risk Assessment	Space weather was probed to pose *an indirect impact on people and the environment* due to interruptions in power supply.	[19]
South Africa	2017 SANSA policy brief	Acknowledged that *although a tremendous amount of work has been done in this area, much of the evidence remains anecdotal, warranting further investigations and studies.*	[20]

In addressing the future risk of GICs and ensuring that societies are better prepared for future geomagnetic storms, researchers cannot work alone. Intervention from governments through policy and legislation is also necessary. Thus, the inclusion of GIC in national risk registers is a good start

towards ensuring a minimisation of future impacts. Governments are gradually improving their readiness for future storms by allocating the necessary resources required to secure their systems and minimize the impacts. One can notice from Table 2.1 that most of the countries that are paying serious attention to GICs are in areas closer to the polar regions. These are areas that have experienced GIC events which caused substantial transformer and power system-related damages. One such event is the 1989 geomagnetic storm which was adjudged the primary cause of the province-wide power system collapse at Hydro-Quebec [10]. Another event is the Halloween storm in South Africa (2003), documented by Gaunt and Coetzee [6].

Although GICs have historically been associated with polar regions, the reported damages to transformers in South Africa around the period of the Halloween storm strongly indicates that power systems in low latitude regions are also susceptible to GICs. Thus, South Africa has also been taking decisive steps towards understanding the threats posed by GICs. The South African National Space Agency (SANSA) and the Electrical Engineering Dfepartment at the University of Cape Town have spearheaded the research in this regard.

The study of GICs in power systems continues to advance as present research within the power systems community is linking present day technology with GICs studies. Some researchers are looking at machine learning algorithms that can be used for detecting GICs in power systems [21-23]. Such studies will potentially lead to improved prediction of GICs in power systems in order to minimise their impacts due to informed design principles. GICs currently affect power systems in various ways, as discussed in the following subsections.

2.1.2 Impacts of GICs on power systems

The effects of GICs are predominant at the high voltage (HV) transmission level of power systems [25], where the low resistance of HV lines compared to low voltage (LV) lines allows for easy flow of GICs [26]. Transformer HV windings also have grounded terminals (for protection), which provide a path for GICs to flow into the network, leading to a range of negative impacts.

The physical impacts of GICs are generally cascaded and intertwined in complex ways as summarised in Figure 2.1. The introduction of GICs into the transformers leads to an increase in magnetizing currents. The increased magnetizing current leads to an increase in the amount of non-active power taken up by the transformer. This may eventually lead to system blackouts as has been the case historically. Further information on this is provided in detail below. This study focuses on the impacts on transformers. Of all power system components, transformers are one of the most susceptible to GICs. Also, the cost of refurbishing an impaired transformer or replacing a damaged one is

significantly high. Extensive physical damages to transformers might impair grid stability and operation [6, 10, 27], causing blackouts with high national and global socioeconomic costs. The response of a transformer to GICs is dependent on its design, thus the pattern of effects leading up to damage varies according to the transformer type. The 3p3L transformer was chosen for the investigations in this study based on its common use in power systems.

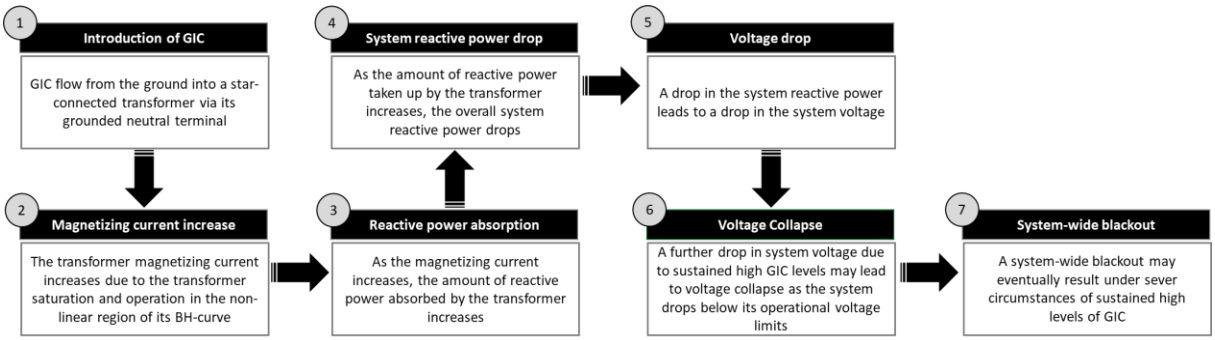

Figure 2.1: Cascaded effects of GICs on transformer reactive power consumption, leading to possible system blackout under severe circumstances.

2.1.3 Impacts of GICs on the 3p3L transformer

The 3p3L is a common transformer core type for small and medium rated transformers [28]. Extensive literature review on the response of this core type indicated that 3p3L transformers are more tolerant to GICs injections compared to the three single-phase three-limb units (3(1p3L)) and three-phase five-limb transformers (3p5L) [10, 29-32]. However, the reported GICs tolerance of the 3p3L transformer [31] might be rather optimistic. Although the design may seem better for the composite power systems, it could be more dangerous for the transformer itself due to higher leakage fluxes [12]. Specific GICs-induced effects on transformers including the 3p3L transformer are discussed below.

i. Part-wave saturation

Transformers are generally designed to operate within specific voltage and current limits, with an operating point specified. A transformer operating under normal conditions has its operating point centred around the zero flux point, with its peak ac flux lying below the knee-point [25]. Several situations can disturb the transformer operating point, pushing it into a region of saturation. An example of such situations would be currents of very low frequencies and dc flowing into transformer windings. These currents drive the transformer beyond the knee-point into the saturated region, which reduces the effective impedance of the core [33]. When the magnitude of the GICs/dc is large

enough to push the operating point into the region of non-linearity, part-wave saturation is initiated [34]. Lv and Zhu [35] alluded to the fact that, the saturation caused by the dc bias (or level of GICs) is directly proportional to the magnitude of the inrushing dc and the duration of the transient process.

Mousavi *et al* [36] pointed out that even small amounts of dc in an alternating current (ac) source can drive a transformer core into part-wave saturation, which greatly distorts the magnetizing current waveform [37]. The sensitivity of a transformer to saturation can be linked to parameters such as its air-gap and tank inductance, core knee-point, relative yoke cross-sectional area, outer limb cross-sectional areas, air-core inductance, applied voltage and the non-uniform distribution of the air path fluxes within the tank [30]. Hence, these aspects of the transformer must be taken into close consideration during its design and when studying the transformer's response to GICs/dc.

ii. ***Harmonic Generation***

The part-wave saturation of a transformer core is normally accompanied by the generation of odd and even harmonics [2, 25]. Harmonics lead to different side effects on the system, which include: additional active and non-active power losses, core overheating, accretion of noise, possible resonance, false operation of relays and interference with communication circuits [30, 38]. The harmonic effects become more significant with increasing transformer rating and size [38], but decrease with increasing harmonic order [24]. Harmonics generated as a result of GICs or dc cause distortions in the current and voltage waveforms, which may further escalate to voltage imbalance within the system [39].

iii. ***Increased non-active power (Q) demand***

The increased part-wave saturation and presence of harmonics present high magnitudes of magnetizing current flowing through the transformer's magnetizing branch, leading to increased non-active power consumption by the transformer [29]. The magnetizing current lags the voltage of the system by 90^0. This results in an inductive circuit which absorbs non-active power [24]. Transformers absorb non-active power through their shunt impedances (magnetizing reactance).

Literature has been split regarding the relationship between GICs and non-active power absorption. Most of the literature covered claim that the amount of non-active power taken up by transformers increases linearly with increasing GICs levels [29, 40-42], while some claim a nonlinear relationship [43], [44]. Understanding the nature of this relationship is imperative for improving transformer models. A nonlinear relationship might present a bigger challenge in improving the models, as a change in parameters might affect this relationship nonlinearly as well, leading to further complexity. The absorption of non-active power leads to various system-related effects which might result in

system-wide blackouts [45]. An improved understanding of the transformer's non-active power uptake may be obtained by studying its response to extreme levels of GICs. The model used in this case needs to be highly reflective of actual physical transformers for the results obtained to be credible. The following sections look at the key aspects of transformer modelling carried out by researchers through laboratory experiments and FEM simulations.

2.2 Transformer Laboratory Testing for GICs

Practical physical transformer laboratory testing has provided good insight on its response to GIC. Due to the complexity of the power system and the difficulty in conducting tests on field power transformers, relatively small-sized transformers have been used for laboratory-based investigations. Transformer laboratory testing has proven to be a critical exercise towards the study of transformer response to dc or GICs. Laboratory scaled transformers are easy to move around and test without dealing with the complexities of power systems. The laboratory testing of transformers is also useful for estimating transformer parameters for modelling, when there is little or no manufacturer data available [46]. A test procedure can also be used as a model validation exercise [47], where simulation results are compared with physical measurements in the laboratory. In conducting laboratory tests, there have been recurrent protocols. Needful areas of focus have been identified following the previous section from existing research and are discussed below.

2.2.1 Flux density distribution measurements

Flux is generated in the same direction in all three limbs of the 3p3L transformer [48]. Under saturated conditions, the magnetization parameters of the transformer increase drastically, increasing the magnetic flux density around the core of the transformer. The transformer is designed to accommodate flux density up to a certain point (the knee-point), determined through its magnetizing curve. Once the flux density increases beyond the knee-point, the core becomes saturated [49]. If the dc levels are high enough, flux may ultimately escape the core as the core approaches the inductance of an air core. An air core has a very high reluctance, similar to that of the surrounding air, hence the outside air becomes an alternative path for flux. Laboratory tests have thus measured the changes in flux density around the core, while identifying specific points along the core that saturate before the rest of the core, which include the core joints and regions closer to the excited windings.

2.2.2 Magnetizing current measurements

The magnetizing current is one of the most common identifiers of transformer saturation as it undergoes part-wave saturation under dc. The increased magnetizing current as a result of GICs

presence leads to a range of other effects, including increased harmonics and absorption of non-active power by the transformer. The magnetizing current will thus be a primary focus in analysing the transformer response.

2.2.3 Harmonics measurement

The saturated magnetizing current is characterized by a range of harmonic components. Low order harmonics are present almost all the time in transformers, as they are caused by the distorted magnetizing current drawn by the transformer [50]. Low order even harmonics are generated due to the presence of a dc component [50]. Some researchers [25, 50, 51] have reported that the presence of both odd and even harmonics characterises the response of power transformers to dc. A focus on both odd and even harmonics is thus imperative when analysing the transformer saturation under dc.

2.2.4 Total harmonic distortion measurements

The total harmonic distortion (THD) describes the sum of the voltage (THDv) and current (THDi) harmonic components in relation to the fundamental. These are also measured to assess the response of the transformer to dc. The THDi for the 1p3L transformer is characterized by a sharp rise, with a peak around the knee-point region due to the relatively low fundamental component with the onset of saturation [52]. A similar trend was noted by Hutchins [29]. The THDv and THDi of the 3p3L transformer will thus be assessed in this research.

2.2.5 Non-active power measurements

A transformer exposed to GICs or dc takes up non-active power with an increase in GICs [52]. Results from reference [30] showed that the 3p3L transformer does not take up appreciable amounts of non-active power up to a certain level of dc. Exceeding this level causes the transformer to enter into saturation, with a rapid increase in the non-active power taken by the transformer. This is in line with earlier investigations in reference [53], [25].

2.2.6 Transformer time response measurement

The transformer time response (TTR) was proposed by Oyedokun [54] to obtain a better understanding of GICs flow and calculations in power systems. This was with the view that the sampling time interval of the magnetic field may influence the peak magnetic field values. The analysis of this investigation showed that the 3p3L transformer had the shortest response time for 300 VA bench-scale transformers. It thus permits the flow of dc current through its windings within the shortest amount of time, due to its lower magnetization impedance and higher magnetizing current. The TTR for all transformer core types was found to decrease with increasing GICs, which was common for both laboratory experiments and simulations.

Even though transformer laboratory tests have had their own breakthrough in research, they remain limited in their application as they cannot be replicated in actual power transformers in service. Transformers are quite expensive; thus, they are hardly available for laboratory tests. Transformer simulations offer an opportunity for modelling transformers of various designs and sizes. Results from laboratory experiments have been utilised for developing simulated models like FEM transformer models. There is an opportunity for extension of these models to bigger models. The following section reviews work done around transformer models.

2.3 FEM Modelling

One of the most essential steps in transformer GICs mitigation is the modelling of transformers, [55, 56]. Transformer models present a good opportunity for developing an understanding of transformer behaviour under exposure to GICs/dc. Once created, transformer simulated models can be injected with GICs/dc at various levels, under different conditions to assess their behaviour. This further helps researchers and designers to deduce insights into areas of intervention required to produce robust transformer designs that can possibly withstand various levels of dc. The Finite Element Matrix (FEM) or Finite Element Analysis (FEA) modelling method is a tool that can assist towards achieving this objective. FEM is a computational technique used to obtain approximate solutions to approximate boundary value problems in engineering. It achieves this by applying a numerical method for solving a combination of differential and integral equations, by dividing the bulky application domain into a number of smaller sub-elements [57, 58]. The power transformer can be broken down into different components where its magnetic behaviour can be analysed through a series of differential equations. The fundamental steps associated with FEA are shown in Figure 2.2. The model is usually developed from physical dimensions associated with a real-world structure. Depending on the level of accuracy required in the solution, the structure is modelled in FEM with varying levels of detail, leading up to a discretized model for analysis.

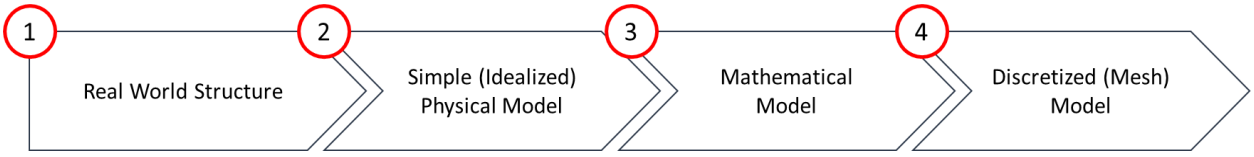

Figure 2.2: Key steps in Finite Element Analysis (FEA)

FEM is mostly attractive for its superior level of accuracy. It has been applied in transformer modelling for calculating the transformer's eddy current and stray losses, electromagnetic field behaviour, temperature gradients and short circuit stresses [58]. FEM is further important for conducting an analysis on the overall and localized flux distribution within the core. Flux distribution

is one of the key indicators for the transformer's saturation state, hence it needs to be closely monitored. Some FEM models have been used in past research for the following studies:

- Power loss tests (copper loss and core loss "significance under dc or GICs")

The saturation of the transformer causes an increase in the amount of off-core flux, which in turn increases the transformer core losses [51, 59]. Due to the magnetic field penetration, the ac loss in the windings mainly contains hysteresis losses, [60]. The calculation of transformer core losses is thus an important part of this research, as core losses may be a consequence of GICs. The modelling and calculation of a transformer's core losses improves the understanding of its response to GICs, and ultimately provides insights on intervention required. One of the key considerations presented by Liu *et al* [59] is the additional core loss by the effect of end stripe. The study in [61] presents a FEM model critical for this calculation involving a 2D scaled down model, which can add value to this present research.

The electrical steel core loss computation shown in equation (2.1) is used in the FEM method[61]:

$$P = K_h f(B_m)^2 + K_c(fB_m)^2 + K_e(fB_m)^{1.5} \text{ [61]} \quad (2.1)$$

Where:

P: Core loss

K_h: Hysteresis loss coefficient (ranges from 1.5 to 2.5)

K_c: Eddy current coefficient

K_e: Excessive loss coefficient (additional eddy current loss)

f: Operating frequency

B_m: Nominal magnetic flux density

The eddy current loss coefficient (K_c) is calculated from the conductivity (σ) and lamination sheet thickness (d) of the core material using equation (2.2). Nowadays, eddy currents are known to account for about 30-50% of total no load losses [57].

$$k_c = \pi^2 \sigma \frac{d^2}{\delta} \quad (2.2)$$

where: δ is the skin depth (defined as the distance within which the fields reduce to 1/e of its maximum value)

- *Magnetic flux densities*

The focus on magnetic flux density has been a growing area of research in transformers under GICs. FEM provides a great tool for analysing and visualizing the distribution of flux within the transformer. This is very key in identifying the differences in saturation for different parts of the transformer as presented by various researchers [62-65].

2.3.1 Challenges in transformer modelling

Although FEM modelling has various strengths and advantages, it also has several challenges, some of which are highlighted below.

- *Large amount of structural detail required for improved accuracy.*

The need for more structural detail remains the key focus of most FEM studies [66]. This is due to the accuracy improvement that comes with it. The downside to increasing structural detail is an increase in computational burden. FEM simulations require the use of computers with above average capabilities, like 4 Gigabytes (GB) of RAM or more depending on the software used and the structure under investigation. More refined models require the development of more mesh elements to produce a solution. This increases the number of iterations the computer must run to get a solution and the computational time [67]. Some institutions make use of high-performance computing, which incurs more costs.

- *Difficulty in modelling of air gaps*

Previous researchers have established the need for the inclusion of joints in transformer models due to their influence on the core saturation [14, 64]. Due to their complex shapes, air gaps have proven to be a challenge to model using FEM. They also have a substantial impact on the transformer performance, hence they require a good amount of attention when modelling a transformer. Some researchers have highlighted the need for better modelling of transformer air gaps, especially for analysing core saturation [68]. A number of researchers have devoted their resources towards the study of the air gaps at the core joints [69, 70] with some studying them under GICs conditions [13, 14, 69, 70].

2.3.2 Recent areas of focus in FEM research

Despite being faced with several challenges in transformer modelling using FEM, researchers have made breakthroughs in certain aspects of the field. Specific areas of FEM modelling have been identified to be of importance. Some of these areas are discussed below.

i. 3D modelling

Most historical FEM tools were built for two-dimension (2D) models, but there has been a recent transition to tools for three-dimensional (3D) modelling. 3D modelling is particularly good for building transformer structures with close resemblance to reality, hence improving the accuracy of the solution. Recent areas of study have considered ways to model different types of joints [63-65, 68], which the 2D modelling environment was not adequately capable of handling. Furthermore, 3D modelling is a powerful tool for evaluating other areas of interest in a transformer like the flux density distribution.. Some researchers have reported improved accuracy with 3D models [40] in the study of flux density distribution, and in the assessment of power losses and temperature changes in the tank and other metallic components of the transformer.

ii. Air gap modelling

To overcome the challenge of air gap nonlinearity and complicated losses, some researchers have proposed ways of replacing the equivalent variable air gap length with a constant length transversal element leading to the same magnetic flux drop [71]. The results of the developed model showed consistency with the recorded laboratory results.

iii. Mesh quality

When modelling a FEM structure, the structure is broken down into smaller units for the computation of the solution. These smaller units are then integrated to reproduce the whole structure. In FEM modelling, these small units are called mesh elements. These mesh elements are used to ensure high quality element shape necessary to avoid artificial numerical stiffening [72]. To this end, the use of automatized mesh sizes, which depend on material properties and frequency range of interest was proposed [72]. This is particularly important in improving the accuracy of the FEM calculations that are necessary for obtaining solutions to the different variables investigated.

iv. Model simplification

Model simplification is one approach that has been used towards overcoming the computational requirements associated with FEM models. Some published research used the approach of applying a uniform distributed core in place of a stranded complex geometry, where the B-H curve of the core is then corrected to provide for better accuracy [48, 67, 73]. The stranded core approach is computationally burdensome and may fail to converge to a solution at times.

v. ***Use of symmetry***

The use of symmetry has been applied in transformer modelling to minimize the simulation times associated with FEM. This is particularly important for simulations conducted in the transient domain, as these require excessively longer times to process [68].

2.4 Transformer research at the University of Cape Town (UCT)

This present work follows a series of publications on transformer research at the UCT. It is built upon the background of critical breakthroughs and findings in transformer research for GICs/dc studies. The existing transformer research covered laboratory experiments and simulations using various approaches as outlined further below.

2.4.1 Transformer experimental testing

Transformer laboratory experimentation has been a key component in understanding the response of transformers to GICs, making use of dc current [29, 74, 75]. A key part in this area has been the development of a laboratory protocol for testing bench-scale transformers by Chisepo *et al* [29, 75]. These studies further identified the measurement components associated with the response of transformers under GICs. These measurement components include: (1) the identification of the magnetizing current at a uniquely defined 'knee-point' on the B-H characteristic, (2) the testing of harmonics, and (3) interpreting the reactive power data as non-active power. An extension of the protocol to other transformers varying in core structures (bench scale) and size (48kVA three-phase three-limb) showed great consistency in the results, proving that the fundamentals of the protocol remain true regardless of the transformer type or size.

Further to the transformer testing, a general power theory developed at UCT established the significant effects of distortions in measuring the transformer non-active power [76]. Through experiments, it was shown that non-active power measurements in a transformer under distorted conditions are significantly higher when measured using the General Power Theory (GPT) compared to conventional IEEE power measurement methods. These results were experimentally consistent in various experiments [29, 53, 77, 78].

Sequel to the aforementioned UCT studies, transformer research has matured. There has been an extension of the aforementioned protocol, so that it is suitable for testing much bigger transformers. Tests were conducted on single-phase four-limb (1p4L) 4.4 KVA 110/202.6 V transformers [13, 14, 68, 79]. Thus, enough certainty has been established around the test protocol and the validity of the test results.

2.4.2 *Transformer FEM simulation at UCT*

FEM modelling has recently been introduced to transformer studies at UCT. The development of transformer models in ANSYS Maxwell have been explored by Chisepo *et al* [14, 68, 78]. The major focus in these studies is the influence of the core joints on the behaviour of the transformer and the evolution of efficient modelling techniques.

2.4.3 *Transformer equivalent circuit models research at UCT*

Transformer equivalent circuit models have also been found to be useful towards studying the behaviour of transformers under GICs. Borrill *et al* [13] and Borrill [85] developed a 1p4L pi-model based on laboratory measurements. These are discussed further in the following section.

2.5 Transformer Equivalent Circuit Models

Although an equivalent circuit model will not be developed in this research as it falls outside of its scope, an understanding of power transformers through their equivalent circuit models is imperative for understanding their behaviour. This assists towards analysing the practical behaviour of transformers and for predicting transformer behaviour in real life. Accordingly, Engineers can design and test for conditions that cannot be physically tested on actual power transformers. The magnetic behaviour of the transformer can also be understood from such equivalent circuit models.

The magnetic behaviour of a transformer core vastly differs when operating in a saturated state (under dc, inrush or other situations leading to saturation). Each component of the equivalent circuit model needs to be physically realizable and should resonate with each physical aspect of a power transformer [81]. Thus, transformer equivalent circuit models are developed using transformer geometrical data and from short-circuit and open-circuit measurements. Equivalent circuit models could be used to compute transformer terminal measurements. The goal in most research has been to move towards models that can be easily computed on Electromagnetic Transients Programs (EMTP) or any other drag and drop software. As part of developing a theoretical understanding of the 3p3L transformer, the following sub-sections discuss some of the models that have been used in literature.

2.5.1 *T-model*

The T-model was created for the study of low frequency operating conditions. As shown in Figure 2.3, it consists of one magnetizing branch with two leakage inductances (one for the primary winding and the other for the secondary winding). It was found to be suitable for producing the transformer

terminal behaviour at steady state, however it yields inconsistent results when the transformer is driven into deep saturation [82].

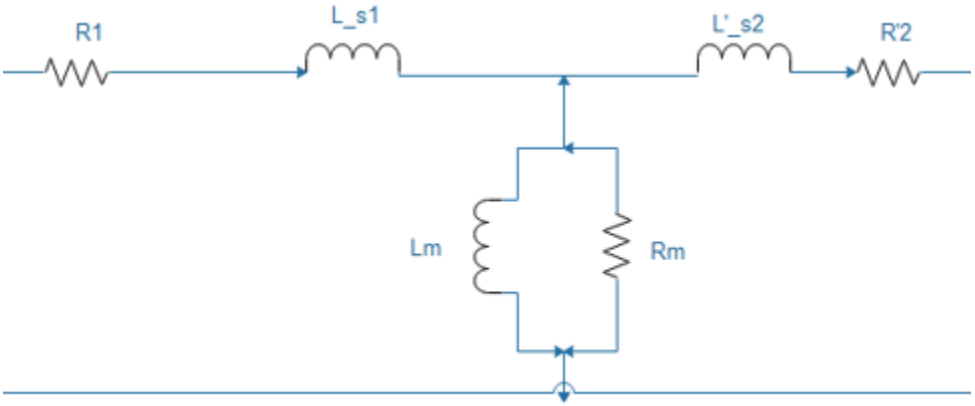

Figure 2.3: Single phase transformer equivalent T-model

2.5.2 Pi-model

The Pi-model shown in Figure 2.4 was adopted for its improved accuracy in the calculation of inrush currents. The model consists of two magnetizing branches with one leakage inductance. The motivation for this model was its resemblance to physical transformers. The magnetizing branches depict the primary and secondary sides of the transformer linked through a leakage inductance (L*s*). The Pi-model considerably replicates the physical transformer behaviour, especially in the deep saturation region. The deep saturation region is of paramount importance in the calculation of inrush currents [79, 80, 82].

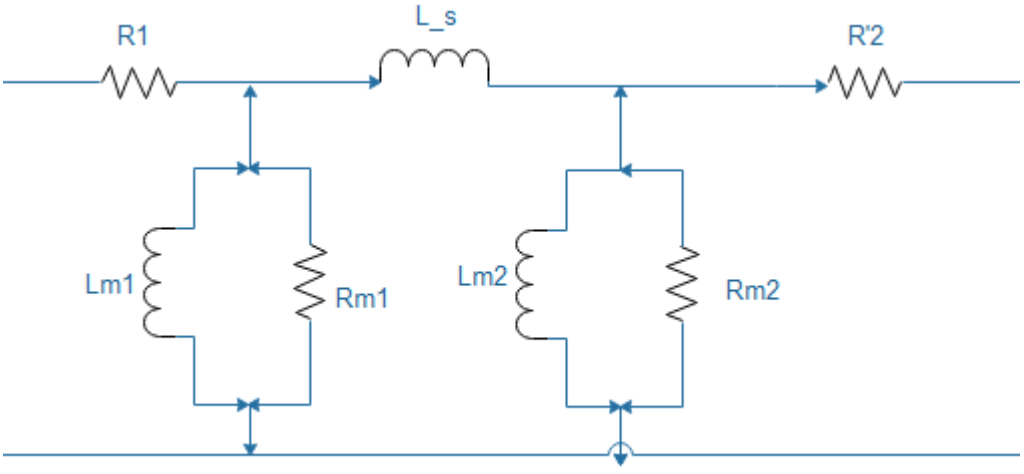

Figure 2.4: Single-phase transformer equivalent pi-model

2.5.3 *Single-phase reversible pi-model*

The single-phase reversible pi-model was developed as an improvement to the pi-model. It was set to overcome the challenge of needing to adjust the model parameters, depending on whether the inner or outer windings are energized. This model can predict transients from excitation of either inner or outer windings without parameter adjustments. It can also compute air core inductance from both windings [81, 83].

2.5.4 *Three-phase reversible pi-model*

With the consideration that most of the equivalent circuit models are developed for single-phase transformers. There have been efforts to extend the pi-model even further to include three-phase transformers [84]. Most Electromagnetic (EM) software offer three-phase transformers built from a combination of three single-phase transformers. The modelling of three-phase transformers has proven to be very important because most of the transformers used by utilities are three-phase. The three-phase reversible pi-model can be used for parameter identification in normal operation and deep saturation. It accurately accounts for the differences in three phase terminal connections and the interaction between phases.

2.6 Chapter Summary

This chapter presented findings from the literature in line with the research questions in section 1.4. A context for the research in this dissertation was set by explaining space weather events that lead to GICs. The importance of this research towards the security of modern power systems is emphasized. The chapter also delineates different considerations for transformer laboratory testing and FEM model development that are relevant to this dissertation. Transformer studies cannot be conducted in separation to the relevant transformer equivalent circuit. Hence, discussions on transformer equivalent circuits were presented towards the end of the chapter to assist in analysing laboratory results and FEM models.

3. Methodology and Laboratory Set-up

3.1 Methodological Framework Overview

This chapter outlines the framework and methodological principles guiding this project. This project follows a series of other related projects which focused on different core structures [13, 14, 29].

The overall methodological approach is summarized in Figure 3.1. The preliminary stages of the project led to some research questions which offered guidance on the trajectory of the project. Detailed protocols for the laboratory tests and simulation were developed subsequently. The rest of this chapter offers an overview of the technical methodological approach for the laboratory and simulation phases of the project, as the project initiation phase was mostly administrative. The laboratory test system is a key aspect of the investigation phase of the technical approach, hence it is discussed in detail.

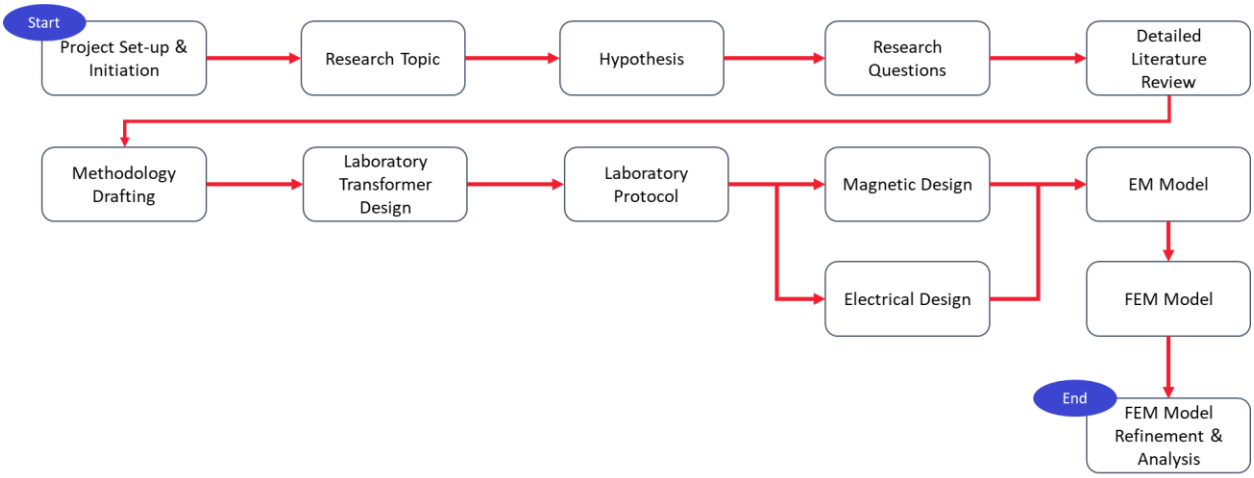

Figure 3.1: Project framework overview

3.2 Laboratory Testing

The overall laboratory test system is shown in Figure 3.2. It is a small-sized test system that was designed as per the project requirements. As the project requires the injection of dc (in lieu of GICs) into a 3p3L transformer, the test circuit needs to allow for the injection and flow of dc. The circuit would be excited from a variable ac voltage source within the voltage range of the transformer under Test (TuT). As mentioned earlier, the flow of dc/ GICs leads to the production of harmonics. Harmonics can be very detrimental to the supply system, hence their flow into the system must be avoided. The use of a source transformer, with a delta primary side is a good way of preventing zero

sequence currents to flow into the system, hence a source transformer was included in the test system. The source transformer also allows for the injection of dc/GICs between the neutral points of the source transformer and TuT, as if it were a real-life network. The source transformer should ideally be rated higher than the load transformer to avoid it saturating before the TuT [29], hence the use of two source transformers.

A load can be connected at the load bus, which should be rated lower than the TuT, in order to account for the non-active power taken up by the TuT during dc tests. The laboratory for the test had a range of load types varying from resistive and inductive loads; this offered flexibility in the type and size of load that can be used. A switch in the dc system is important for controlling the injection of dc.

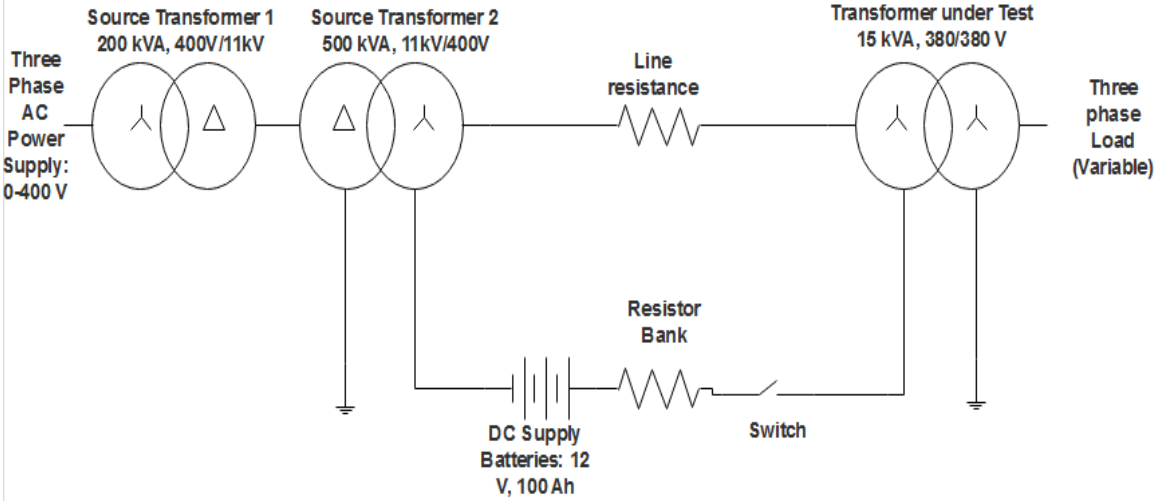

Figure 3.2: Proposed Test System with a battery connected for dc supply

3.2.1 Source transformer availability

Even though one transformer is enough for this project, two source transformers were available for use: Source Transformer 1 and Source Transformer 2, rated at 200 kVA and 500 kVA respectively (Figure 3.2). The two source transformers are less susceptible to saturation compared to a single source transformer. Also, the use of two source transformers ensures that the amount of non-active power drawn by the TuT is significantly less than the power rating of the source transformers.

3.2.2 Protection

Protection for the test system was provided by several circuit breakers. One breaker was installed before the variable power supply (variac), which was rated at 110 A. The variac also had three 60 A circuit breakers installed on its output side. An isolator was also present between Source

Transformer 1 and Source Transformer 2 (on their HV sides). The dc supply line was also protected with a 100 A switch for easy switching during tests, or in case of emergencies.

3.3 FEM Simulation

A simulation protocol was developed after the laboratory protocol. Previous Simulation work at the University of Cape Town focused on single-phase four-limb 3x(1p4L) transformers.

In order to carry out the work required in FEM modelling, it is important to pick the right tool. Several simulation tools with various capabilities exist in the market. The tool for this research was picked based on an analysis of the various common tools (Figure 3.3). Most of these tools seemed adequate for the requirements of the research in this dissertation. Cost and accessibility were however a major issue for tools with advanced capabilities. Freely available tools like FEMM do not have 3D capabilities, which limits the accuracy of obtained solutions. Tools with 3D capabilities like Solidworks and COMSOL cost about US$4000. Even though it also comes costly, ANSYS Maxwell was picked based on its competence in comparison to other tools, its availability at the University of Cape Town and its common use by different researchers [57].

Figure 3.3: Assessment of FEM simulation tools

ANSYS Maxwell has a powerful library for EM analysis. One of its advantages is the different ways in which transformers can be excited, providing for voltage, current or external circuit excitation. This provides for dc excitation under various cases. ANSYS Maxwell further provides for the selection of relevant boundary conditions. Boundary conditions define the magnetic field behaviour at interfaces or at edges of the particular problem region [85].

A FEM model of the TuT will thus be developed using ANSYS Maxwell. The model will be developed using the laboratory transformer data supplied by the manufacturer. The core data will be very key in this part of the project. According to Chisepo [14], the calibration of a FEM model of a transformer with ac measurement data can result in a realistic model that can be used for studies involving transformer response to dc excitation. The developed FEM model will undergo structural refinement based on the results acquired from the laboratory to improve its accuracy. Results acquired from such a model would assist in developing a better understanding of the actual conditions in a power transformer during GMDs [14].

3.4 Chapter Summary

This chapter discussed the methodology and theoretical framework of this research. The methodology involves testing a 3p3L 15 kVA laboratory transformer and developing a FEM model of the transformer for simulations, making use of the right tool.

4. Laboratory Protocol

The laboratory protocol used to investigate the response of the 3p3L transformer to dc/GICs is outlined in Figure 4.1. The protocol firstly addresses the issue of compliance, especially for the TuT. Compliance is checked against the data provided by the manufacturer. The testing involved no load tests and load loss tests. A detailed investigation of the transformer saturation under dc will be conducted to identify critical levels of dc that contribute to the saturation of the transformer. The protocol proceeds to outline the relevant tests identified from the literature review section to enhance the understanding of the transformer's response to dc/GICs. Other necessary tests will be conducted to enhance the understanding of the transformer's response to dc/GICs. The high-level protocol outlined in Figure 4.1 is further explained in subsequent sections.

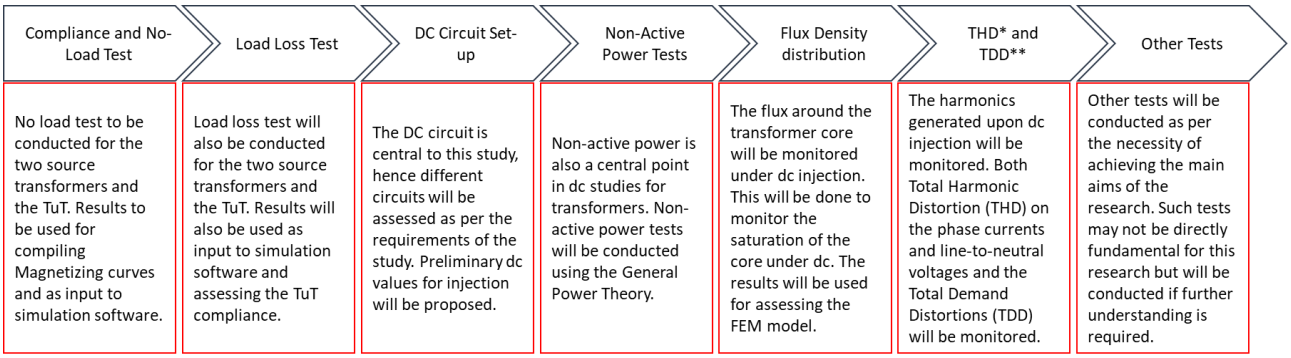

Figure 4.1: Detailed laboratory protocol

4.1 No load Loss and Excitation Current

A single-phase representation of the no load test circuit is shown in Figure 4.2 for the first source transformer (200 kVA). A similar circuit was used for source transformer 2 and the TuT. The detailed procedure and material requirement for the no load testing of all the transformers is outlined in Appendix A. The no load test results were used for computing the V-I curves and determining the parameters of the transformers.

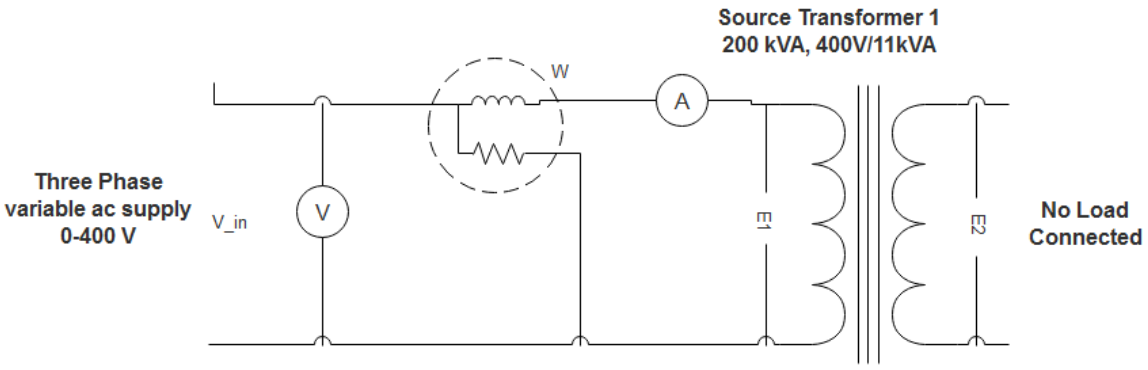

Figure 4.2: No Load Loss Test Circuit

4.2 Load Loss and Impedance Test

A load loss test will be carried out following the no load test. This test will be carried out on the TuT. The set up for this test is shown in Figure 4.3. The detailed load loss test list of required equipment and testing procedure is outlined under Appendix A.

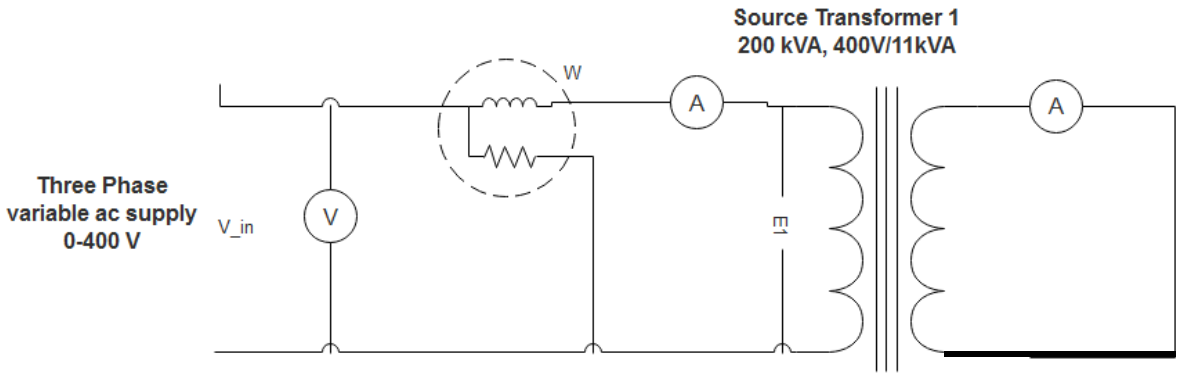

Figure 4.3: Short Circuit test Circuit

4.3 DC Circuit

The effectiveness of a dc circuit depends on its ability to emulate real life GICs cases which cause transformers to saturate. The dc circuit will be used to inject constant dc values instead of varying dc source. This is in order to keep consistency with the simulation tool, which was not geared for varying dc levels (which is the case for GICs). A good dc circuit needs to fit the following criteria for it to be suitable for such an experiment:

a) Range of dc values

A circuit with a wide range of dc excitation values leading the transformer into deep saturation is more ideal than one that does not lead into deep saturation.

b) Suppression of ac in the neutral

AC flow into the transformer's neutral because of imbalance may end up affecting the batteries used as dc supply in some cases. AC thus must be suppressed as much as possible, while still allowing dc to flow. The use of an inductor as explained in section 4.3.2 is one way of doing this.

c) Minimal battery discharge

The batteries may discharge during the experiment. This may affect the nature of the result as the dc in the neutral will not be steady. GICs have also been found to vary slightly with time, hence these changes are not entirely against the requirements of the set-up, but a good tracking of the dc current with time needs to be ensured.

The key equipment that will be used for the dc circuit include the following:

4.3.1 Battery (dc voltage source) and resistor banks

Batteries have been used by several established researchers to study the effects of dc bias on transformers [13, 14, 54, 86, 87]. Through preliminary testing, it has been noted that a battery is susceptible to discharge over the course of dc excitation. While most tests were conducted for a period of 2 – 4 minutes, similar to real life GICs cases, the dc level could not perfectly settle at one value as the battery discharged. The rate of discharge increased with the increasing level of dc injection. This may affect laboratory results and introduce disparities between laboratory results and simulation results – which are based on constant dc values. The resilience of the batteries can be increased by connecting the batteries in parallel, hence increasing their power and longevity during testing. The battery set-up will be connected as shown in Figure 3.2. The detailed procedure for testing each dc source is given in Appendix A.

4.3.2 Single-phase inductor

The inclusion of a single-phase inductor in the dc circuit helps to suppress any ac current that may leak into the neutral wire because of imbalance in saturation. The overall circuit set-up is as perFigure 3.2, with the inclusion of an inductor between the TuT and the dc circuit (Figure 4.4).

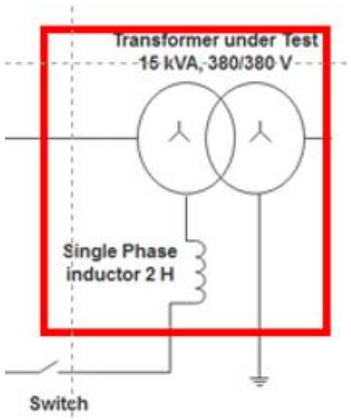

Figure 4.4: DC injection circuit involving a single-phase inductor, battery bank and resistor bank [12]

i. ***DC excitation values***

A protocol for determining the dc values to be used for dc excitation tests on transformers was developed by Oyedokun [54] as stated under the following steps.

a) Calculate the load current to dc ratio.

$$k_{LD} = \frac{I_r}{I_m}(pu) \tag{4.1}$$

where: I_r is the rated line current and I_m is the magnetizing current.

b) Calculate the dc level (I_{dc}) in pu. I_{dc} coupled with the AC currents should not exceed the rating of the transformer.

$$I_{pu} = \frac{I_{dc}}{I_m}(pu): \tag{4.2}$$

c) Inject dc into the transformer neutrals, such that the dc level per phase follows the inequality:

$$1 \leq I_{pu} \leq k_{LD} \tag{4.3}$$

d) Higher dc levels will be introduced to determine the response of the transformer in deep saturation. The maximum level of dc to be injected will comply with conductor restrictions and the observed transformer behavior in order not to permanently damage the transformer windings.

4.4 Non-Active Power Tests

The non-active power taken up by the transformer will be measured using both conventional IEEE compliant measurement instruments (Yokogawa WT1800 Power Analyzer) and the General Power Theory (GPT) developed extensively by Malengret and Gaunt [76, 88, 89]. The measurements for the GPT computation will be carried out as outlined in Figure 4.5. This experiment will seek to:

- Investigate the effect of dc on the non-active power taken up by a 3p3L transformer
- Investigate the presence of distortions on the load side of the TuT
- Compare non-active power absorption using conventional IEEE and GPT methods under dc excitation
- Understand the influence of distortion on non-active power computation under extreme dc excitation

Accordingly, the non-active power measurements will include:

- non-active power taken up by the transformer with increasing dc.
- non-active power taken up by the transformer with increasing input voltage.
- non-active power taken up by the transformer with increasing load current.
- Impact of the nature of load.
- Effect on the nature of saturation when there are different types of loads present.

The protocol for these measurements is outlined in detail under the Appendix A.

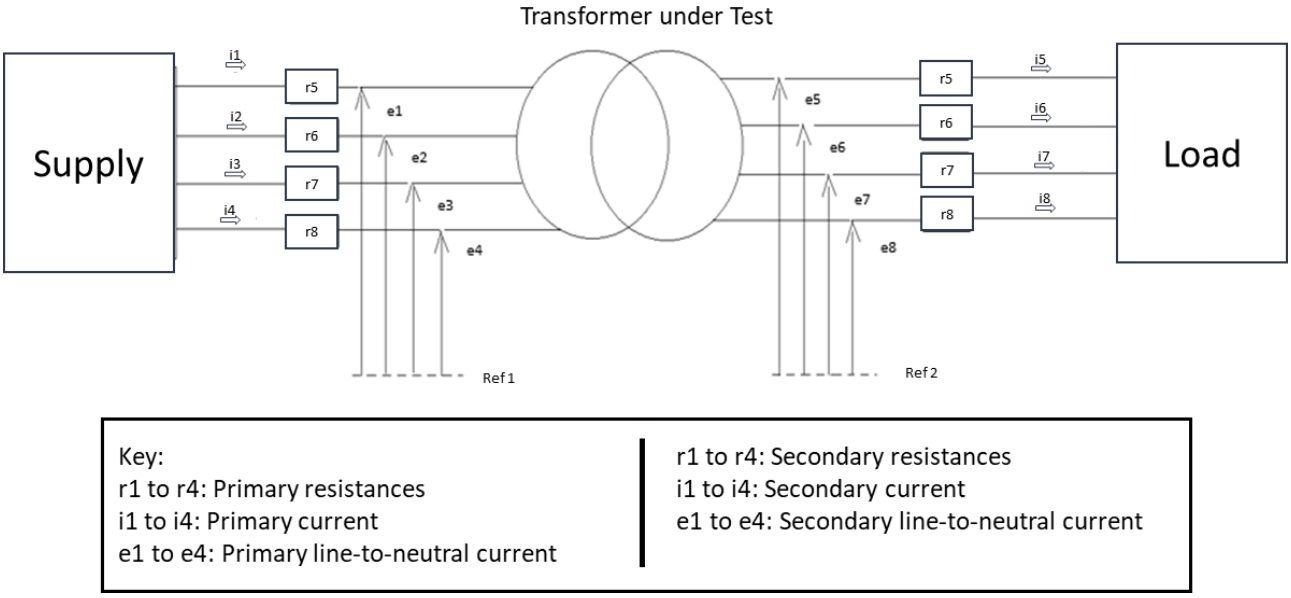

Figure 4.5: A 4 wire system for non-active power measurement using the General Power Theory (GPT)

4.5 Flux density distribution

An experiment will be conducted to measure the flux density distribution of the TuT using search coils. The operation of the search coil is based on the principle that a change in magnetic flux would induce an electromotive force across the search coil, which is proportional to the magnetic flux density.

The aims of this experiment are:

- To identify saturation patterns on the core and areas more vulnerable to deep saturation.
- To identify modifications that may need to be made on the transformer to decrease the level of saturation.

The following basic protocol will form part of the procedure guiding this experiment.

a) Prepare 1 mm thick, insulated fine wire to be used for search coils.

b) Wind two-turn search coils around each limb of the core and the yokes, with twisted tails brought out.

c) Connect the ends of the tails to a voltmeter.

d) Assembly air search coils around the corner-joint and t-joint areas, ensuring that off-core stray flux cuts through the cross-section area of the coils. Attach the coils to the core using masking tape. Air search coils would consist of twenty turns as the level of flux density is much smaller compared to the core [13, 14]. The twenty-turn (20) air search coils will be installed as shown in Figure 4.6. The core and air search coils were placed at positions that were identified to be prone to early saturation [13, 14, 80]. A few other search coils may be added when necessary during the investigation for the purposes of acquiring deeper understanding.

e) Energize the transformer with different levels of dc and record the voltage level across the voltmeter connected to each search coil.

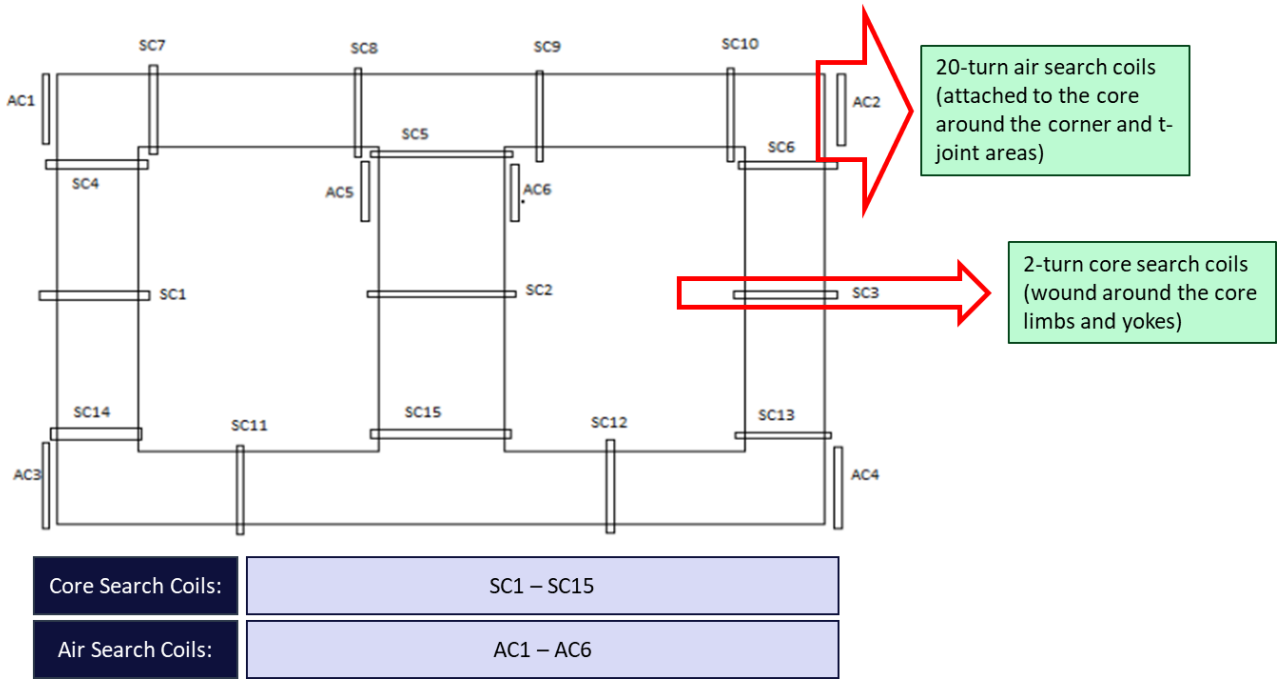

Figure 4.6: 3p3l Core and air search coil placement

4.6 Total Harmonic Distortion (THD) and Total Demand distortion (TDD) under dc

The THD and TDD are used to monitor the distortion in a system due to harmonics. According to Morsi *et al* [90] , the TDD needs to be kept within certain acceptable limits to minimize system losses, heating and malfunctioning of system equipment. The TDD is the total rms harmonic current distortion as a percentage of the maximum demand load current, as shown by equation (4.4).

$$TDD = \sqrt{\frac{\sum_{h=2}^{\infty} I_h^2}{I_L^2}} \tag{4.4}$$

where:

I_L: Maximum demand load current (fundamental frequency component)

The THD and TDD will be monitored under resistive and inductive load conditions with: increasing dc, increasing input voltage, increasing resistive load and increasing inductive load.

4.7 Other Tests

A couple of other tests which are not primary to the project will be conducted to facilitate further understanding of the transformer behavior under dc. A few of these tests are discussed in the following sub-sections.

4.7.1 Open phase test

Open phase situations are not rare occurrences for power systems, mostly in medium voltage (33 kV and below) distribution networks [91]. These may be because of broken conductors, loose connections or a blown fuse. With the introduction of more Distributed Generation (DG) sources, this problem is expected to become even more pertinent [91]. Since the TuT falls within the family of transformers that are susceptible to open phase (failure of a phase) conditions, it is important that the transformer is tested for such cases. The TuT will be tested for its response to dc when one of its primary phases fails. The tests will be carried out by opening one phase at a time as per Table 4.1 below. Each test will be conducted under no load conditions with increasing input voltage and increasing dc.

Table 4.1: Open phase testing

Open Phase Test (PTF) Label	Open Phase
PFT1	A
PFT2	B
PFT3	C

4.7.2 Transformer Time Response

The time response of the transformers would be analyzed, following the work of Oyedokun[54]. Oyedokun [54] concluded that the 3p3L transformer has the shortest time response as it permits dc flow in the windings much quicker. This would be analyzed using a Yokogawa (WT1800) Power Analyzer. This would be tested as part of the main circuit testing in Figure 3.2 utilizing the following procedure:

a) Set up the dc resistor connections for the dc circuit to be tested.
b) Energize the ac system by turning on the variac to the nominal voltage.
c) Have one person working on the Yokogawa to capture readings.
d) Switch on the dc circuit while the other person captures the waveform on the variac (capturing of readings must be done simultaneously with switching before the system reaches steady state).
e) Compute the time response by calculating the settling time of the current waveforms after switching on dc.

4.7.3 DC injection on inner winding or outer winding

Conventional transformers used for either stepping voltage up or down consist of HV and LV windings. The HV winding is usually located closer to the core because of its lower current, hence lower heat is produced. This is advantageous for the core as heat generation leads to further core losses. This experiment makes use of an isolation transformer with a 1:1 ratio. This test will thus investigate the response of the transformer to dc when injected with dc either on the inner winding or the outer winding. This would provide clarity on the effect of having the energized winding closer to the core on the transformer's saturation. The flux density distribution will be monitored through a range of dc tests.

4.8 Chapter Summary

This chapter presented the laboratory protocol to be followed during the transformer testing. A rigorous laboratory protocol was put together, with close guidance from previous research at the

University of Cape Town. Only the test protocol critical for the analysis of the transformer response is presented in the chapter. Other miscellaneous protocols are presented in the Appendix A. The next chapter outlines the initial execution of the protocol by exploring some of the preliminary laboratory experiments. Compliance tests are carried out to check whether the transformer functions as per the design requirements and in line with the information provided by the manufacturer.

5. Preliminary tests

5.1 Transformer Under Test visual inspection

The Transformer under Test (TuT) shown in Figure 5.1, was a three-phase three-limb (3p3L), 15 kVA, 380/380 V, 50 Hz core type transformer, manufactured by Modisync (Pty) Ltd in Johannesburg, South Africa. The 3p3L was accompanied by a similar 3p5L transformer, which was designed to have similar ratings. Reference will be made to the 3p5L transformer whenever necessary for comparative purposes. The 3p5L transformer is however not the primary focus of this study.

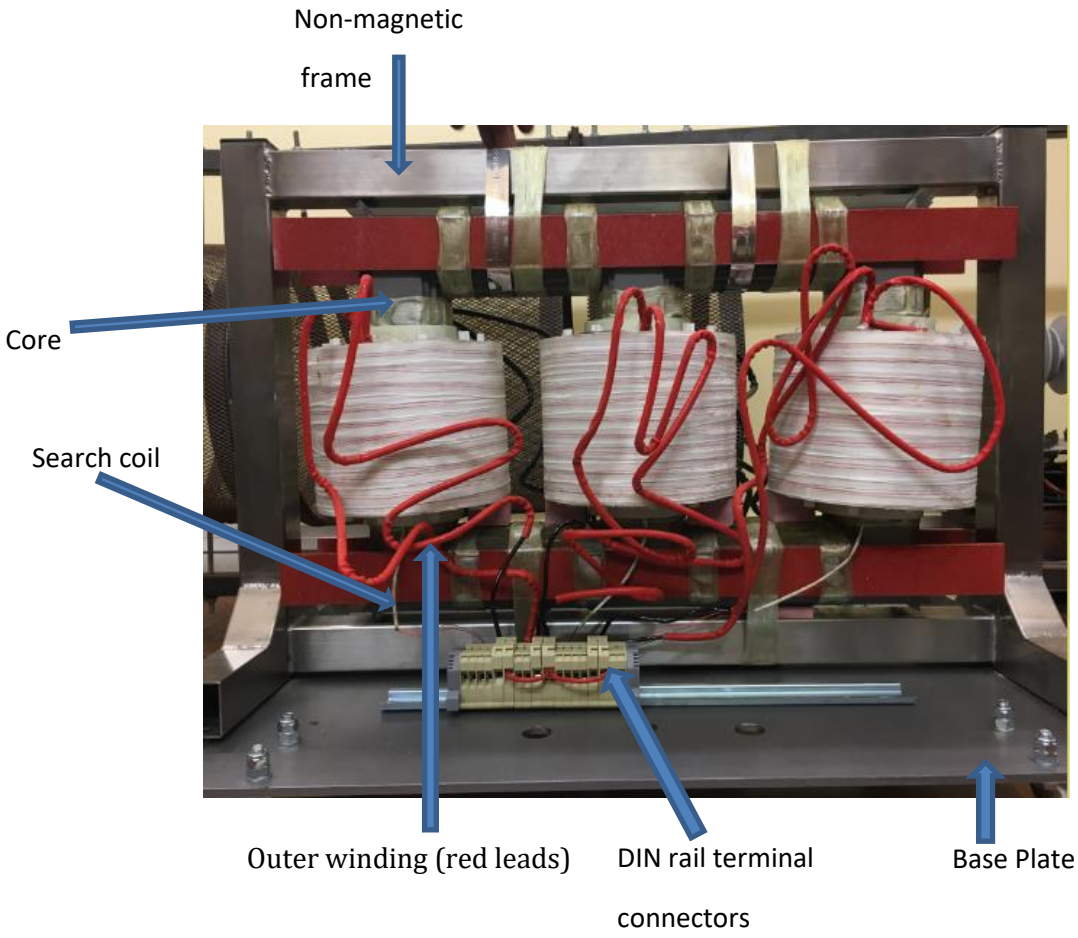

Figure 5.1: Transformer under Test

The TuT shown in Figure 5.1 was specially designed for greater amount of flexibility in testing. It came with a detachable tank to allow access to the transformer windings and core. The core was made of four steps, with mitred core joints to emulate the design of industry scale large power transformers. The core laminations were held in place with GPO3 (glass reinforced polymer) strips.

The core was also supported on a non-magnetic 304 stainless steel frame. The bell tank was made of 3 mm mild steel plates, while the base plate was made of 6 mm mild steel. A clear distinction was made between the primary (inner) windings and secondary (outer) windings, which were colour coded with black and red respectively. The transformer windings were enamel covered copper wires of 3.55 mm diameter. With enamel, the diameter of the copper wires is 3.702 mm.

5.2 Compliance Testing Results

Compliance testing was conducted before exposing the transformers to rigorous testing. These test results were compared to the manufacturer given values. The preliminary tests conducted are discussed in the following subsections.

5.2.1 No load test results

The TuT no load test was conducted to determine its magnetizing (V-I) curves, and the magnetizing current value at the McLymans knee-point of the transformer. The knee-point values are important for understanding the transformer behaviour and are to be used as input to the FEM model. The transformer no load tests were conducted with and without the tank, with its inner and outer windings energized separately. Figure 5.2 shows the magnetizing curve for the case when the inner windings were energized without a tank on. It can be noted from Figure 5.2 that the transformer knee-point voltage is at around 162 V (0.74 p.u) (line-to-neutral), which falls below the transformer operating voltage of 219 V (line-to-neutral). This is a critical finding which might fundamentally affect the behaviour of the transformer and the point at which it will eventually be operated. The magnetizing current of the transformer is the current flowing through the transformer at the knee-point voltage under no load conditions. The magnetizing current was recorded to be 126 mA.

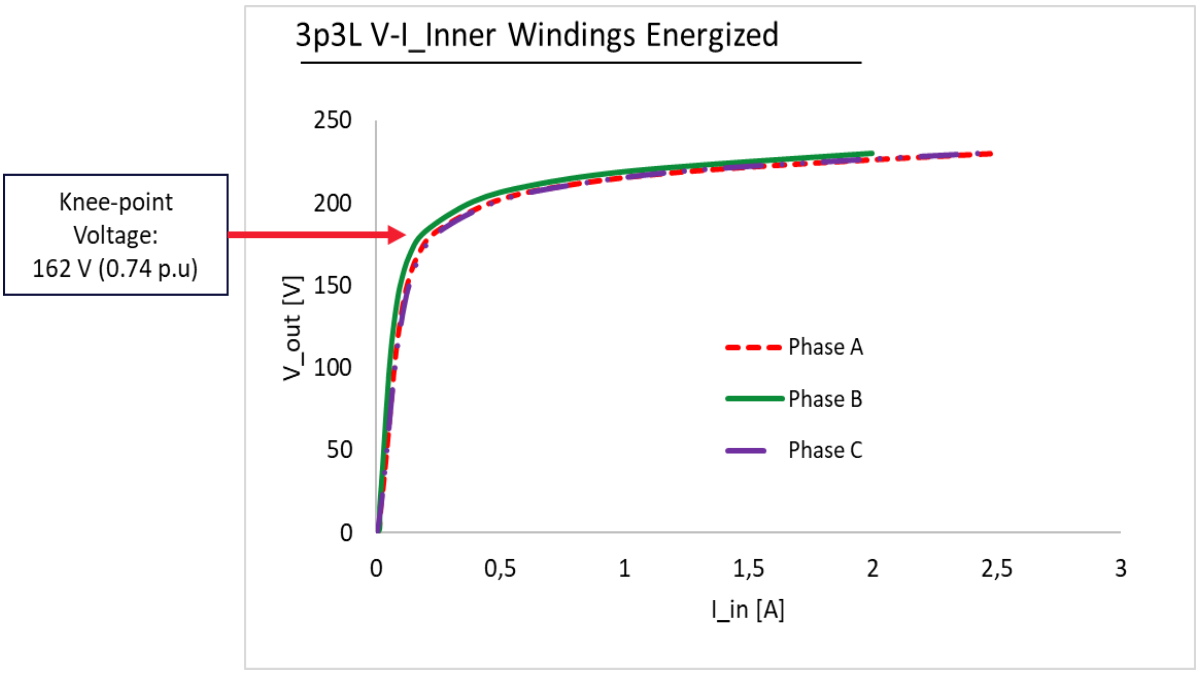

Figure 5.2: 3p3L transformer V-I curve computed from a no load test

The no load test was conducted for each of the transformer phases, energizing the inner windings first and then the outer windings of the transformer to ensure that the transformer works under a range of conditions. The energization was also done with and without the transformer tank to assess its influence on the operation of the transformer. The results for these tests are outlined in Figure 5.3, which shows the knee-point voltages and magnetizing currents of the different phases of the transformer.

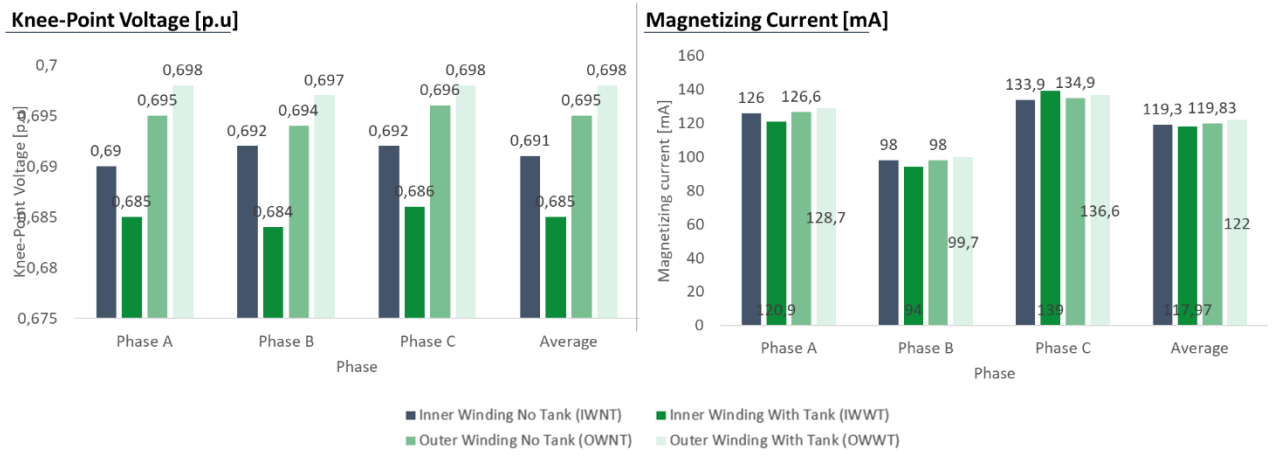

Figure 5.3: TuT knee-point line-to-neutral voltages and magnetizing current

As seen from Figure 5.3, the magnetizing current values are barely affected by the energization of either the inner or outer winding since there is no overarching trend apparent between the different cases. The inclusion of the tank seems to have some minimal effect on the transformer knee-point voltage. An example of such impact can be deduced from the inner winding results with and without tank. The same seems to be true for the magnetizing current, although at a lower magnitude compared to the knee-point voltage. There is further an exception of phase C magnetizing current, with a different behaviour compared to phase A and B, where the magnetizing current is higher without the tank than with the tank. This difference is negligible nonetheless as the transformer is operated in its linear region, with minimal off-core flux.

The B phase magnetizing current generally appears to be lower than the other two phases (about 26.8% lower than the C phase for the inner winding with no tank (IWNT) case), with a similar trend noticeable in the B phase knee-point voltages (line-to-neutral) voltages. This is due to the increased reluctance path experienced by the B phase magnetic flux, which must feed flux into two equal and parallel paths, unlike the other two phases. The magnetizing currents of the A and C phases appear to be slightly different as well. For each case, the A phase current is about 6% less than the C phase current. This is because of a difference in the total magnetic path length (MPL) seen by the flux from the two energized limbs. The difference in MPL is a result of the slight differences in the equivalent corner joint gaps, hence affecting the total reluctance seen by each limb flux. This will be investigated further by the energization of each winding at a time and monitoring the core flux sharing between the limbs. Overall, the knee-point voltage for all phases appears to be much lower than the manufacturer specified rated voltage of 219 V/phase. This will be investigated further in the following chapter.

5.2.2 Load loss test results

The load loss test was conducted following the no load test. The load loss test results are shown in Table 5.1 These results will provide useful input to the development of the FEM model.

Table 5.1: Short circuit test results

Input Current			Input voltage [V]			Active power [W]		
Phase A	Phase B	Phase C	Phase A	Phase B	Phase C	Phase A	Phase B	Phase C
22.106	22.807	22.829	9.447	9.516	9.679	116.9	122.1	127.5

It is worth noting that the load loss voltage appears to be much lower than the specified V_{SC} of 19.3 V, by about 10 V per phase. This is due to the lower operating point of the transformer, which was also different from what the manufacturer specified.

5.2.3 Transformation ratio

The transformation ratio of the transformer was designed to be 1:1. The transformer input and output voltages were recorded at no load (at the rated voltages), to compute the transformation ratio. The results are shown in Table 5.2. The transformation ratio was compliant with the design specification of the transformer and the information provided by the manufacturer.

Table 5.2: Transformation ratio computation

	Phase A	**Phase B**	**Phase C**
V_primary [V]	210.83	210.31	210.67
V_secondary [V]	210.65	210.3	210.51
Transformation ratio	1.0009	1.000	1.0008

5.2.4 Winding resistances

The winding resistances were also measured as part of the preliminary testing of the transformers to check for compliance with the calculated values. Considering the temperature dependence of winding resistances, equation (5.1) below was used to calculate the actual winding resistances from the measured values. The calculated and measured results are shown in Table 5.3. The calculations and measurements were conducted for both the inner and outer windings to maintain consistency with the other tests, hence Table 5.3 is reflective of both cases.

$$R = R_m \frac{234.5 + Ref.Temp}{234.5 + Meas.Temp} \tag{5.1}$$

where:

R: actual winding resistance at standard room temperature

R_m: Measured winding resistance

Ref. Temp: Standard room temperature

Meas. Temp: Temperature during measurements

The measured winding resistances were compliant with the calculated winding resistances, with a consistent 2.2% difference between measured and calculated resistances for both inner and outer windings..

Table 5.3: Winding Resistances

	Inner Winding			**Outer Winding**		
	Phase A	Phase B	Phase C	Phase A	Phase B	Phase C
R [ohms]	0.176	0.176	0.176	0.225	0.205	0.215
R_m [ohms]	0.180	0.180	0.180	0.230	0.210	0.220
Difference [%]	2.2	2.2	2.2	2.2	2.2	2.2

5.2.5 Core flux

The transformer rated volts per turn (EMF) of the core is 1.5671 V, hence the two-turn search coils were expected to give a reading of 3.134 at the rated voltage of 219 V/phase. A test involving the two-turn search coils around the centre of the wound limbs recorded a voltage of 3.03 V (1.515 V per turn). The recorded values were found to be within 1% of the volts per turn specified by the manufacturer.

5.2.6 Core and Copper Losses

At a design flux density of 1.703 T, the transformer rated losses were given by the manufacture to be 1.4 W/kg. The calculated expected core losses based on the transformer mass would then amount to 71.4 W, while the manufacturer recorded 69.83 W. The core losses recorded in this compliance test amounted to 75.78 W. This value is about 6.1% higher than the design value of 71.4 W and about 8.5% higher than the manufacturer specified value of 69.83 W. These observations may be due to the transformer operating well beyond its actual knee-point voltage. Thus, it is operating in its early saturated region, hence the increased losses, especially around the joints.

The manufacturer also provided the estimated copper losses of the transformer to be 425 W at the rated current. The copper losses from short circuit test amounted to 366 W, which is 13.9% lower than the manufacturer specified copper losses.

Upon completion of the compliance tests, it was noted that even though there were a few discrepancies between some of the test results and the manufacture data, the transformer was generally suitable for the required experiments as such discrepancies were within acceptable limits. One issue of major concern was the operating point of the transformer, with it showing signs of saturateion at the specified operating point of 219 V/ph. This required further investigation, and hence the 3p5L transforemer was then looked into.

While visually inspecting the 3p5L transformer which accompanied the TuT, it was noticed that the outer limbs of the core had 10mm diameter holes which were used for stacking the core. Upon inquiry with the manufacturer, it was clarified that the holes were included in the 3p3L transformer as well, although these were not visible through inspection as they were covered by the windings and the clamping material. The impact of the holes would be investigated further in the next section.

5.3 Investigation of the Impact of Holes in the Transformer Performance

This section provides an assessment of the impacts of the holes punched on the core of the 3p3L transformer on its test results. An illustration of the holes is shown in Figure 5.4 from a similarly designed 3p5L transformer return limb. A picture of the holes could not be taken on the TuT as they were covered by the windings and the clamps on the yokes.

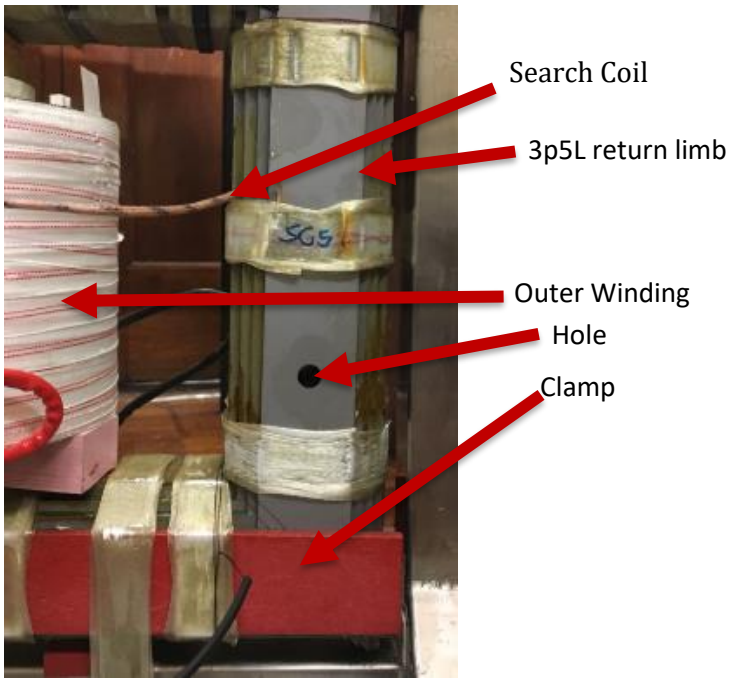

Figure 5.4: 10 mm diameter holes in a similarly rated 3p5L transformer

The exact location of the holes per transformer was not specified on the transformer manual. The manufacturer only specified the number and approximate locations of the holes which are shown in Figure 5.5. Since these may not be the exact locations, further investigations were required as this information is a crucial input to the FEM model.

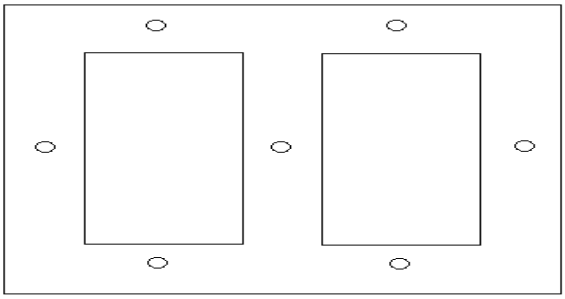

Figure 5.5: 10 mm diameter hole placement on the 3p3l transformer under test.

Following the compliance testing of the transformer in the previous subsection, it was noted that the operating point of the transformer was lower than the operating point specified by the manufacturer. The suspicion was that the transformers were either not designed to specifications or the holes were having a major contribution towards the transformer's early saturation. This called for further investigation into the extent of the impact of the holes on the transformer behaviour. The holes basically introduce an air gap into the core, which offers a reluctance different from the rest of the iron core. An understanding of the influence of the air gap seemed to be a good starting point towards understanding the influence of the holes.

5.3.1 Understanding the air gap

Air gaps usually exist in transformer cores around the joint areas. They are formed due to the placement of lamination sheets. These air gaps in conjunction with shifted core steel packages cause inter-laminar flux components which lead to flux inhomogeneities and higher loss [92]. The air gap presented by the hole is different from conventional air gaps found in joints, which are usually represented with a uniform depth [93-95]. The hole air gaps are distinct in that they are cylindrical in shape and are punched from one side of the core to the opposite across the laminations as shown in Figure 5.6. The air gap from the hole does not cover the whole width of the core, thus it leads to air gap reluctance parallel to the surrounding core reluctance. The depth of the air gap along the flux path varies from 0 to 10 mm.

The transformer core was made of high permeability, low reluctance magnetic steel (M5). Air gaps present a low permeability, high reluctance path to magnetic flux. The air gaps influence the shape of the B-H curve of the magnetic circuit, while increasing the saturation current [94, 95]. This also leads

to flux fringing, where flux lines are no longer confined within the core but occupy the surrounding space. This effect on the magnetic circuit might affect the efficiency of the transformation and induction of voltage by the transformer, especially under saturated conditions.

The presence of the hole is expected to deflect the flux lines along the core. The availability of core material around the gap would result in flux cross linkages to utilize the low reluctance path as shown in Figure 5.6. This could cause localized saturation within the core area surrounding the hole, leading to early saturation of the core.

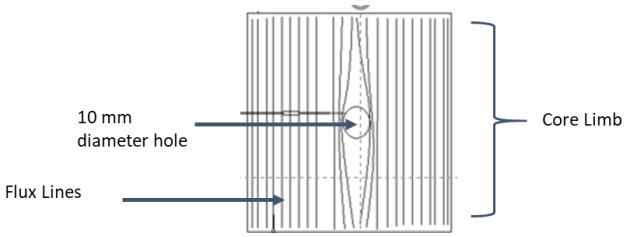

Figure 5.6: Core section including a 10 mm diameter hole and flux lines.

The presence of the holes leads to an increase in the overall reluctance of the magnetic circuit. The impact of the hole on the surrounding flux lines is shown as the lines are not parallel to the flux lines in other areas of the same core section. This influences the overall distribution of flux and flux concentrations in the neighborhood of the gap areas, leading to localized losses [96]. This influence reflects in the lower operating point of the transformer, which is different from the operating point specified by the manufacturer. The manufacturer may have designed the transformer to operate at 219 V (line-to-neutral) without factoring in the influence of the holes. Hence, the effective operating point is lower than the designed operating point. Further investigations were required to understand the impact of the holes on the transformer flux distribution.

5.3.2 Influence of the holes on the core flux distribution

As part of investigating the impact of the holes on the operation of the transformer, two-turn search coils were installed around certain sections of the core (labelled SC1-SC15) and twenty-turn search coils were installed to capture stray flux (labelled AC1-AC6), as per Figure 4.6. Search coils were placed around the core to capture voltages induced by the flux across the search coil.

According to Borill *et al* [97], the expectation is for a uniform flux density within the core limbs and along the yokes, such that: SC1 = SC4 = SC14; SC2 = SC5 = SC15; SC3 = SC6 = SC13; SC7 = SC8; and SC9 = SC10. The right limb of the transformer was picked for this investigation, using search coils SC3, SC6 and SC13 The right limb search coil readings (SC3, SC6 and SC13 were almost the same for lower voltages (up to 200 V) (Figure 5.7). At higher voltages, (at 202 V and 219 V), the search coil voltage at SC3 and SC6 increased by 1% more than the SC13 voltage as shown in Figure 5.7. This

indicates flux loss in the lower part of the limb, which may be due to the presence of a hole. There was an increase in localized saturation around the holes because of a high concentration of flux density. The same result was noticed for all three limbs.

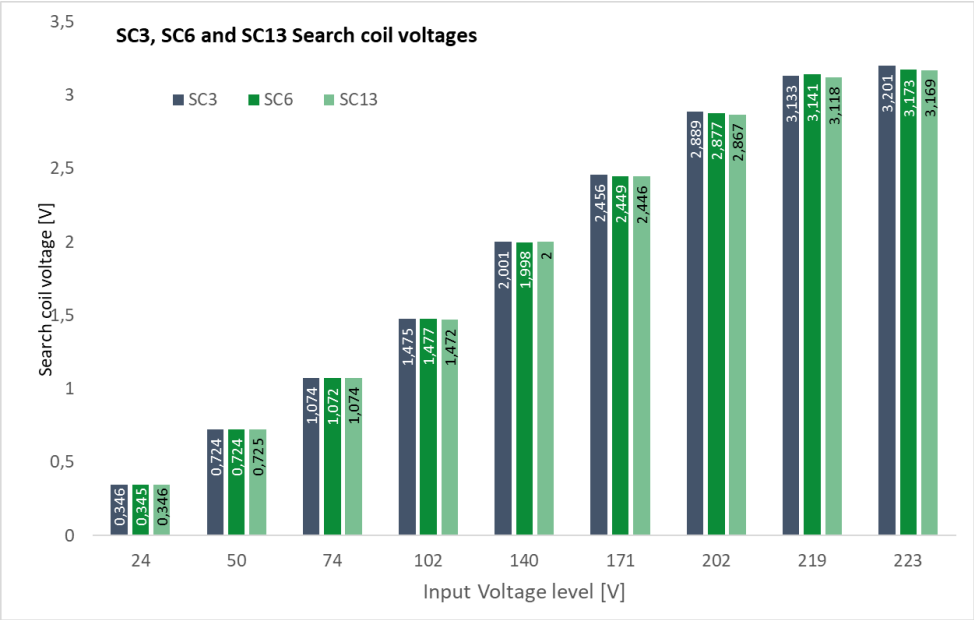

Figure 5.7: Wound right hand side outer limb search coil results.

From Figure 5.7, one can see that SC3 and SC6 have slightly higher induced voltage compared to SC13 at higher input voltages (about 0.9% higher). Since these are expected to be similar, as is the case for the lower voltages, there appears to be something happening between search coil SC6 and SC13. This difference means that the initial assumption of the holes being in the middle of the limb may have not been accurate. The holes appear to be located further down the limb, somewhere closer to SC13, which is the reason for the lower reading on SC13 under saturation. Less flux is captured by SC13 wound around the limb due to a fraction of the flux fringing around the hole. In deep saturation, the permeability of the transformer drops drastically, approaching that of air. The air surrounding the core then suddenly becomes an optional path for flux to flow, causing an increasing amount of fringing and stray flux. The same result was experienced for the left limb, where SC14's induced voltage appeared to be higher than those of SC1 and SC4. Thus, it can be deduced that the hole has an influence on the core flux. Further insight was gained on the actual location of the holes, which is towards the end of the limb. To further test this new insight, the air search coil recordings were explored.

The air search coil (AC1 to AC6) voltage outputs were analyzed under varying voltage levels. Figure 5.8 shows the air search coil results at varying levels of input voltage. The air search coils started giving voltage readings from about 200 V, signaling saturation before the rated voltage (219 V). This

corresponds with the core search coil voltage readings. Upon inspection, it was noted that the laminations were a bit loose towards the corner of the SC3 joints. The looseness of the laminations further widened the gaps between individual laminations, hence further increasing the reluctance of the path. Further evidence of early saturation of the SC3 joint was the presence of a buzzing sound from about 210 V/ph of input voltage. The degree of looseness and the overall unevenness in the joints led to differences in the recorded search coil voltages. Further differences may have been as a result of small differences in the search coil cross-sectional area, although this would have been a minor contributor as caution was taken to ensure that the search coils are around the same size.

Well-designed and manufactured transformers should not saturate below the transformer operating voltage. They are expected to give air search coil readings at input voltages above the design operating voltage of the transformer. The knee-point should be above the operating voltage, hence saturation should commence above the design operating voltage. Further analysis on the flux density distribution is provided in Appendix B.

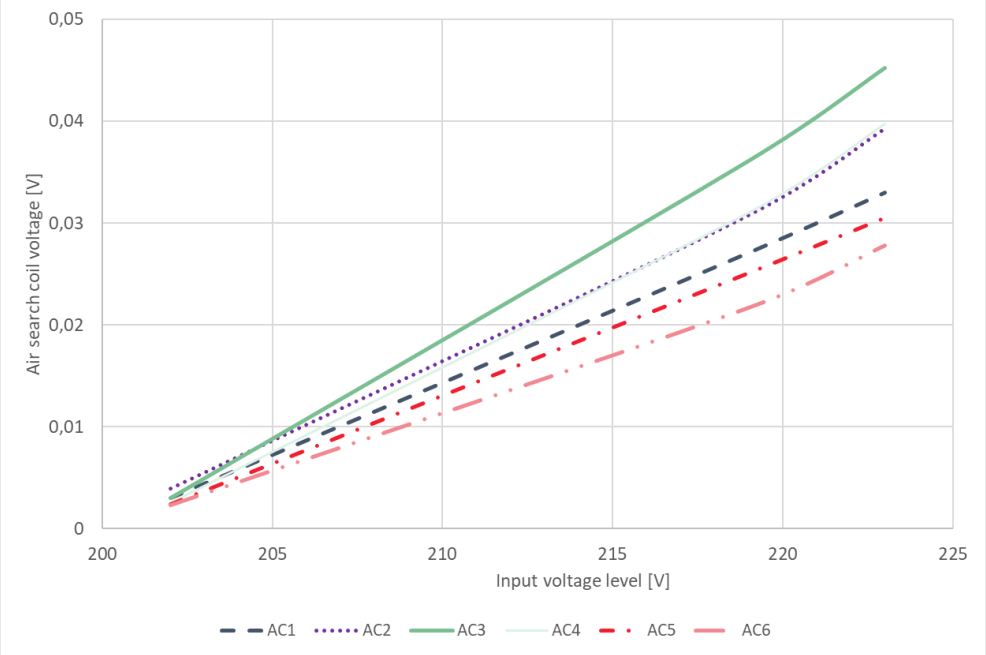

Figure 5.8: Air search coil results

5.4 Derating the transformer

The TuT was designed for an operating voltage of 219 V/ph. The magnetizing curve computed after the no load test revealed that the operating voltage lies above the McLyman knee-point voltage of about 167 V/ph, signalling that the transformer is already in saturation. To validate this claim, a theory for saturation extracted from [98] was used to further investigate the state of the transformer

at both the rated and knee-point voltages of the transformer. This proved that the transformer is already in saturation, as shown Table 5.4

$$For: I_{peak} < 2 \times I_{average} : No\ Saturation \quad (5.2)$$

$$For: I_{peak} = 2 \times I_{average} : Saturation\ begins \quad (5.3)$$

$$For: I_{peak} > 2 \times I_{average} : Saturation \quad (5.4)$$

Table 5.4: TuT Saturation check

V_point	Voltage [V/ph]	I_{peak} [A/ph]	$I_{average}$ [A/ph]	$2 * I_{average}$ [A/ph]	Decision	Saturated?
V_{rated}	219	2.7751	0.9988	1.9976	$I_{peak} > 2 \times I_{average}$	Yes
V_{knee}	167	0.2848	0.1446	0.2892	$I_{peak} < 2 \times I_{average}$	No

From the analysis above, it is evident that at the rated voltage, the transformer is already in the region of saturation. Thus, it was de-rated to be operated at a voltage within the linear region (below the knee-point), at 160 V(line-to-neutral). To prevent the transformer from easily creeping into the saturated region under minor distortions or dc levels, it should not be operated too close to the knee-point. Also, the operating point should not be too far from the knee-point for economic reasons.

5.5 Chapter Summary

This chapter presented preliminary and compliance test results for the TuT. One of the key findings of this chapter was the influence that the holes on the core of the transformer had on the overall transformer behaviour. Early saturation of the transformer due to its core led to its operating point being de-rated from 219 V (1 p.u) to about 160 V (0.73 p. u).

The chapter further highlighted the need to clearly understand the performance of the TuT's core when conducting experimental tests and simulations. The behaviour of the core has been seen to be significantly impacted by the presence and placement of the holes. This can be seen through the early saturation experienced by the core. The core was made to closely resemble actual laboratory scale transformers with mitred cores to combat early saturation [80]. The impact of this on the operating point of the transformer is discussed in the following section.

6. Discussion on Laboratory Test Results

6.1 Introduction

Upon satisfaction on the suitability of the TuT for the purpose of this research through compliance testing, this chapter focusses on a rigorous testing of the 3p3L transformer under dc, drawing from the laboratory protocol. The tests began with a no load test of the TuT under dc. Further tests involved the inclusion of resistive and inductive loads in the testing process. The 3p3L transformer was tested in parallel with a similarly rated 3p5L transformer (focus of another study). Some comparisons between the two transformers were made in a few parts of this chapter, although the focus was on the 3p3L.

6.2 No load DC Tests

This section outlines the results of the 3p3L transformer testing with no load under dc. The transformer was exposed to open circuit testing, with dc current applied between the neutrals of source transformer 2 and the TuT. Terminal measurements were taken using the Yokogawa WT1800 power analyzer. These tests ultimately helped in the understanding of the saturation of the transformer under dc, identifying critical points of saturation. This will be used as a point of comparison for the FEM simulation.

6.2.1 Magnetizing current

The transformer magnetizing current was analyzed under different dc levels injected into the TuT neutral. Under no load conditions, the current flowing through the primary side of the transformer through the magnetizing branch is viewed as the magnetizing current due to the high value of the shunt resistance. Upon injection of various levels of dc, it was noticed that the current waveforms showed peaks on one half-cycle of the waveforms; a consequence of dc presence called part-wave saturation. To provide a clear picture of what this part-wave saturation looks like (for both the 3p3L and 3p5L transformers), an arbitrary dc value of 24 A/ph was injected to both transformers, where the current waveforms would be clearly distinguishable. Figure 6.1 shows the TuT's magnetizing current compared to the 3p5L transformer's magnetizing current under the excitation of 24 A/ph dc, captured over a time series. Part-wave saturation can be noticed from both waveforms but at different intensities or magnitudes. This can be seen by the uni-directional peaks on the one half cycle, and a flat half cycle on the other hand. The two half cycles should ideally be similar and sinusoidal for perfect waveforms. But from the graphs, the one half cycle (in the direction of the injected dc) develops to a point that the other half cycle appears to be flat.

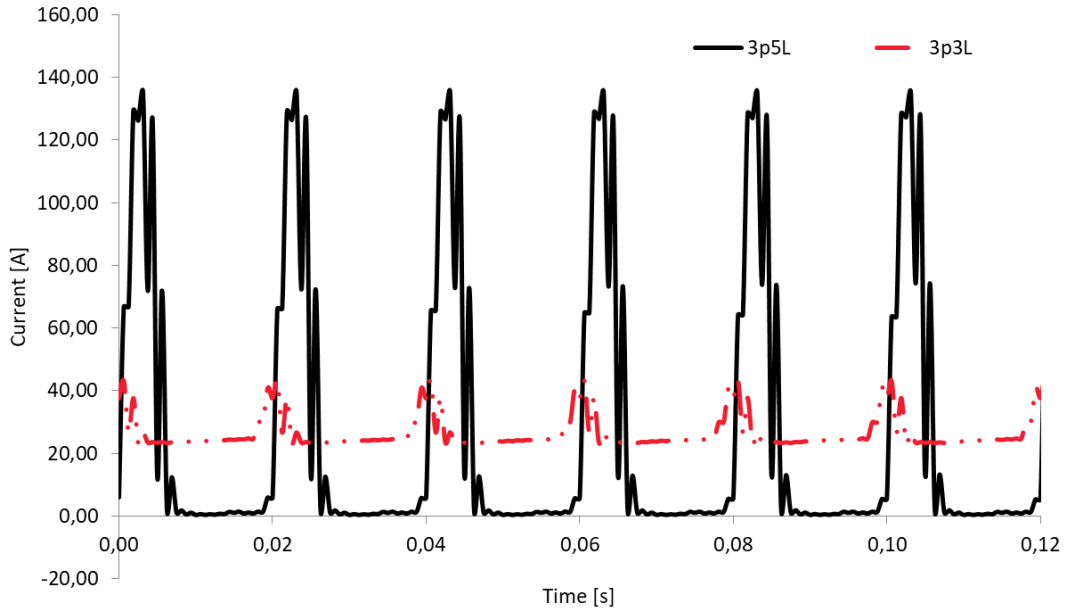

Figure 6.1: 3p3L and 3p5L transformer magnetizing current waveforms at 24 A/ph dc

The 3p3L magnetizing current waveforms shown in Figure 6.1 appears to be shifted up from the horizontal axis, as opposed to the 3p5L waveform which is pinned to the horizontal axis. This pattern has been found to be unique to the 3p3L transformer [51]. The shifting is due to the return dc flux in the 3p3L transformer which is shared with the primary flux along the limbs. All the limbs are occupied by excitation flux, and hence there is no alternative return path for the dc flux, except through the excited limbs. It can be noted from Figure 6.1 that the 3p3L magnetizing current waveform is shifted up to the dc value injected per phase, thus showing a link to the amount of dc injected and the associated dc or zero sequence flux. This is however not the case for the 3p5L transformer, where dc or zero sequence flux can make its return via the unwound outer limbs, thus having limited presence in the excited limbs. The magnetizing current can be used to assess the transformer saturation under dc, which is the subject of following section.

The displacement of the zero axis appears to be minimal in transformers with outer limbs and not proportional to the injected dc. This is due to the outer limbs taking long to saturate compared to the dc excited limbs. These results are consistent with the findings of Chisepo *et al* [87], whose research portrayed similar findings for a 1p4L 4.4 kVA transformer.

6.2.2 Transformer saturation

The mini spikes noticed on the magnetizing current waveform in Figure 6.1 raise a suspicion that the transformer may have been operating in a saturated region at a dc injection of 24 A/ph. The asymmetric nature of the waveform and the sub-peaks are evident signs of a transformer operating

in its saturated state with harmonics present. One of the main goals of this study is to identify the level of dc that exactly leads to the transformer saturation. Different approaches were taken in the following sub-sections to conduct this analysis.

i. Saturation point check using the Price method

According to Price [51], a linear relationship exists between the transformer exciting current and the induced GIC/dc [51]. The ac input under a no load condition was used for this analysis as shown in Figure 6.2. The graph depicts the change in ac with increasing dc excitation. The input ac current was kept constant at 0.06 A/phase through the experiment, with only the dc component changing.

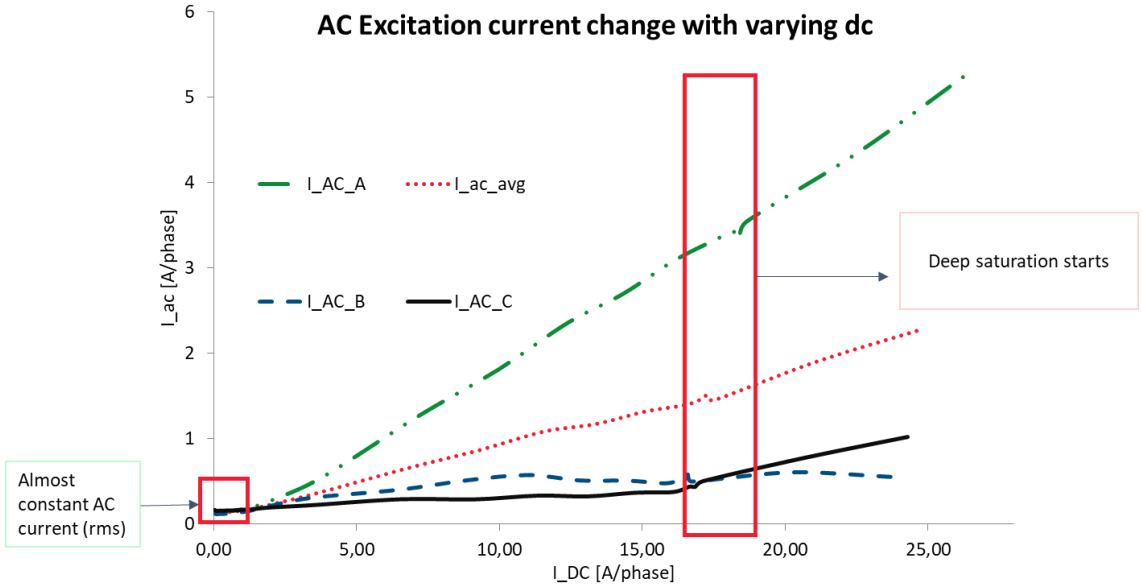

Figure 6.2: 3p3L ac excitation level change with varying dc input

Figure 6.2 shows that at lower values of dc input, the ac current remains almost constant at a low magnitude. A linear relationship starts to show beyond a dc input of about 1.8 A/phase (8% of rated current/phase). According to Price [51], this is the point where the transformer starts to saturate. The ac current magnitudes in the three phases are clearly different. The difference increases with higher values of dc injection. This distinction indicates some current imbalance between the different phases as a result of dc injection. This imbalance is due to a disproportionate share of the dc injected into the neutral among the three phases of the transformer. There was no control over the actual flow of dc into each phase, but the actual dc values were monitored through the Yokogawa power analyzer. This was dependent on the resistance of each phase, which includes; the actual transformer phase resistances, the dc circuit resistance and the wiring used for the dc circuit. The marked point between 15 and 20 A/ph of dc injection was another interesting point in the transformer saturation. This was suspected to be the start of deep saturation of the transformer.

ii. Saturation point check using the McLyman method

McLyman [98] takes a different approach at identifying the saturation of a transformer. The McLyman saturation rule states that saturation begins when the current $I_{peak} = 2I_{average}$ [98]. The change in the peak and average current values of the magnetizing current under dc can be seen in Figure 6.3. The Yokogawa WT1800 power analyzer records the average current as I_{rmn}, which is the rectified mean value of the waveform calibrated to the waveform true rms, using the following equation (6.1):

$$I_{rmn} = \frac{\pi}{2\sqrt{2}} \frac{1}{T} \int_0^T |f(t)| dt \tag{6.1}$$

Equation (6.1) rectifies the period (T) of the signal to determine its average (I_{rmn}), and then applies a constant value. The value of this constant was used to compute the true rms value from the input signal.

The I_{rmn} value was the same as the I_{dc} average value, except for dc0.25 and dc0.5. The very low values of dc had minimal impacts on the transformer. The startling finding is that the transformer remains unsaturated even at dc values as high as 34 A/phase, according to the McLyman rule. This appears to be a misleading result, with the transformer magnetizing current total harmonic distortion peaking up to about 70%. Some of the air search coils started indicating leakage flux at about 13 A/phase of dc, which clearly shows that the transformer was already in the saturation region. The McLyman rule seemed to be limited in identifying this. The reason for this result lies in the way in which the 3p3L transformer saturates under dc as opposed to other transformer models. A similarly rated 3p5L transformer was also tested and it was noticed that its part-wave saturation is different from the 3p3L as shown in Figure 6.1. Part-wave saturation in a 3p5L transformer involves magnetizing current spikes in one half of the wave cycle, while the waveform remains un-shifted and centered along the horizontal axis. Part-wave saturation in the 3p3L involves a shift in the magnetizing current waveform by the dc value. The McLyman saturation rule might hold for other transformer models but not for the 3p3L model. For it to hold for the 3p3L, the vertical shift in the waveform must be accounted for.

Figure 6.3 below shows the 3p3L transformer's magnetizing current positive peak, average and negative peak graphs. It is clear from Figure 6.3 that the 3p3L magnetizing current positive peak increases at a much faster rate compared to its average value and its negative peak. This faster increase can be seen from point A (0.12 A/ph dc) to point B (4 A/ph dc). There appears to be a greater increase in the positive peak beyond point B. Figure 6.3 also shows the non-linearity in the

transformer saturation. This nonlinearity can present some challenges when predicting the way a transformer would behave at a certain level of dc.

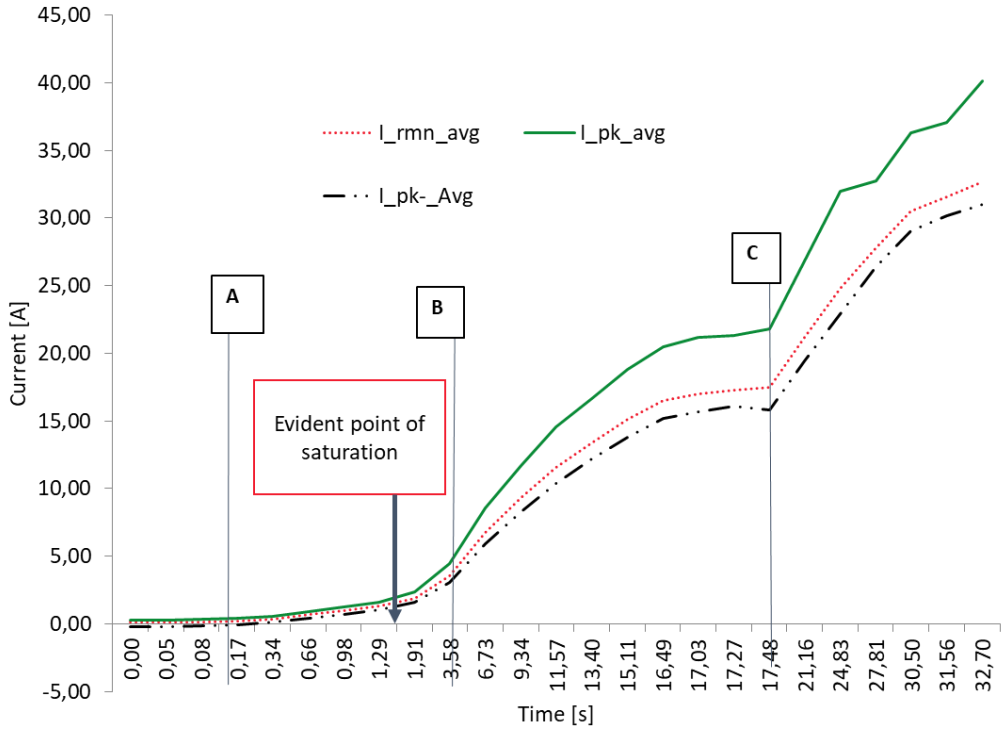

Figure 6.3: 3p3L Transformer I_peak+, I_peak- and I_average values at varying levels of dc input

After noting its limitations for 3p3L application, the McLyman rule was then revised to fit the vertical shift in the 3p3L transformer magnetizing current under dc saturation. The revised rule says:

$$\text{Let: } I_B = I^-_{peak\_old} + I^-_{peak\_new} \tag{6.2}$$

The peak and average current values can thus be re-calculated using the set of equations below.

$$I^+_{peak\_new} = I^+_{peak\_old} - I_B \tag{6.3}$$

$$I^+_{average\_new} = I^-_{average\_old} - I_B \tag{6.4}$$

Equations (6.2) – (6.4) were used in a spreadsheet to re-calculate the new values from the old values that were supplied by the Yokogawa WT1800 power analyzer raw data. The new check for saturation adopted from McLyman is as follows:

$$\text{For: } I^+_{peak\_new} < 2 \times I^-_{average\_new}\text{: Not Saturated} \tag{6.5}$$

$$\text{For: } I^+_{peak\_new} = 2 \times I^-_{average\_new}\text{: Saturation begins} \tag{6.6}$$

$$\text{For: } I^{+}_{peak\_new} > 2 \times I^{-}_{average\_new}\text{: Saturated} \tag{6.7}$$

The above set of equations can be summarized as:

$$\text{For: } (I^{+}_{peak\_new} - 2 \times I^{-}_{average\_new}) < 0\text{: Not Saturated} \tag{6.8}$$

$$\text{For: } (I^{+}_{peak\_new} - 2 \times I^{-}_{average_{new}}) > 0\text{: Saturated} \tag{6.9}$$

The revised saturation check equations were used to identify when the transformer saturated under dc. The results are shown in Figure 6.4 which gives a clear distinction between the transformer's saturated state and non-saturated state.

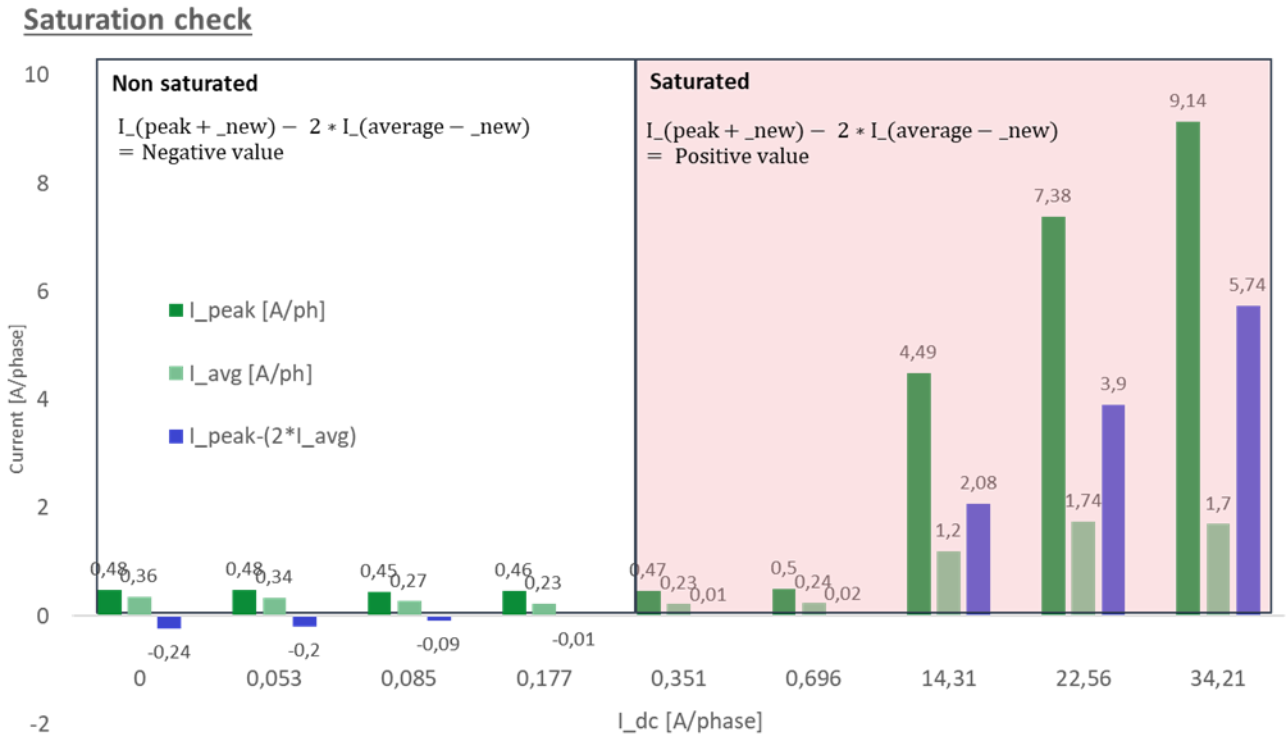

Figure 6.4: TuT saturation check under dc using the revised McLyman rule

As seen on Figure 6.4, the results from the revised McLyman method show that the transformer starts saturating at around 0.3 A/phase of dc (1.3 % of rated current). This result is evidently different from the original McLyman [51] method applied previously.

Following this assessment, it can be concluded that the transformer begins to saturate at 0.3 A/phase of dc injection, as the presence of dc increases the magnetizing current. The effect of saturation on the magnetizing current is more evident at around 1.8 A/ph, which is the same point for both the

revised McLyman rule and the Price method used earlier. Further assessments were done to solidify this finding.

6.2.3 Saturation due to current Total Harmonic Distortion

The current total harmonic distortion (THDi) is also one of the major consequences of dc injection into a transformer. The TuT THDi data was analyzed by plotting the THDi for each phase over a range of dc injection (Figure 6.5). The results show that the 20% THDi limit in IEEE std 519 [99] is reached with a dc injection of about 0.9 A/ph (0.04 p.u of the transformer's rated current). The transformer evidently saturates as the amount of THDi increases. There appears to be a small dip at point A of Figure 6.5, with a dc input of about 6.1 A/ph (0.27 p.u). A similar THDi dip has been noted in literature [29]. The dip appears to be a sign of the transformer getting into deep saturation. The THDi appears to be approaching a constant value after the dip, indicating that the transformer is at a constantly saturated state (deep saturation). The initial sharp rise in the THDi was identified in prior studies to occur when the dc bias drives the transformer to the knee-point region of its B-H curve [52], which is caused by the relatively low fundamental harmonic component at the start of saturation. The peak is soon followed by the dip. The phase B THDi appears to be smaller than those of phases A and C. In the preceding experiments, the magnitude of the magnetizing current for phase B was smaller due to the larger magnetic path length experienced by the flux generated in the mid-limb. The small magnetizing current led to the smaller THDi experienced in that phase. Further analysis was conducted to investigate the individual harmonic composition of the transformer excitation current under dc at no load, as discussed in the following section.

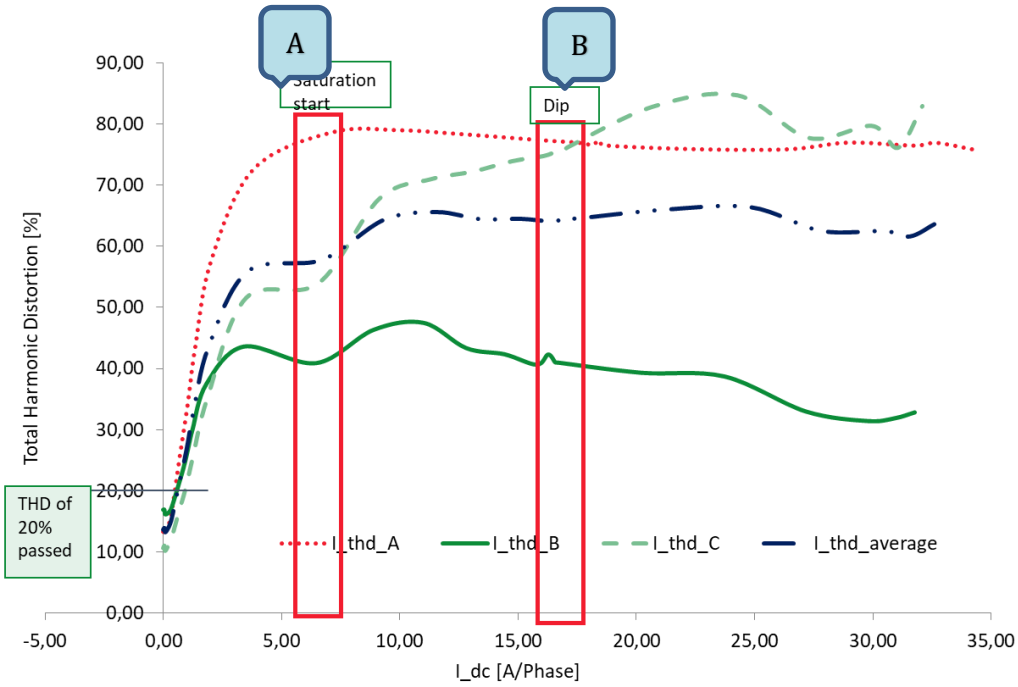

Figure 6.5: 3p3L Input current total harmonic distortion (THD) under dc with no load

6.2.4 Saturation from harmonic components

The transformer harmonic components were analyzed under no load with increasing dc levels. The results for up to the 10th order harmonic are shown in Figure 6.6. The figure shows only the harmonic components of the red (A) phase, as all the three phases appeared to behave in a similar manner. Recordings were made up to the 10th order harmonics due to the negligible values of higher order harmonics.

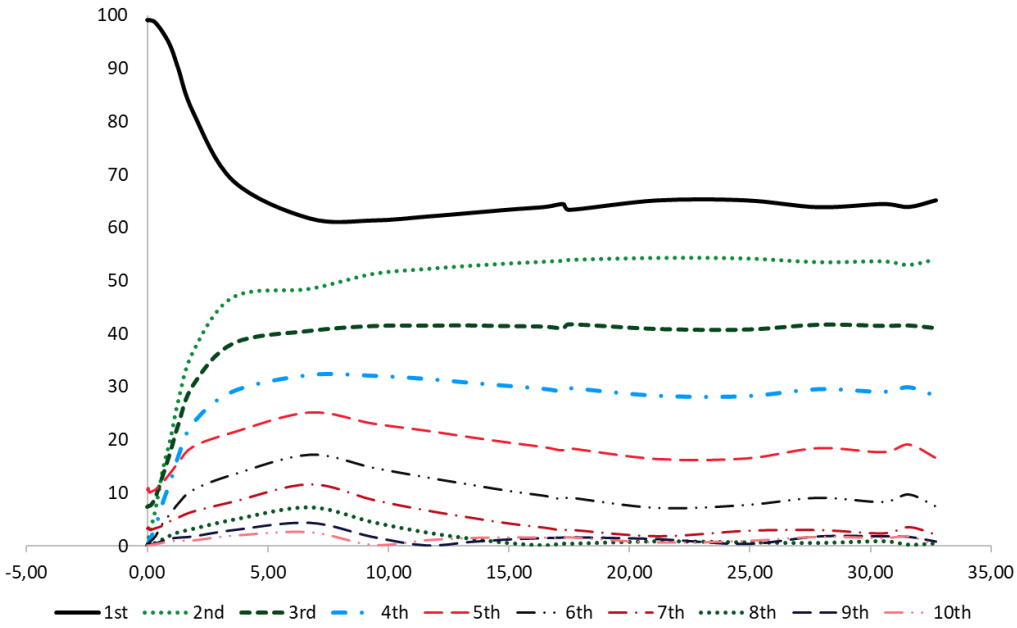

Figure 6.6: 3p3L Transformer harmonic components under dc

The most obvious trend is the increase in the harmonic order magnitude (except the fundamental), with increasing dc, while the fundamental harmonic decreases. There also appears to be a dominance of odd (3rd, 5th and 7th) and fundamental components at lower dc values (below 0.17 A/phase). For 3p3L transformers, the magneto-motive force (mmf) of the triplen harmonics is in the same direction and in phase, hence the trajectory of the triplen harmonic flux is extended to outside of the core [100]. Their magnitude is however reduced by the high reluctance path, which is why the 3rd harmonic appears to be smaller than the 5th harmonic even with no dc present. The even harmonics start emerging at 0.17 A/ph. The fundamental component starts dropping significantly beyond injection of 0.34 A/phase. The fundamental harmonic drops from 99% to stay constant at around 60% for much higher dc values.

Another significantly obvious trend is that all harmonic orders increase to a maximum at 6.73 A/ph of dc, after which there is a decline in each harmonic order magnitude with increasing dc. The decline levels off to a constant value at about 17 A/phase of dc. The rate of decline appears to increase with harmonic order. Higher harmonic orders seem to diminish at higher dc bias values. Each harmonic order appears to have about two distinct peak values associated with it. The 2nd and 3rd harmonic orders have two peaks which appear on either side of the flat regions, whereas the flat region does not exist for higher harmonic orders. This trend was specially analyzed and reported by McLyman [52] . It was identified that there appears to be a 90° difference between the two maximums, which

becomes more pronounced with increasing harmonic order. This is the reason why higher harmonic orders reach their first peak faster (at lower dc values) than lower harmonic orders.

The results appear to be very similar to the analysis by Price [52], even though the transformer used in that particular study was a single-phase three-limb transformer. The rise of even and odd harmonics appears to be similar across the harmonic spectrum. Odd harmonics are caused by the distortion in the transformer magnetizing current, while the even harmonics are caused by the dc component [50] . It thus makes sense for their trends to be similar, as the rising dc bias level leads to a similar distortion increase in the magnetizing current.

6.2.5 Non-active power measurements

Non-active power is also viewed as one of the indicators of saturation in power systems. This was also analyzed under no load with increasing dc by making use of the conventional IEEE method and the General Power Theory (GPT). The Yokogawa WT1800 power analyzer used for measurements complies with standards IEC76-1(1976) and IEC76-1(1993) [101, 102]. The GPT duly accounts for distortions and imbalance in the calculation of non-active power, as opposed to the conventional measurement meter. Most of the present instrumentation makes use of IEC methods hence this is compared to the GPT method. It is clear from Figure 6.7 that the transformer's non-active power computed using the GPT is much higher than that computed with the IEEE method. The difference between the two trends (GPT vs conventional) widens with increasing dc, accounting for the increasing magnitude of distortions. Previous studies have identified the non-active power to follow the fundamental current component [66]. This dip evident before 5 A/ph of dc seems to be associated with the inception of deep saturation. The dip seems to be common in Figure 6.2 to Figure 6.7. Saturation before this point is only preliminary, hence most of the flux remains trapped within the core. The dip point appears when the flux begins to find alternative paths to flow outside of the core, hence the deep saturation inception point is met with a minor drop in reluctance as the flux navigates a new path.

With respect to the non-active power taken by the transformer, the vastly reported linear relationship between the non-active power taken up by the transformer and dc current soon takes shape after the minor dip.

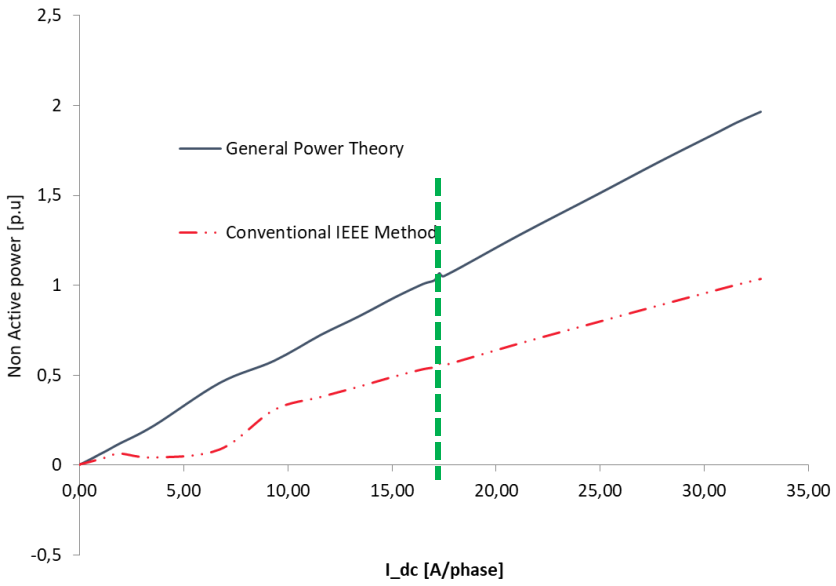

Figure 6.7: non-active power taken up by the TuT under DC no load

6.3 DC Tests with Load

In the previous section, the unloaded transformer saturation under dc was assessed using various measures. This provided some good insight on the critical dc values associated with saturation. This section seeks to outline the influence of loading the transformer under exposure to dc, hence the focus is placed on a few tests that are associated with the different types of load. Tests were conducted to assess changes in Total Harmonic Distortions (THD), Total Demand Distortions (TDD), harmonic components and non-active power as elaborated further below. The different loads used include resistive loads, inductive loads, and a combination of the two. Arbitrary loads were selected based on availability and suitability for this experiment, while maintaining uniformity in the size of the loads used.

6.3.1 TuT Total Harmonic Distortion results under dc excitation

The Total Harmonic Distortion (THD) was analyzed under various load conditions under dc excitation. The results for a resistive load of 5.5 kW are shown in Figure 6.8, where there is a clear distinction between the current THD and the voltage THD. The transformer V_in, I_in THD values were measured at the primary side of the transformer while the V_out and i_out THD values were measured at the secondary side.

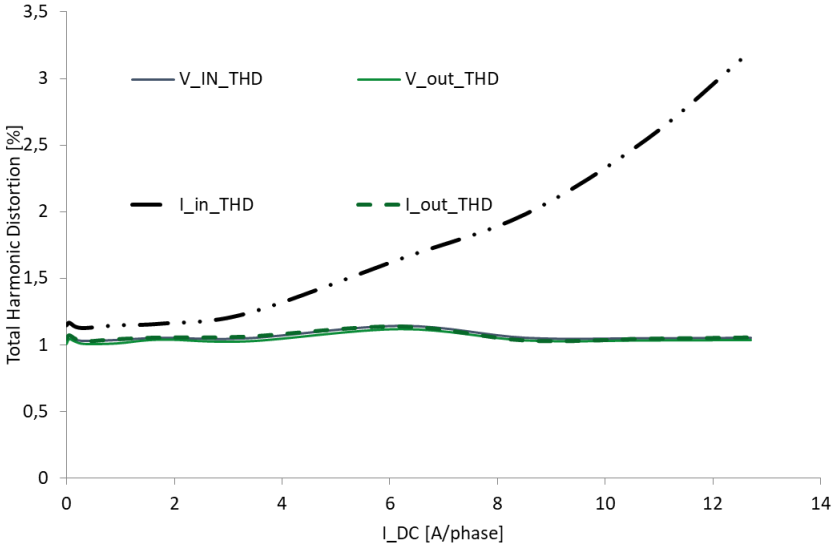

Figure 6.8: Total Harmonic Distortion under dc for 5.5 kW resistive load

It can be noted from Figure 6.8 that the voltage and secondary current THD remain constant for a range of dc values. Much higher dc values could not be investigated due to the limited rms current that could be recorded by the measurement instrument. It can be noted that the 5% THDv limit was not surpassed for the range of dc applied [103] . The primary (input) current THD (THDi) appears to increase non-linearly with increasing dc. This increase is due to the increased amount of magnetizing current drawn by the transformer with more dc being injected. The transformer thus acts as a load itself, with an increased amount of non-active power intake. The amount of current flowing into the load remains constant as the load does not change.

6.3.2 Total Demand Distortion results under dc excitation

The Total Demand Distortion (TDD) is regarded as a more realistic way to monitor distortion on the load side. The TDD is expressed as a function of the rated load current. The TDD (in and out) of the transformer with varying dc injection and a 5.5kW resistive load are shown in Figure 6.9.

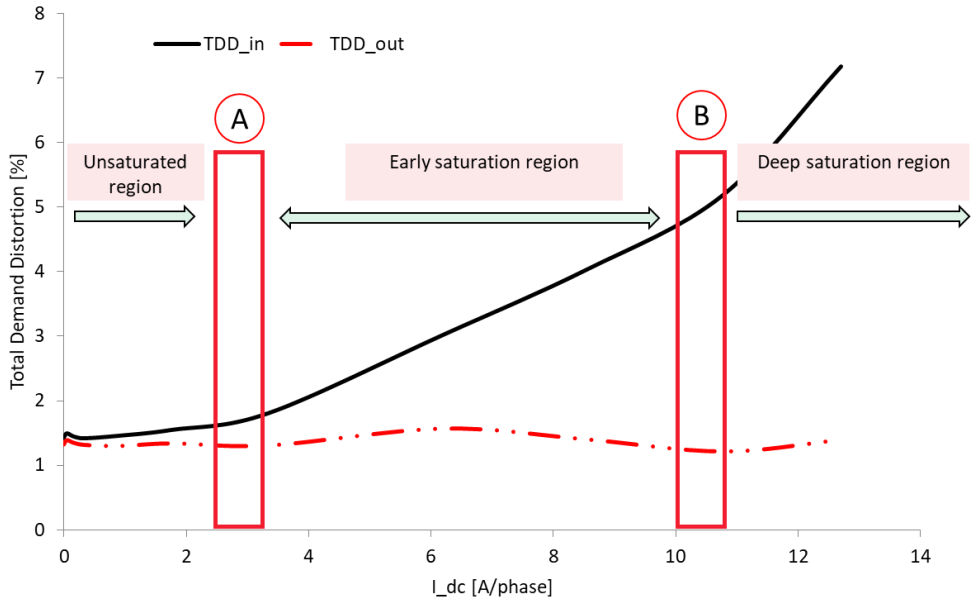

Figure 6.9: Transformer Total Demand Distortion (TDD) for a resistive load of about 5.5 kW under dc

The Total Demand Distortion (TDD) of the transformer appears to be constant for lower dc values, up to around point A (3.53 A/ph dc which is 15% of rated current) in Figure 6.9. A somewhat linear behavior appears in the region between A and B (10.8 A/ph dc which is 48% of rated current) signaling a region of saturation as TDD increases, after which the TDD appears to increase at a much faster rate with more dc being applied. The transformer is deemed to be entering a deep saturated region. A similar behavior was noticed with the use of an inductive load and the combination of an inductive and resistive load. The B point is also somewhat the same for all three load cases. For a given load type, the calculated TDD values appear to be generally higher than the THDi values, for both primary and secondary currents. The TDD uses the load current as a denominator, hence showing the level of distortion seen from the load end. Previous studies [29, 33] have recorded a linear relationship between the TDD and dc current. The type of source used is very key to the computation of the TDD. Weak sources tend to lead to a greater distortion as they possess a much higher demand current relative to their rated current [100]. The reverse is true for stiff sources.

6.3.3 Harmonic components

The individual harmonic components were explored under loaded conditions. The results are shown in Figure 6.10 for the case of a 5.5 kW resistive load with increasing dc.

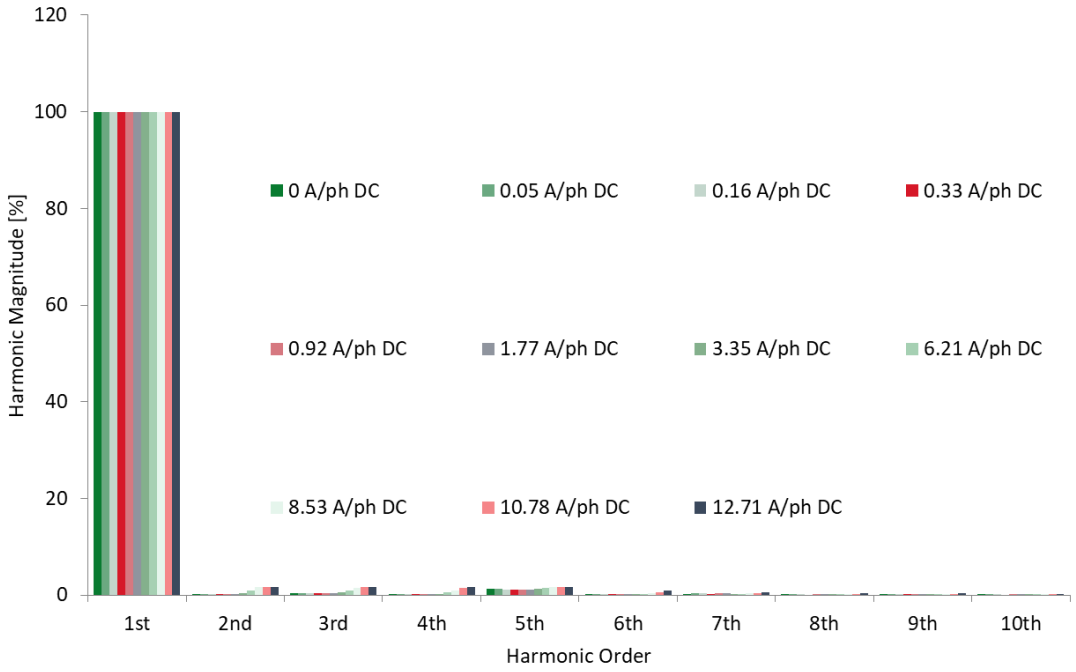

Figure 6.10: 3p3L transformer load current harmonic components for 5.5 kW resistive load

The harmonic component results (Figure 6.10) show the presence of only the 5th order harmonic component from no dc. Such presence of 5th order harmonics has been recorded for a 4.5 kVA transformer with different nonlinear loads [104]. A similar dominance of 5th order harmonics was recorded for the case of an inductive load and a combination of an inductive and a resistive load. The inductive load however had very minimal amounts of low order even and odd harmonic. The 5th order harmonic component has been found to largely contribute towards the increase in transformer losses. This harmonic order remains constant for dc values up to about 6 A/ph, which is the same point where other low order harmonics (2nd, 3rd and 4th) begin to appear (Figure 6.13). A study by Zynal and Ala'a [105] showed that the application of a 5th order harmonic filter reduced the percentage loss increase from 13.26% to 5.04%.

6.3.4 Non-active power drawn by the transformer

The amount of non-active power absorbed by the transformer was measured under varying dc excitation and for various loads. The results of this experiment are shown in Figure 6.11. Generally, there is a linear increase in non-active power absorbed by the transformer with increasing dc excitation.

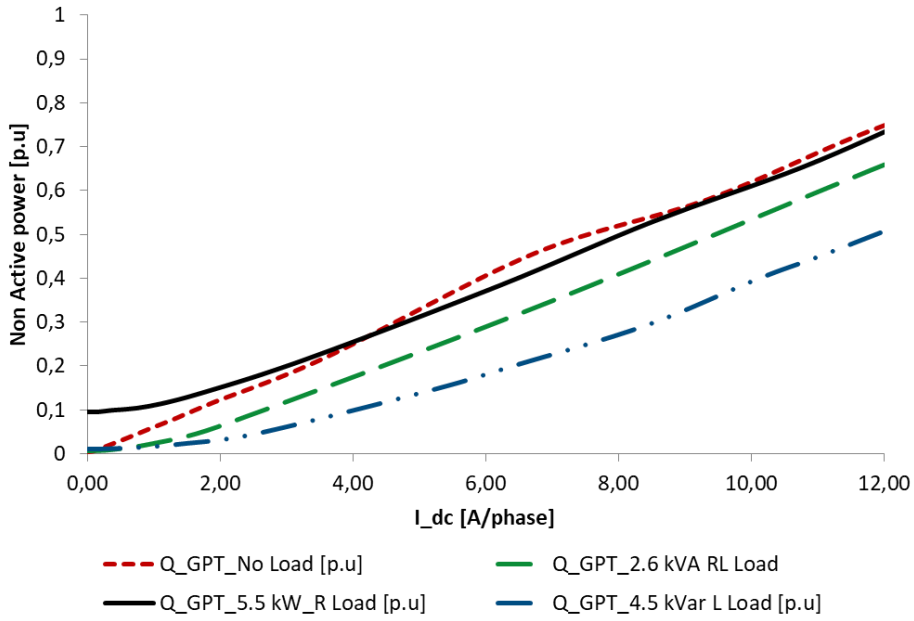

Figure 6.11: non-active power taken up by the transformer under no load and various load conditions

As can be seen from Figure 6.11, the amount of reactive power taken up by the transformer at no load is similar to when a reactive load alone is connected. The lowest amount of reactive power is taken when a reactive load is connected. The reason for this is that when an inductive load is connected, it also takes up a certain amount of reactive power to itself, whereas when there is no inductive load, all the reactive power is taken up by the magnetizing branch of the transformer. This is the reason a combination of inductive and resistive loads sits between the two extremes (resistive load vs inductive load). This is also proven by the fact that when no load is connected, the transformer takes up similar amounts of reactive power as when a resistive load is connected.

6.4 Other DC Tests

Other dc tests were conducted to build further understanding of the transformer's response to dc under various cases.

6.4.1 Transformer winding reconfiguration under dc excitation

Three-phase transformers can be configured in different ways. Different configurations offer different advantages for power system operators. However, these configurations impact the paths which are taken by different harmonic components [106]. The transformer primary and secondary winding configuration was changed from a star-star to a star-delta configuration for further dc testing to analyze the impact this has on the generation of harmonics. For this analysis, THDi and THDv values were measured at different levels of dc injection. The results for this experiment are

shown in Figure 6.12. As in section 6.3.1, there is an increase in THDi and THDv as the dc excitation level increases. THDv is not shown on this figure since it has previously been indicated that dc has minimal effects on its magnitudes.

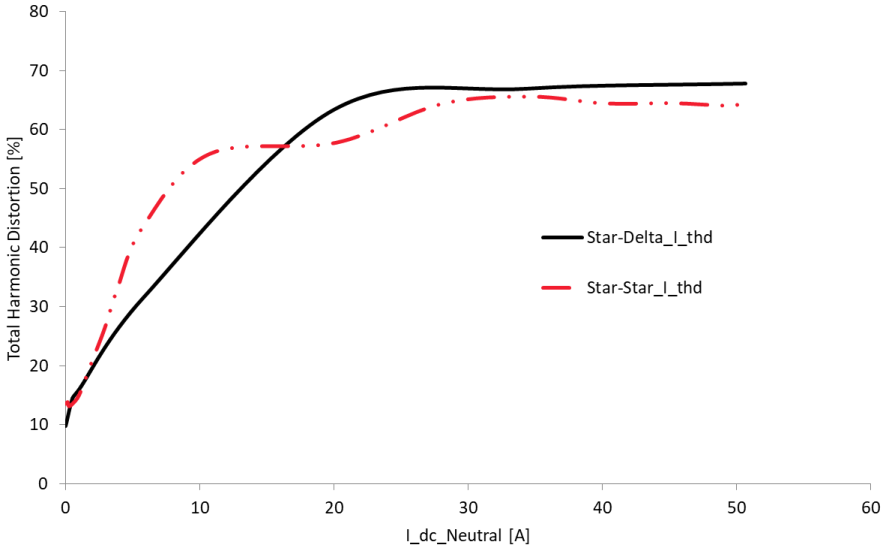

Figure 6.12: 3p3L Transformer THD for when configured in a star-star and a star-delta configuration

The primary THDi appears to be affected by the reconfiguration both at low dc and high dc values. The recorded THDi appears to be lower for the star-delta connected transformer at low dc values, while this changes at about 16 A dc [5.5 A/phase]. From that point onwards, the star-delta connected transformer THD is higher than the star-star connected transformer. These differences are largely due to the content of the harmonic orders, which affect the THD. The largest difference in the THDi measured for the two configurations was around 12% (at around 3A/phase dc). Figure 6.13 shows the individual harmonic components for the star-delta connected transformer showing an increase in harmonic order magnitude with increasing dc.

One of the noticeable trends from Figure 6.13 is the decreasing magnitude of the fundamental component with increasing dc, while the reverse is true for all other harmonic orders. At lower dc values (below 6 A), there is a large dominance of odd harmonics. The trend of decreasing harmonic magnitude with increasing order becomes very clear once the 6 A dc mark is reached. For lower dc values, the system is dominated by the 3rd order harmonic component as the delta-connected secondary provides a path for 3rd harmonic components of the magnetizing current. This case is like the star-star connection, hence the minimal differences between the THDi values and individual harmonic components profile. The minimized presence of the 3rd harmonic components in the

excitation current is because of the ungrounded neutral; this causes the 5th harmonic to be dominant at low dc values. These results are consistent with those obtained in a comparative analysis of the star-star and the star-delta configurations [107].

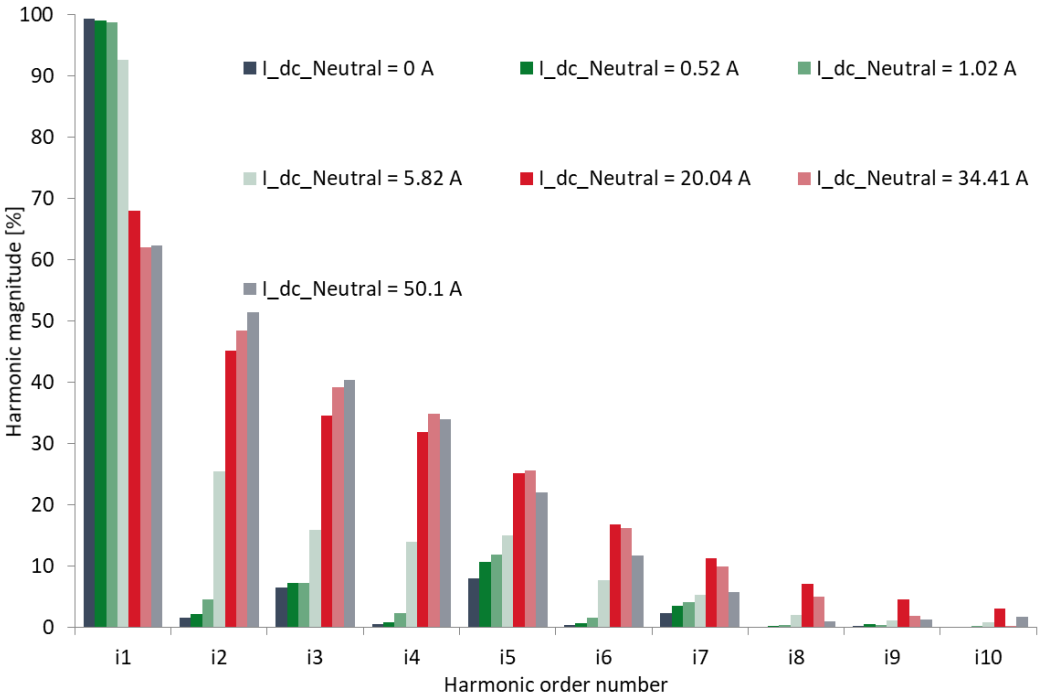

Figure 6.13: Harmonic components for when configured in a star-star and a star-delta configuration

6.4.2 Open Phase Test

To further investigate the behavior of the 3p3L transformer against other core types, the transformer was tested with one phase open. The transformer was configured in a Y-Y (star-star) configuration under no load. The open phase case for the 3p3L is compared to the 3p5L. The results in Figure 6.14 show that with one phase open, the 3p3L transformer behaves similarly to the 3p5L transformer. In this case, the zero-sequence flux now has a return path within the transformer. This result shows that a dc excited transformer with a failing phase can suffer from severe distortions. It is worth emphasizing that while 3p3L transformers have a greater GICs withstand capability, the loss of a phase coupled with GICs significantly increases magnetizing current ($I_{\_mag}$) and most likely non-active power absorption.

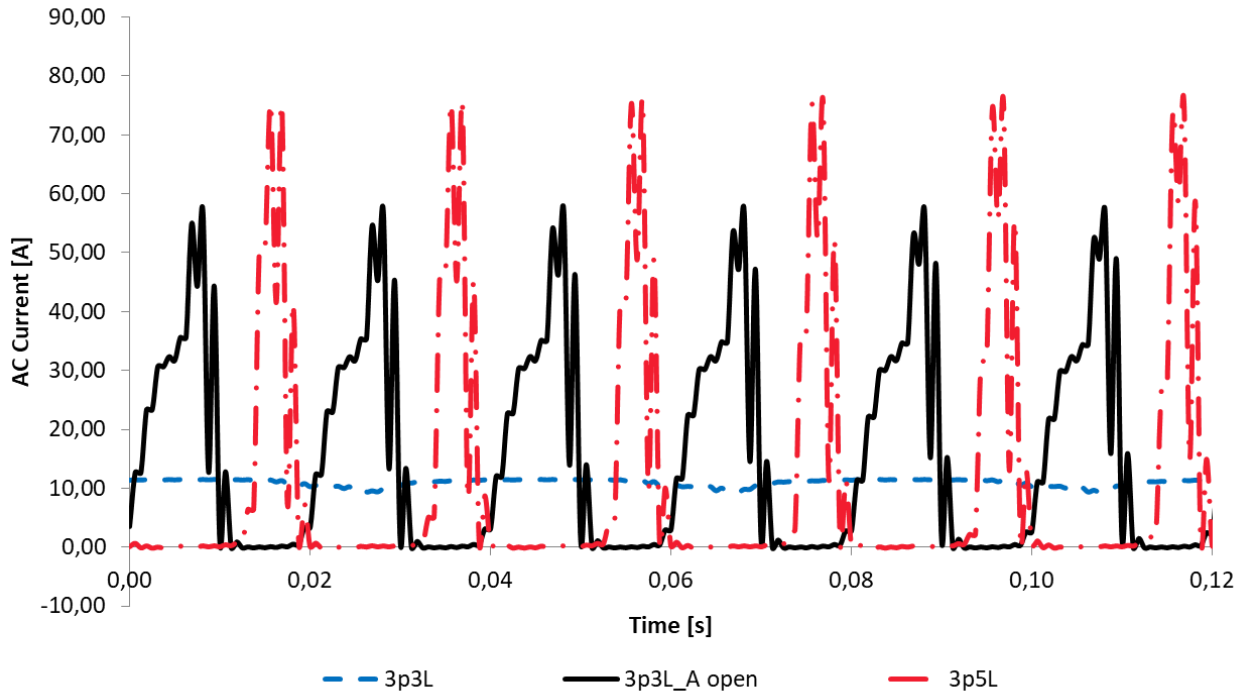

Figure 6.14: Magnetizing current waveforms at 30 A dc

6.4.3 Transformer time response

The time response of the transformer was also monitored under dc excitation. This was done by capturing the excitation current waveforms using the Yokogawa WT1800 power analyzer. Instantaneous current waveform values were stored from a few milliseconds before switching on the dc source for the duration of one (1) second. Figure 6.15 shows an example of such excitation current waveform when 6.74 A/phase dc was injected, with a settling time of 0.325 s. The waveform duration was shortened to between 0.75 to 0.95 s to improve readability. The time response was noted as the time from when the dc source was switched on until the new average value of the waveform was equal to the dc value.

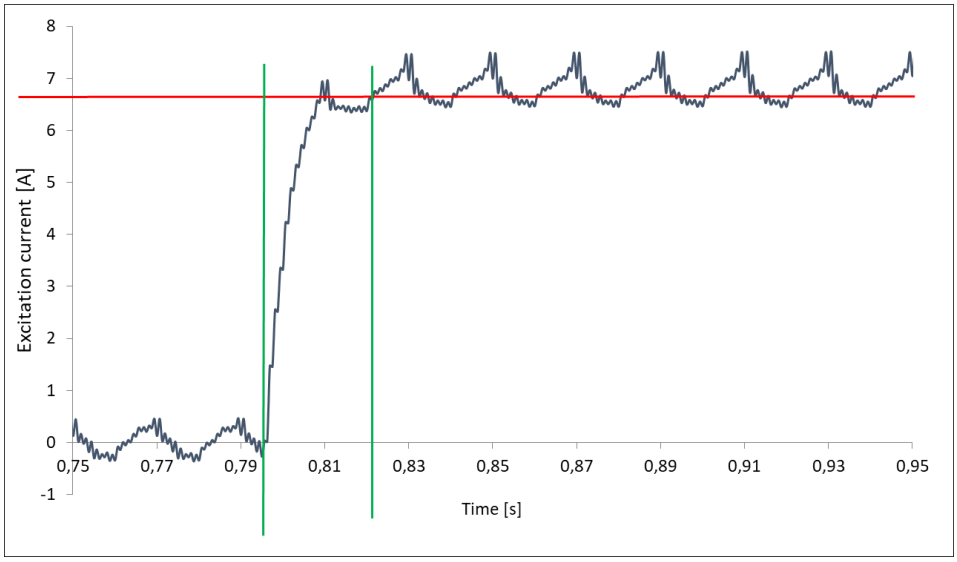

Figure 6.15: Exciting current waveform for dc current injection of 6.74 A/phase

The above method was applied for the full range of dc values tested, with the results shown in Figure 6.16. Care was taken to demagnetize the core (by turning the input voltage all the way to zero and switching the system off for a few minutes) and resting it for a few minutes before introducing a new dc value. This was done to avoid different dc values affecting each other due to their sustained effects on the core because of remanence flux.

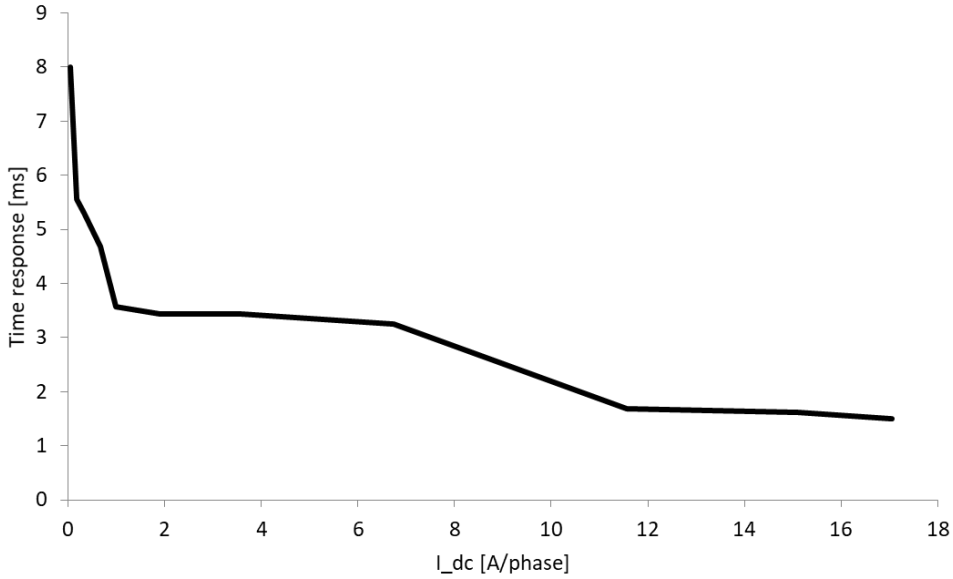

Figure 6.16: 3p3L Transformer time response under dc excitation

The results show the expected trend of decreasing time response with increasing dc level. A very steep decline is noted for the very low dc injection (around 0.25 A in the neutral), after which the gradient of the graph begins to drop. The response time appears to be approaching a constant value for much higher values of dc excitation. The drop in the transformer time response is due to the constantly changing core material damping coefficient, as ($\tau = R_m L_m$; R_m = core loss resistance; L_m: magnetizing inductance), which drops with increasing dc. The different noticeable steps on the graph are associated with the state of saturation of the transformer. The rate of decay flattens as the transformer gets into deep saturation, approaching air-core inductance, which is a constant value. The time response can thus be expected to remain constant in a deeply saturated transformer.

6.5 Chapter Summary

An in-depth discussion on the laboratory results was presented in this chapter. The testing focussed on identifying the critical levels of dc that are associated with the different levels of saturation of the TuT. This discussion is largely based on the test results to be used as a benchmark for the development of the FEM models. Discussions were made by analysing the experimental and calculated results, comparing the results to similar findings in literature where possible. Further insight was gained from other tests that were viewed to provide further understanding of the transformer response to dc.

7. FEM Model Development

This chapter discusses the different approaches taken to develop an optimal Finite Element Matrix (FEM) model which can closely replicate the laboratory transformer behavior. The software package that was used for this investigation is ANSYS EM v18.2. It is a high-performance interactive software package, which uses Finite Element Analysis (FEA) to solve 3D electric, magnetostatics, eddy current and transient problems [108], making use of magnetostatics and transients solutions.

The framework for developing the FEM model is outlined in Figure 7.1. The framework shows the strategic approach taken, starting from the preparatory work done to set up FEM. A 2-dimensional (2D) model was then developed, leading up to a solid 3D model to be used as a base case. Various explorations are carried out to provide in-depth structural details which assist towards the development of a refined FEM model.

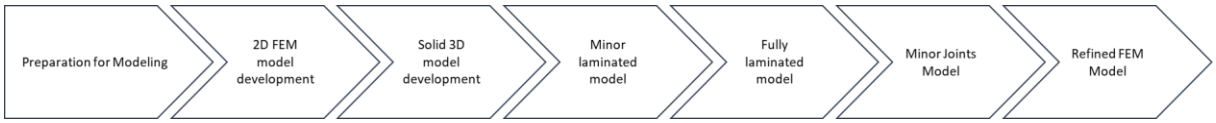

Figure 7.1: Framework for FEM model development

To set-off the simulation phase, some preparatory work had to be done to ensure readiness for simulations.

7.1 Preparations for Simulation

A big part of the preparatory work was focused on clarifying the link between the laboratory tests, and how the results from the testing phase will be used for the FEM simulations. This is discussed further in the following subsection.

7.1.1 Laboratory Results to give input to FEM model

As indicated previously, the FEM models will be developed using the laboratory results as a benchmark. The performance of the model will be compared to the laboratory measured results of the physical 3p3L transformer using the key elements associated with the transformer response to dc, which include the no load input current, magnetizing current, excitation voltage, non-active power, THD and flux density distribution. Such parameters will include the ones shown in the laboratory results summary in Table 7.1. These results speak to the behavior of the core in carrying out magnetic induction and efficiency in transforming the primary voltage to the output voltage. Further basis of comparison will be the search coil values used to capture the magnetic flux density.

Table 7.1: Laboratory test results to be used as basis of comparison for FEM model development

Parameter	Phase A	Phase B	Phase C
Input Current [A]	0.14	0.11	0.15
Input Voltage [V]	158.74	158.53	158.52
Output Voltage [V]	158.71	158.54	158.58
Input Active Power [W]	14.06	7.80	21.86
Input Reactive Power [Var]	17.39	15.60	21.77
Input Apparent Power [VA]	22.36	17.44	23.70
Current THD [%]	1.11	1.21	1.02

7.1.2 FEM model excitations

One of the key elements of FEM involved defining excitations (field sources) and boundary conditions. The inner windings were voltage excited with defined voltage equations, while the outer windings were current excited. All winding terminals were defined to be stranded, with 140 turns per winding, as per the physical transformer. Voltage excitations define the difference in voltage across two faces of the conductor, while current excitations define the total current (amp-turns) through a loop cross-section, [108]. To be able to minimize the magnitude of inrush currents, the transformer windings were excited with slow rising voltage equations as shown below, with phase differences applied:

$$Phase\ A: V = V_{peak}\left(1 - e^{-50\times time}\right)\cos\left(2\pi \times 50 \times time\right) \quad (7.1)$$

$$Phase\ B: V = V_{peak}\left(1 - e^{-50\times time}\right)\cos\left(2\pi \times 50 \times time - \frac{2\pi}{3}\right) \quad (7.2)$$

$$Phase\ C: V = V_{peak}\left(1 - e^{-50\times time}\right)\cos\left(2\pi \times 50 \times time + \frac{2\pi}{3}\right) \quad (7.3)$$

where: *time:* is an intrinsically defined Ansys variable for time.

7.2 2D Model

A 2D model was then developed and analyzed as a starting point of the FEM model development. This was to allow for a good understanding of how the model runs at the de-rated voltage of 160 V/ph rms and compare its results with the laboratory measured results at the same voltage. Another model was run at 220 V/ph rms for a better understanding of the effects of saturation on the model.

7.2.1 *Approach*

The most common way of developing a 2D model in ANSYS is through converting a 3D model to a 2D model, which is the approach taken in this research. A 3D solid model was thus developed first (but this will be analyzed under the 3D section of the thesis). When converting a 3D model to a 2D model, a lot of structural information can be lost in the process. The physical 3p3L transformer consists of a stepped core model, which cannot be accounted for in the case of a 2D model. A 2D model treats the core as a rectangular shape, with a certain depth. The model depth must be estimated for stepped core geometries. The method used here was based on the volume of each core step section on the physical transformer. The sum of those volumes was then divided by the FEM 2D model width and the height of the selected section. In this case, the left limb was selected as shown in Figure 7.2. The model was created with 1 mm core joints at the T and corner joints.

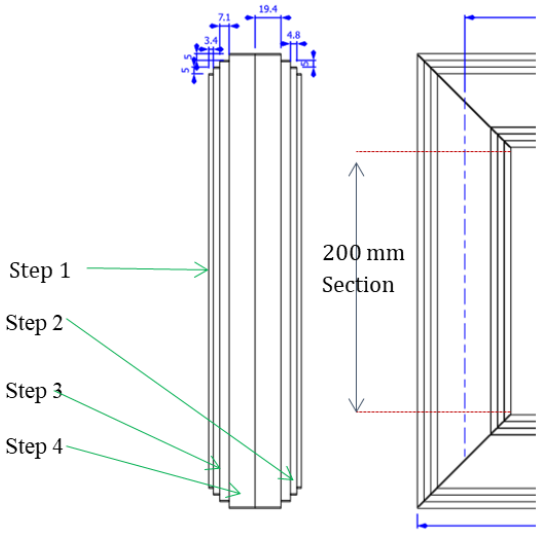

Figure 7.2: TuT 2D model depth computation

The volumes from the different steps were thus:

$V_1 = (200 \times 40 \times 3.4) \times 2 = 54000\ mm^3$
$V_2 = (200 \times 50 \times 4.8) \times 2 = 96000\ mm^3$
$V_3 = (200 \times 60 \times 7.1) \times 2 = 170400\ mm^3$
$V_4 = (200 \times 70 \times 19.4) \times 2 = 543200\ mm^3$

$$V_{total} = V_1 + V_2 + V_3 + V_4 = 863600\ mm^3 \quad (7.4)$$

$$d = \frac{V_{total}}{l_{FEM} \times b_{FEM}} = \mathbf{61.69\ mm} \quad (7.5)$$

Where:

$d = FEM\ Model\ depth$

$l_{FEM} = Length\ of\ FEM\ model$ = 200 mm

$b_{FEM} = Width\ of\ FEM\ model$ = 69 mm

The final FEM 2D model is shown in Figure 7.3, which is planar, but having its depth accounted for in the software and taken into account when running the model. The model was run at the de-rated and rated voltages to assess its performance against the laboratory results.

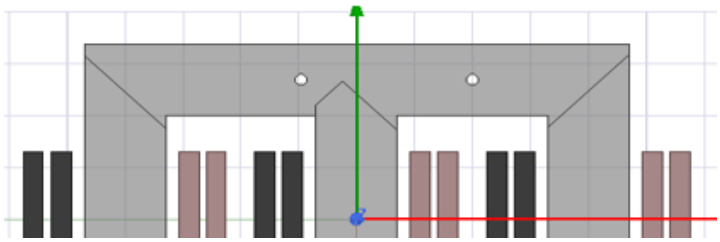

Figure 7.3: 3p3L FEM 2D model developed on Ansys Maxwell 18.2

7.2.2 2D Model Results

Table 7.2 outlines the magnetizing current results of the 2D model with the joints. The results appear to be much larger than the laboratory tested results. The orientation of the joints appears to be key in the transformer behavior in the case of the 2D model. The lack of detail makes each joint air gap to cut through the entire core section. This increases the losses in the joint region as the core flux must find ways to bridge onto the yokes from the core. The difference between the outer limbs and the inner limb is also very evident. The much smaller magnetizing current of the inner limb is due to the much larger reactance the central limb flux faces as it splits into the two top yokes.

Table 7.2: FEM 2D model Magnetizing current a 160 V/phase excitation

	Phase A	Phase B	Phase C
FEM I_mag Results [mA]	298.22	125.91	277.70
Laboratory I_mag Results [mA]	140.90	110.00	149.50
Difference [%]	+111.6	+14.5	+85.8

There appears to be some larger discrepancies between the laboratory results and the 2D FEM model of the transformer. Much of this is due to the loss of detail when building a 2D model. This prompts an exploration of the 3D FEM modelling of the transformer, applying the required amount of transformer detail.

7.3 Solid 3D Model

Following the 2D model, a 3D model was analyzed to investigate the differences between 3D and 2D models. The first 3D model developed was the solid model, initially modelled without holes and then with holes (cf. section 5.3)

7.3.1 Approach

The full transformer solid model, with its structural components was developed as shown in Figure 7.4. The core cross-sectional area was constructed to be in steps from the start. To simplify the overall simulation time, the initial models were run without the non-magnetic structural parts (i.e. tank, base plate and the frame). The structural parts are displayed on the figure for context. Exclusion of the non-magnetic structural parts greatly reduced the amount of mesh elements produced, hence the amount of equations to be solved during the simulation and the simulation time was greatly reduced.

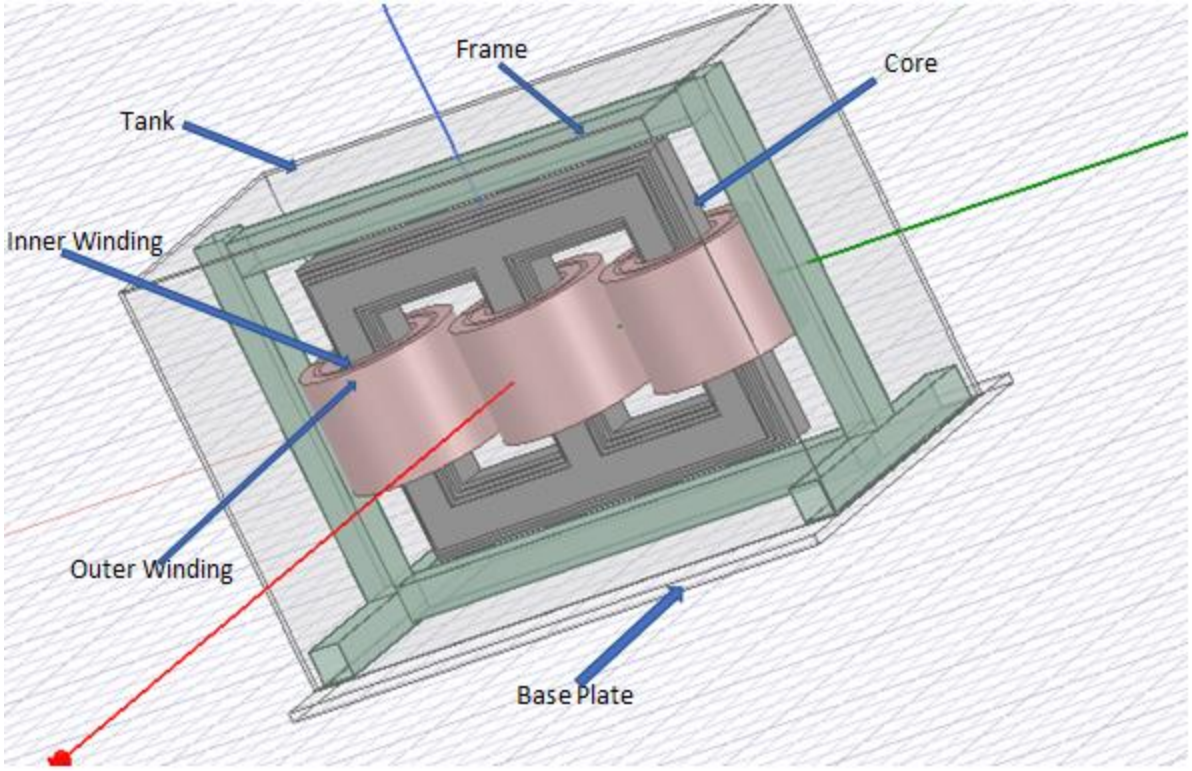

Figure 7.4: Full 3D Solid model with structural parts developed on ANSYS 18.2

7.3.2 Solid model results with no Tank

The solid 3D model results outlined in Table 7.3 show 34% less magnetizing current compared to the laboratory measured magnetizing current. The solid model is a highly efficient model with minimized core losses. Losses are minimized by the omission of the lamination detail and lack of joints.

Table 7.3: TuT 3D solid FEM model with no tank results

Parameter	Phase A	Phase B	Phase C	Average % difference from lab results [%]
Input Current [mA]	91.81	55.03	89.33	-34.00
Input Voltage [V]	159.81	159.81	159.81	+0.6..
Output Voltage [V]	159.27	159.30	159.31	+0.40
Flux Linkage [Wb]	0.51	0.50	0.50	N/A
Total Input Reactive Power [Var]	37.58			-68.60
Total Core Loss [W]	29.52			-46.000

7.3.3 Solid 3D model results with tank

The transformer came fitted with a mild steel tank and base plate. Due to its magnetic nature, the tank is often used as a return path for off-core flux, mostly for the 3p3L transformer. Thus, investigations were conducted concerning the amount of flux captured by the search coils, which was found to be very small compared to the actual core flux by a factor of about a thousand. The distribution of flux around the tank is shown in Figure 7.5.

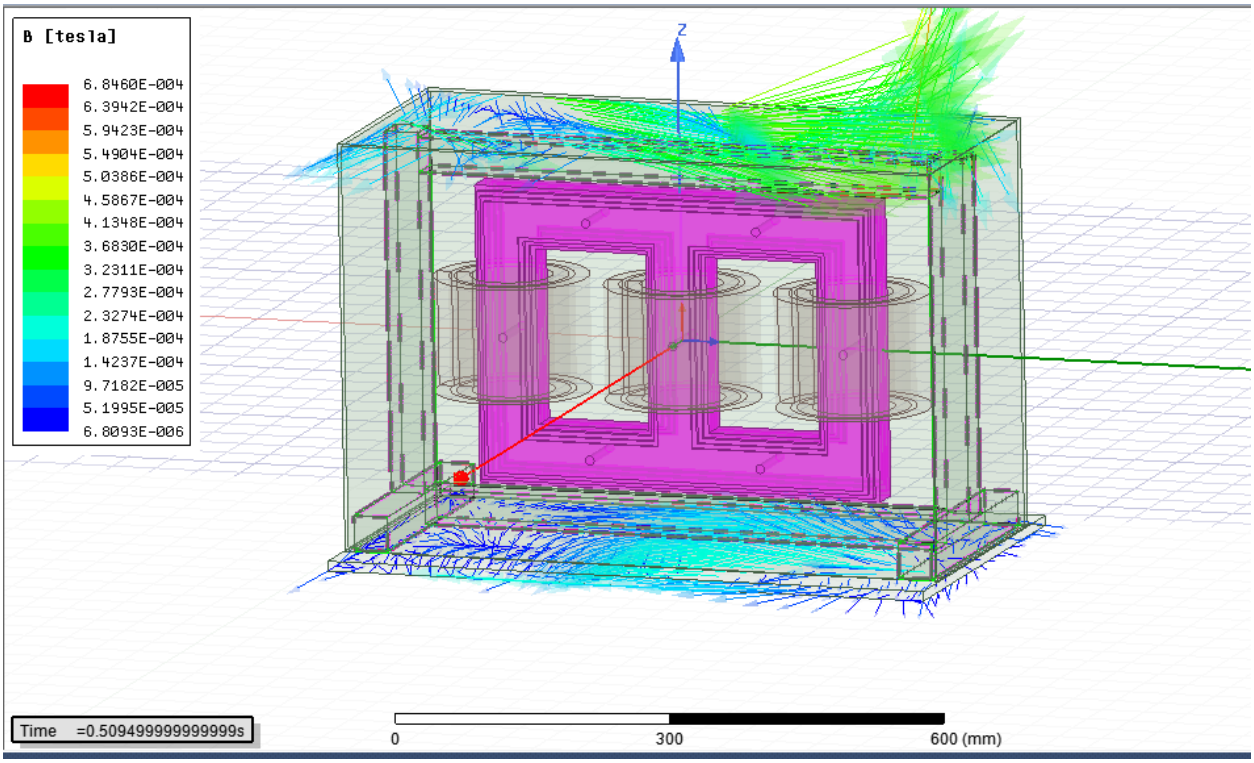

Figure 7.5: Solid 3D model tank and base plate flux

The tank flux appears to be as a result of stray flux from the windings as opposed to leakage flux from the core. This is due to the amount of air-gap space between the core and the tank. The transformer was also excited in the region of its linearity; hence no core stray flux would be expected in this case. Further evidence of this is shown by the terminal results given in Table 7.4, where the transformer magnetizing current (input current) values appear to be unaffected by the presence of the tank.

Table 7.4: 3D Solid model with tank terminal results.

Parameter	Phase A	Phase B	Phase C	Average % difference from lab results [%]
Input Current [mA]	91.99	54.68	89.39	- 34 .00
Input Voltage [V]	159.81	159.81	159.81	+0.30
Output Voltage [V]	159.28	159.30	159.31	+0.60
Flux Linkage [Wb]	0.51	0.50	0.50	N/A
Total Core Loss [W]	29.62			-46.00

A visualization of the magnetic flux density distribution in the core as per Figure 7.6, shows the behavior of the flux lines around the transformer holes. Flux lines can be seen to be deviating from their rolling direction to make their way around the hole. This shows that the transformer is operating in its linear region, with the core unsaturated. Thus, flux lines find alternative paths within the core, avoiding the high reluctance air path through the holes.

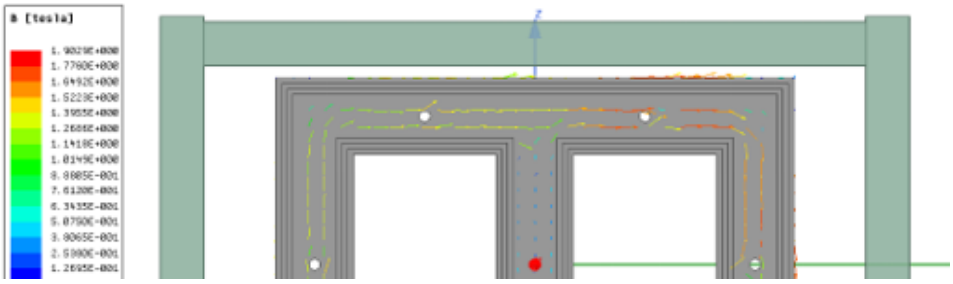

Figure 7.6: Flux lines for the 3p3L transformer at the rated voltage and the influence of the holes at the rated voltage

7.4 Laminated Model

In pursuing a detailed FEM model to increase the accuracy of the FEM results, laminations were introduced into the model at various phases as discussed in the following subsections.

7.4.1 Minor Laminations

The transformer model was further improved by introducing minor laminations to the model. Laminations were initially introduced as air gaps between the core steps as can be seen in Figure 7.7. To find the optimal laminations that closely replicate the laboratory transformer behavior, four phases of minor laminations were investigated. Mechler *et al* [96] states that due to the periodical repetitive nature of the lamination sheet patterns (which may total several hundreds of laminations),

it is not necessary to study the whole lamination package. A finite number of lamination groups can be assessed each time.

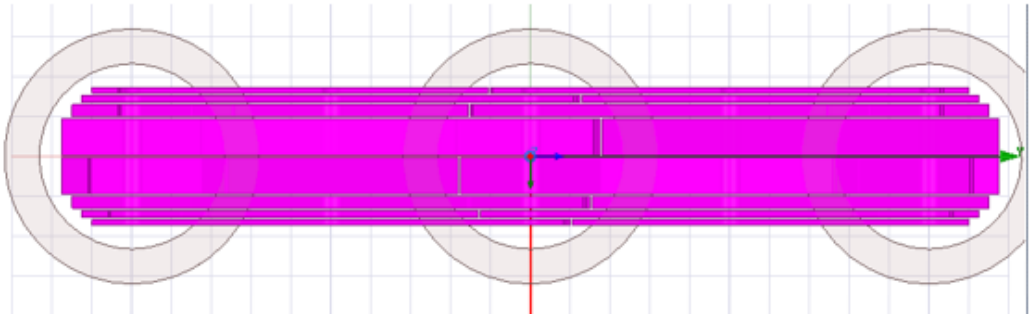

Figure 7.7: Transformer minor laminations between core steps.

i. Approach

The approach for introducing the laminations made use of the 0.96 stacking factor supplied by the manufacturer. Using the stacking factor, 4% of each core step was removed to form an air gap at the end of each step. The rest of the 96% was left as the part occupied by laminations. This approach involved four different phases of lamination as shown in Figure 7.8 with brief discussions.

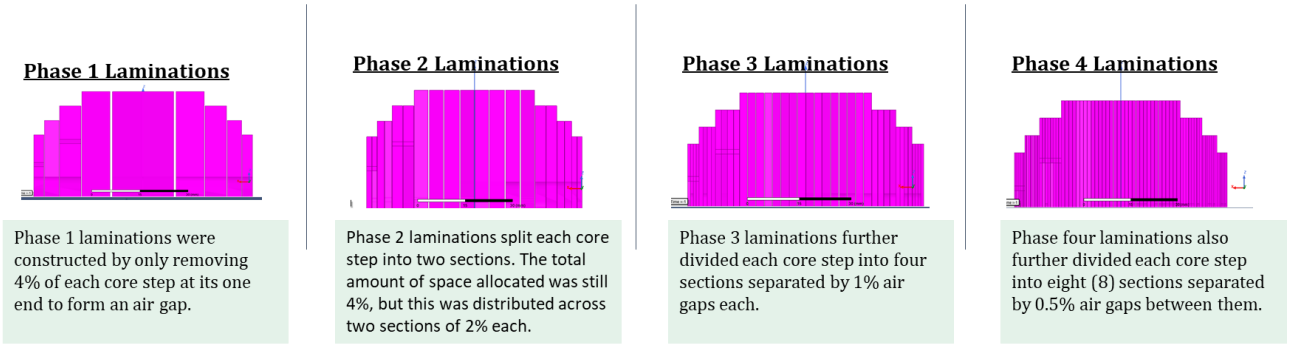

Figure 7.8: Lamination phases

ii. Minor laminations model FEM Results

The FEM results of the minor laminated model are shown in Table 7.5. Once the phase 1 laminations were introduced, it was realized that the ANSYS Maxwell software would either run out of memory or crash before reaching steady state. The values before steady state are erroneous and cannot be used as a basis for comparison. The large memory consumption and long simulation times were due to the amount of surface area introduced by the different lamination slabs. This problem would only persist further if the other lamination phases are introduced. This called for the use of symmetrical models, which could minimize the amount of structural detail and the memory requirements. To start off, half symmetry was explored with the phase 1 laminations applied.

The results from running the symmetrical model with phase 1 laminations, are displayed in Table 7.5. The results show a large 75% increase in the magnetizing current compared to the actual laboratory transformer. This is due to the space between the core laminations modelling air gaps at the core joints. These were uniform gaps which spread across the model depth. The large increase in magnetizing current ($I_{\_mag}$) was due to the isolation of laminations, which increased the losses between them. In normal transformers, adjacent laminations would make contact at various points, thus providing path linkages for flux between the laminations, avoiding the air path.

Table 7.5: Laminated model preliminary FEM results

Parameter	Phase A	Phase B	Phase C	Average % difference from lab results [%]
Input Current [A]	0.58	0.45	0.54	+75
Input Voltage [V]	159.81	159.81	159.81	+0.3
Output Voltage [V]	159.11	159.20	159.24	+0.6
Flux Linkage [Wb]	0.496	0.490	0.491	N/A
Current THD [%]	0.887	0.204	0.453	1.0
Total Core Loss [W]	39.81			-7.4

7.4.2 Fully laminated model

The fully laminated model was developed to fully resemble the physical transformer model as shown in Figure 7.9. The gap between individual laminations was calculated using the manufacturer specified stacking factor of 0.96. Hence, each lamination plate amounted to 0.3 mm thick according to the manufacturer data.

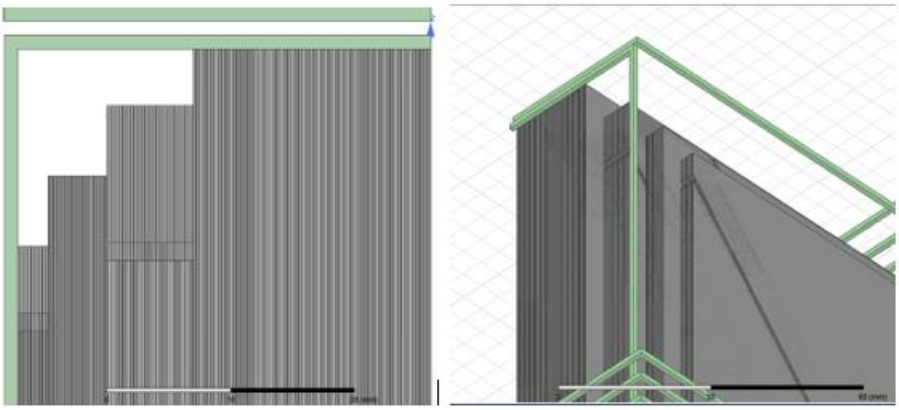

Figure 7.9: FEM 3D Fully Laminated Model

Running the fully laminated model of the transformer proved to be a challenge for even the most advanced computational capabilities. The UCT high performance computing cluster was used for this simulation, with 64 core nodes utilized, each running on about 16 GB RAM. Even with the high performance computing cluster, the model kept crashing before the transformer could reach steady state. FEM views each lamination plate as an independent structure, with no links to the adjacent sheets, hence there are no linkage paths for flux except through the air. The software then applies meshing for each of the individual structures. This increases the amount of computational burden and the amount of memory occupied by the solution. Once the allocated memory runs out, the model crashes. Hence, a solution could not be derived for such a detailed model, hence the first phase of laminations was used going forward.

7.5 Modelling Core Joints

To further explore the amount of structural detail required in the 3D FEM model, the core joints were modelled with air gaps.

7.5.1 Minor joints model

As part of improving the resemblance of the FEM model to the physical transformer, minor corner and T-joints were applied to the model. This was done through introducing 1 mm air gaps at the points where the physical transformer has joints. The 1 mm was the average of the gap lengths measured at multiple points.

i. Approach

The approach taken in modeling the joints involved the application of a uniform airgap across each core step. This was done similarly both for the corner joints and the T-Joints. Figure 7.10 shows the T-joint of the transformer, which can be seen to have four-step laps. The overall core also had laminations grouped in four (4) steps.

Figure 7.10: 3p3L Transformer Top T-Joint

Taking a slightly different approach when introducing the minor joints model, the four-step laps were applied in sections across the four core steps. One joint was applied on one core step. This arrangement is shown in Figure 7.11, showing that the joint detail is not the same as the physical transformer joint detail shown in Figure 7.10. This is envisioned to minimize the simulation time FEM would take to process the model as there are less edges.

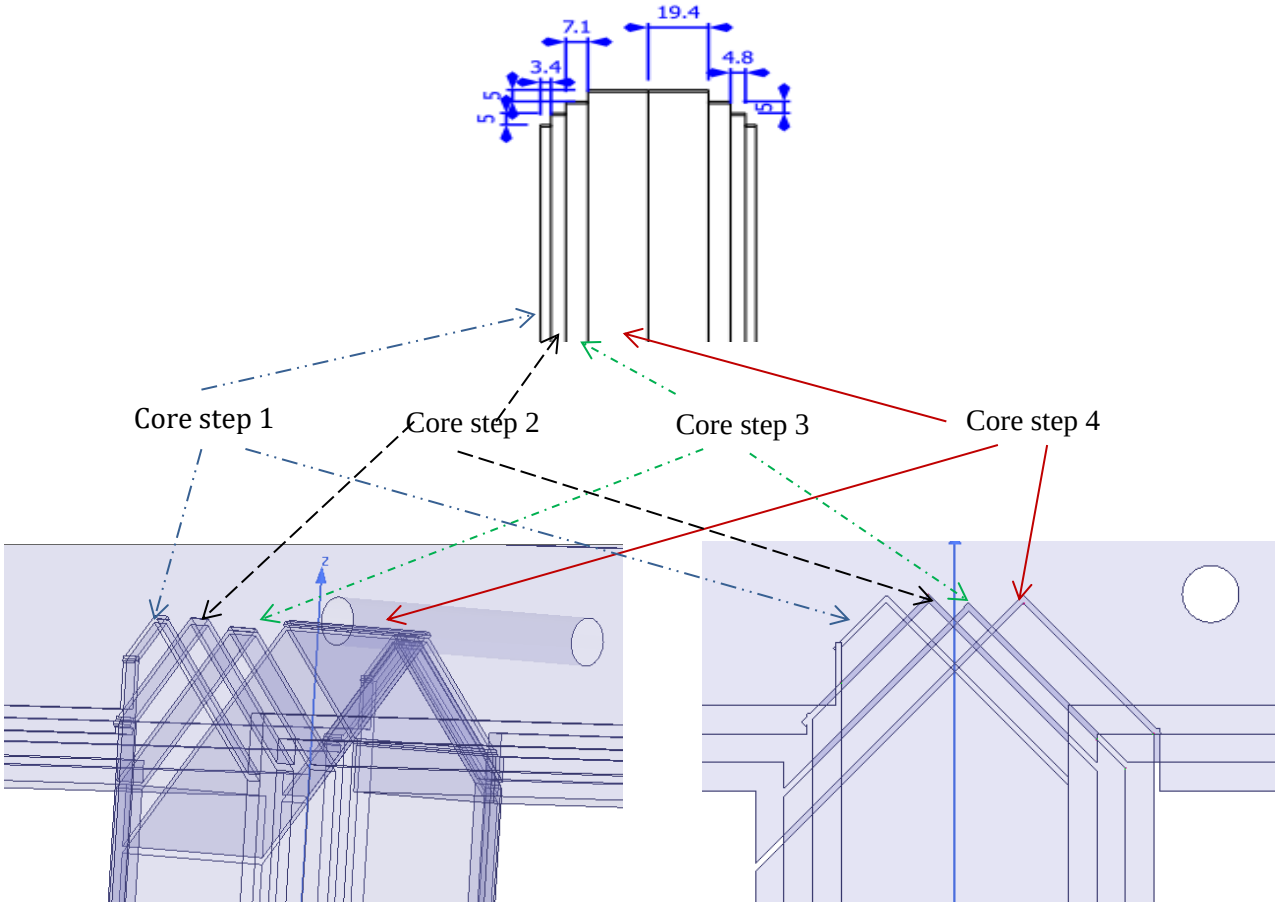

Figure 7.11: Transformer Minor T-Joints.

In the above Figure, Core step 1 has blue arrows, core step 2 has black arrows, core step 3 has green arrows and core step 4 has red arrows.

The same approach was taken to model the corner joints of the model. Symmetry was applied to project the top T-joint gaps onto the lower T-joint gaps. The joints were made by building a rectangular solid structure at the origin, with the thickness of the joint gap. This was rotated by 45° to fit the orientation of the gaps. Next, the structure was translated to the position of the joint air gap

and subtracted from the main core, leaving an air gap space. This was done for the individual air gaps applied in each step.

ii. ***Simulation Results***

The FEM simulation results for the model with equally sized minor joints for both the T-Joints and the corner joints are shown in Table 7.6. The results from the phase A appear to be quite close to those of phase C. Phase B, however, appears to have values much higher compared to phase A, e.g. for the input current. This is due to the design of the T-joints in the mid-limb compared to the corner joints of the outer limb. Even though the joint air gaps were made to be of the same size, the T-joints were made to stagger between the different core steps as per the physical transformer, whereas the corner joints were not staggering (non-mitered). The very large increase in magnetizing current compared to the laboratory measured results is due to the reasons stated earlier i.e. laminations appear as isolated objects in the 3D FEM model. The lack of point of contacts between laminations presents substantial air gaps in between them, resulting in increased losses. The mitering on the T-joints consisted of elongated air gaps across each step of the core. This causes flux lines to travel across longer crammed distances to escape the air gaps. This largely increased the overall path reluctance and led to an increase in input current.

Table 7.6: Results Summary

Parameter	**Phase A**	**Phase B**	**Phase C**	**Average % difference from lab results [%]**
Input Current [A]	0.257	1.48	0.381	+66
Input Voltage [V]	159.47	159.01	159.21	+0.4
Output Voltage [V]	159.44	158.90	159.13	+0.34
Input Apparent Power [VA]	42.63	220.19	58.64	+67.9
Flux Linkage [Wb]	0.513	0.507	0.511	N/A
Current THD [%]	0.31	0.14	0.23	1.07
Total Input Reactive Power [Var]	313.14			+82.5
Total Core Loss [W]	35.63			-18.5

iii. ***Input current harmonics results***

The harmonics of the input currents were also captured as part of the experiment. The results (Figure 7.12) show a large dominance of the 3rd harmonic components. Harmonic components also appear

to diminish with rising harmonic order. In a similar study on a 3p3L transformer, Kohli *et al* [48] recorded that there was a significant occurrence of even harmonics even with increasing saturation. This was explained to be because of the high reluctance path of the 2D model. Thus, further investigation in this area is required as the model is being developed.

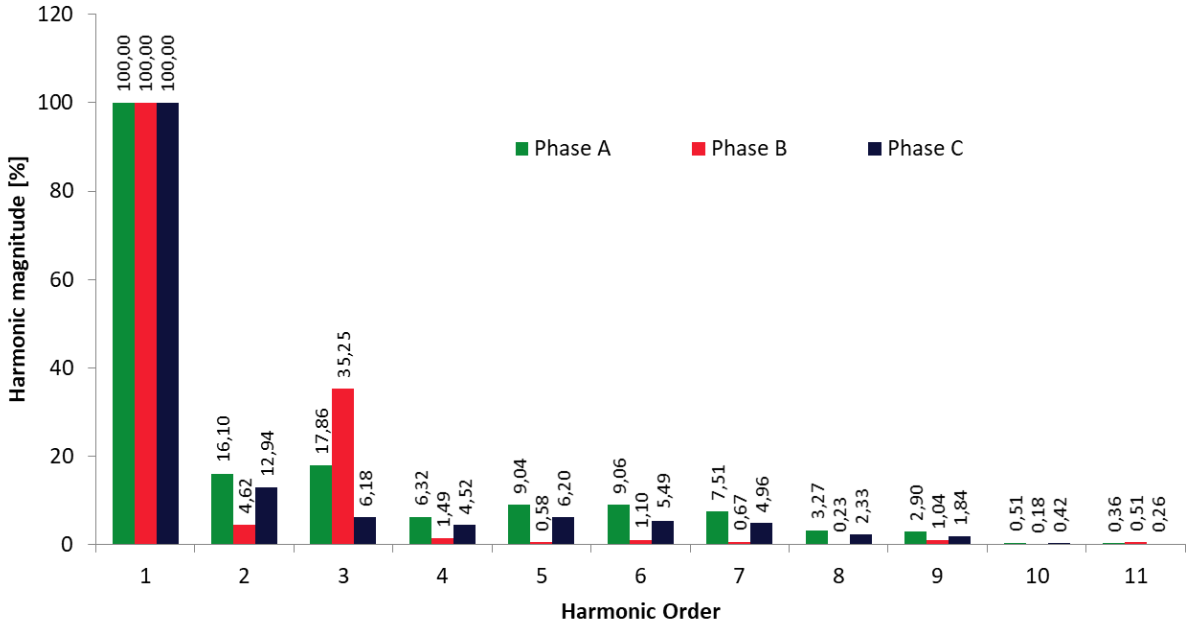

Figure 7.12: 3p3L FEM Harmonic Components for model with similar T and corner joints at 160 V input voltage

iv. ***Flux density vector***

Figure 7.13 shows the flux density vectors within the core of the transformer. A flux density nearing 1.7 T can be noted around some parts of the top T-joint and top left corner joint. It can be noted that these higher flux densities appear around areas where the flux vectors deviate from their straight path. At this point, they are interlinking between lamination stacks (or layers) to escape the air gap. Thus, they become crammed along similar paths and cause an early saturation of those deviation paths. Similar deviations can also be seen around the holes. As the transformer is operating in its linear region, most of the flux remains within the core. Areas of saturation can also be seen on Figure 7.14 and Figure 7.15.

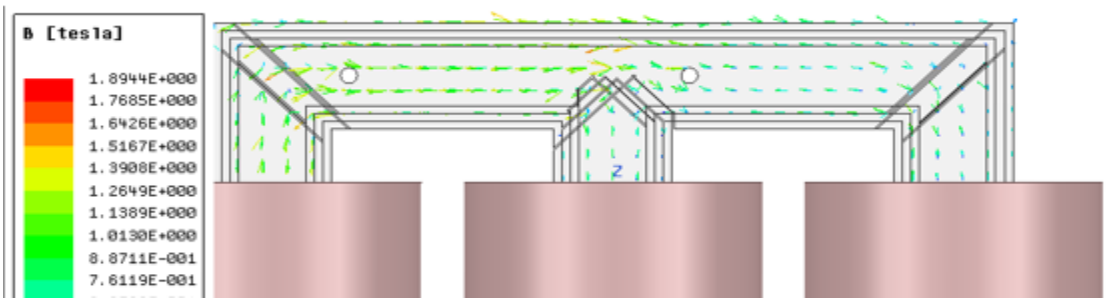

Figure 7.13: FEM model showing core flux density vector distribution when excited at 160 Vrms with both T-joints and corner joints present and with similar joint detail.

The magnitude of the flux appears to be much bigger around the holes closer to the excited phase limb (Figure 7.14). This is due to the air gaps around the holes, which are much bigger than the gaps at the core joints. Thus, the holes have a bigger influence on the core saturation.

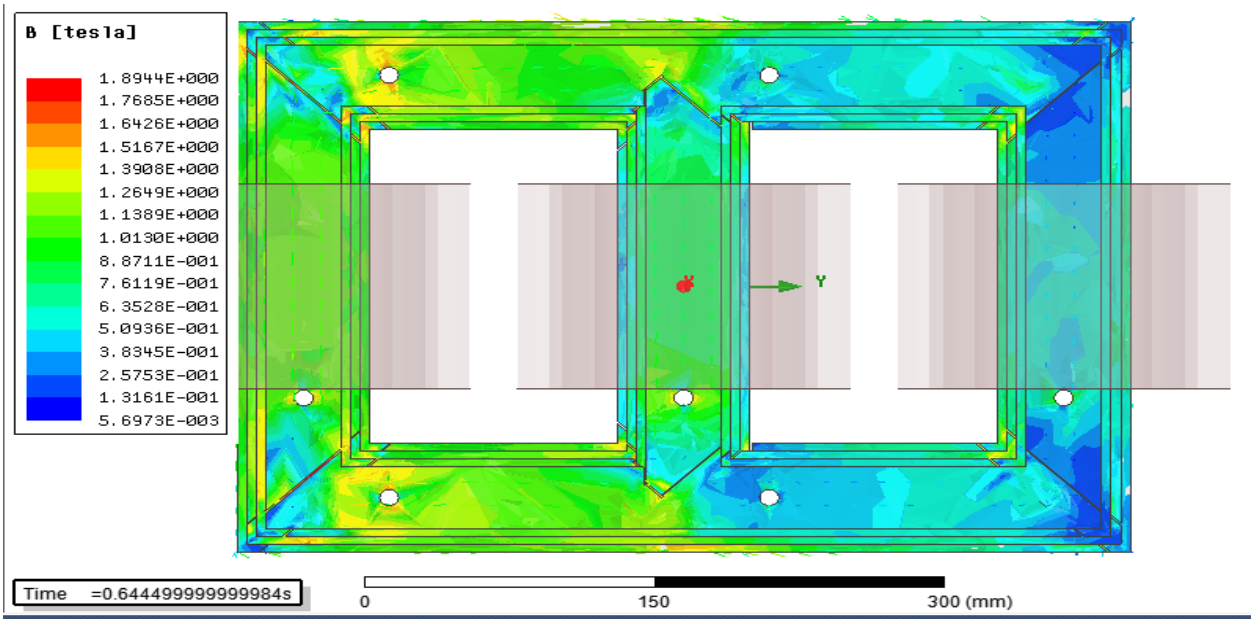

Figure 7.14: FEM model showing core flux density magnitude distribution when excited at 160 Vrms with both T-joints and corner joints present and with similar joint detail.

A closer look at the core T-Joints in Figure 7.15 further shows how the T-joints appear to have an increased amount of saturation around the region, with flux density values peaking to about 1.8 T, above the normal 1.7 T for this core type.

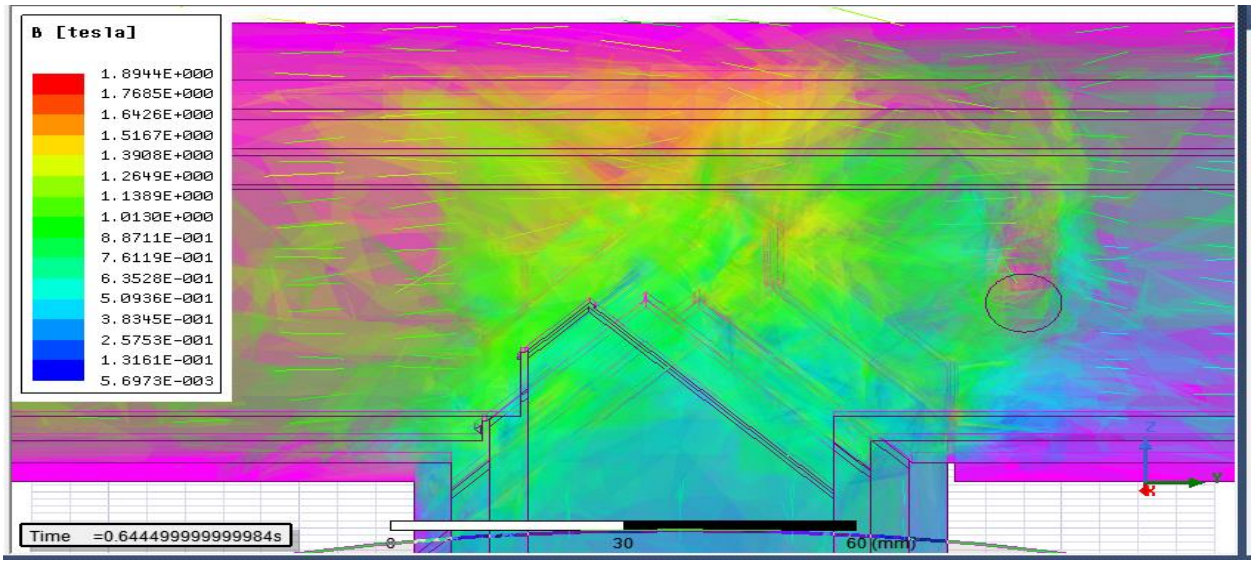

Figure 7.15: FEM model showing flux density around the T-joint of the 3p3L transformer where the T-joints had similar joint details as the corner joints

From the analysis above, it can be concluded that the holes and the joints are the key structural features contributing the most towards the core saturation. Since the holes are existent with clearly defined dimensions on the physical transformer, not much could be done in refining them in the model. The joints however were refined further when building the refined model (section 7.6).

Overall, the results show an increased amount of saturation around the T-Joint area due to the complexity of the T-Joints. The design of the step-laps in bulk across the different core steps appears to escalate the amount of saturation due to the elongated width of the air gap space. The staggering steps (4-step laps) make the flux lines switch directions several times, over longer distances (about four times) compared to the corner joint flux, hence it makes sense for the current to be four times larger in the B-phase winding due to the increased path reluctance. To counter this, further detail was applied on the T-joints, while the corner joints remained the same. Further refinement was then required.

7.6 Refined Model (Minor Joints Model with Improved Mid Joints)

The model presented earlier saw the development of minor T-and corner joints. These were of an equal amount of detail, presenting air gaps across each core steps. Gaps were staggered between different steps. The previous section revealed a large discrepancy in the magnetizing current of the mid-limb, which was much higher than the two outer limbs. This called for more focus on the T-joint detail.

7.6.1 Approach

The approach taken to refine the T-joint seeks to minimize the width of each joint gap, so that it does not spread across the whole core step. Joint gaps in each step will be divided into four different parts which will stagger (mitered) to resemble the actual transformer core, as shown in Figure 7.16. This amount of detail will only be applied to the T-joints, leaving the corner joints the same to see the difference as the T-joints contributed the most towards saturation. In conducting this simulation, search coils were also introduced around the same areas as in the laboratory transformer.

The locations of the search coil can be seen in Figure 7.17. The search coils labelled SCx are set to monitor the core flux density through the core. These were constructed to follow a circular pattern around the core structure for improved accuracy in capturing flux density across the core. The air

search coils labelled ACx were constructed to be twenty (20) turn search coils to monitor stray flux around the core joints. These were made square to resemble those used in the laboratory experiment. The AC_holex search coils were also 20 turn search coils installed inside the upper 10 mm diameter holes to monitor flux making its way into the holes.

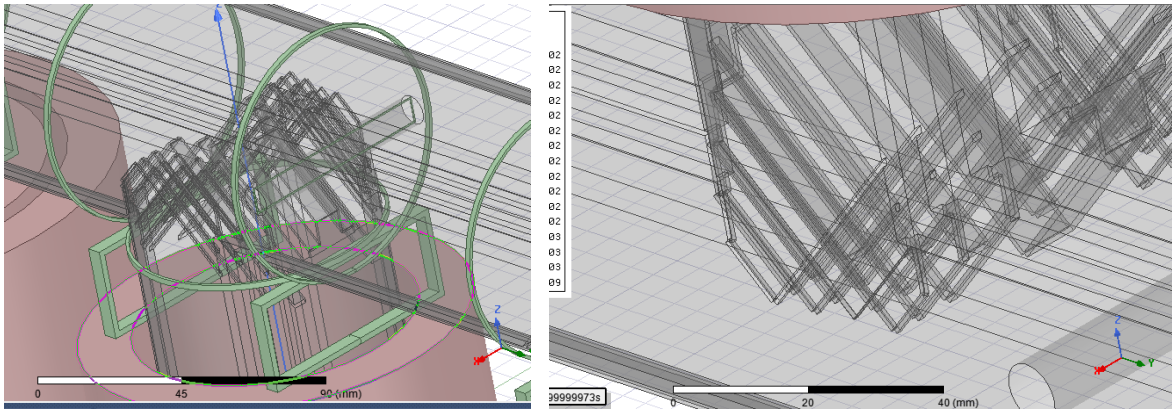

Figure 7.16: Refined T-joint models with more detail for the upper and lower T-joints, respectively

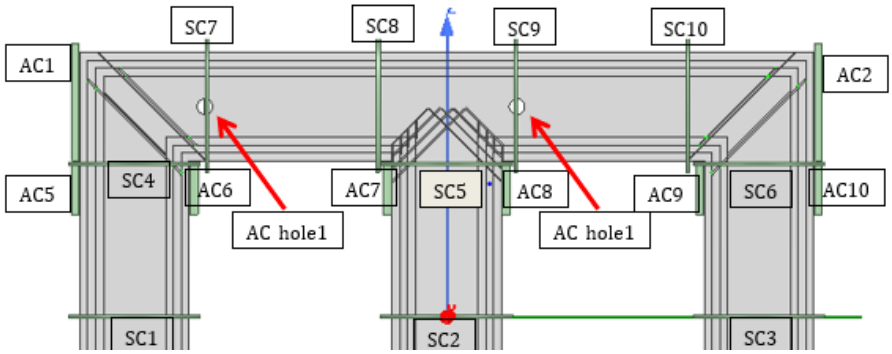

Figure 7.17: Search Coil Locations

7.6.2 Results for the model with refined T-joints

After the refinement of the mid limb T-joints, there was a significant improvement in the transformer terminal measurements as shown in Table 7.7. The average magnetizing current dropped from about 66% to 6.8%. The total apparent power also dropped by about 60%. This improvement is largely due to the refinement process that was applied to the T-joints. This decreased the density of flux along a path while escaping the air gaps to find alternative ways. The decreased flux path and reluctance lowered the amount of current required for the induction process to take place. The lower current meant less power requirement.

Table 7.7: Summary of results for FEM model with refined T-joints

Parameter	Phase A	Phase B	Phase C	Average % difference from lab results [%]
Input Current [A]	0.1666	0.1138	0.1523	+6.8
Input Voltage [V]	159.81	159.81	159.81	+0.76
Output Voltage [V]	159.25	159.29	159.30	+0.42
Input Apparent Power [VA]	26.61	18.17	24.31	+8
Flux Linkage [Wb]	0.513	0.508	0.510	N/A
Current THD [%]	0.31	0.14	0.23	+79.6
Total Input Reactive Power [Var]	69.09			+20.7
Total Core Loss [W]	34.23			-21.7

7.6.3 Flux Density

Further analysis of the model was done by assessing the flux density. It can be seen from section 7.6.2 that the model seems to perform very similarly to the laboratory tested transformer, hence the flux density will also be a good check for this compliance. Figure 7.18 shows the flux density distribution in the core. The losses and stray flux around the T-joint dropped. The change of direction from the mid-limb into the right and left yoke appears to be much smoother compared to the previous model in Figure 7.14 and Figure 7.15. This is largely due to the minimized width of the air gaps across each core step. The gaps have been minimized to a quarter of what they were in the previous model. This has largely minimized the distance that flux lines must take to escape the air gap while travelling in one path. The division of the air gaps into four different parts further gave the flux in each core step different options other than having to travel to the adjacent core step to escape the air gap. The information on the flux density was summarized into the search coil measurements shown in Table 7.8.

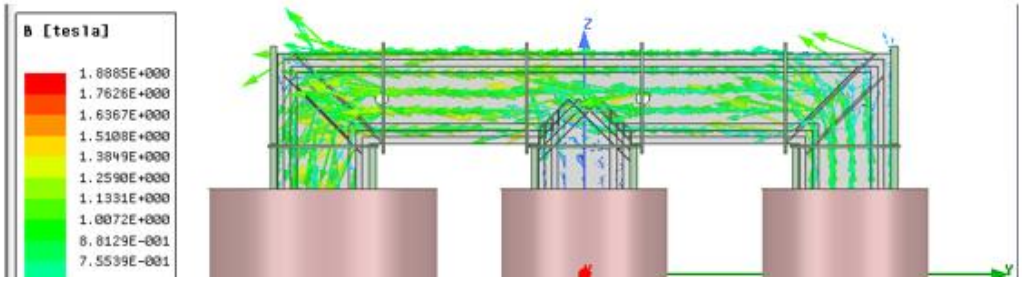

Figure 7.18: Flux density for 3D FEM model with refined T-joints and no laminations

Table 7.8: Search coil results for 3D model with refined T-joints and no laminations

Core Search Coils		Air Search Coils	
Search Coil	Search coil voltage [V]	Search Coil	Search coil voltage [V]
SC1	2.2274	AC1	0.0071
SC2	2.2317	AC2	0.0047
SC3	2.2293	AC3	0.0041
SC4	2.2244	AC4	0.0046
SC5	2.2298	AC5	0.0026
SC6	2.2261	AC6	0.0051
SC7	2.2225	AC7	0.0025
SC8	2.2225	AC8	0.0024
SC9	2.2247	AC9	0.003
SC10	2.2252	AC10	0.008
		AC_hole1	0.0004
		AC_hole2	0.00012

The core search coil results in Table 7.8 all appear to average a 2.2 V reading. This reading is in-line with the laboratory average of 2.23 V. The similar readings show that most of the core flux is kept within the core as the transformer was set to operate in its linear region. The air search coil readings are quite low. No readings were recorded from the laboratory experiment at this voltage. Fractional components of stray flux may have appeared during the laboratory experiments, but these would have been too small to be captured by the measurement instruments.

7.6.4 Harmonics

The transformer current harmonic components were also captured as part of this experiment. These results are shown in Figure 7.19. There is a general decrease in the harmonic magnitude with increasing order. The higher amount of the A phase harmonics is due to the higher amount of dc being split to the A phase at the instance at which the phase was excited with voltage.

Low order harmonics are also visible in the transformer's harmonic spectrum. High order harmonics were too small to show on the graph; hence these were neglected. The results appear to correlate with the laboratory measured results, which showed a high dominance of the 3rd and 5th order harmonics.

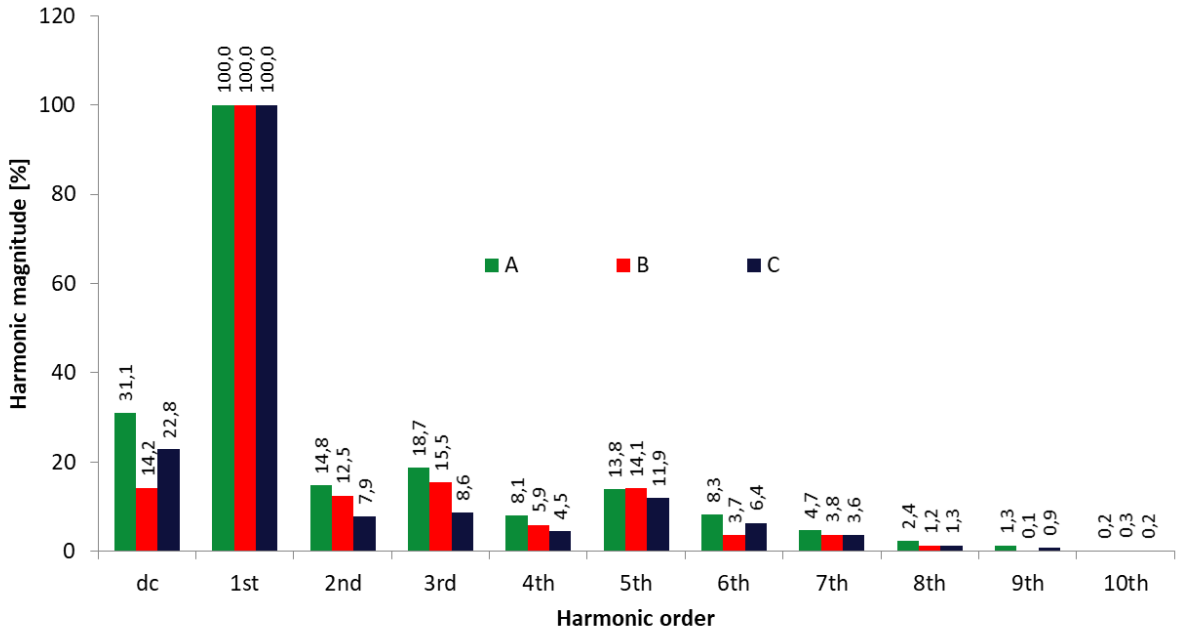

Figure 7.19: Transformer harmonic components for the refined T-joint model

7.7 Chapter Summary

This chapter presented the development of the FEM model of the TuT. Various approaches and techniques were applied to obtain a refined model. The approach followed involved developing solid 2D and 3D models, laminated models, and models where symmetry was later applied to minimise computational burden. A key contribution of this chapter is the presentation of approaches for developing these models, which can be easily followed and replicated by researchers carrying out similar studies. The refined model presents results that bear close resemblance to the laboratory test results, while converging to a solution within a reasonable time, without the simulation crushing.

8. FEM DC Test Results

8.1 Introduction

The final FEM model with terminal results closely matching the physical laboratory transformer was used for dc testing. This aided the analysis of the model transformer's behavior under dc and a check for compliance with the physical transformer response to transients.

8.2 DC Values

The dc values injected into the FEM model were directly adopted from dc levels measured for each phase at the lab. This allowed for the comparing laboratory and simulation results on a per phase basis. The dc values injected are shown in Table 8.1:

Table 8.1: DC excitation values vs. magnetizing currents for FEM model

DC Excitation Label	Phase A dc [A]	Phase B dc [A]	Phase C dc [A]
DC0	0.00	0.00	0.00
DC0.125	0.0532	0.0493	0.0497
DC0.25	0.0848	0.0774	0.0794
DC0.5	0.1734	0.166	0.167
DC1	0.3492	0.3255	0.3312
DC2	0.6932	0.6386	0.6503
DC3	1.0223	0.9387	0.9712
DC4	1.3518	1.2395	1.2638
DC5	1.9796	1.8464	1.8954
DC6	3.8203	3.4194	3.5075
DC7	7.049	6.563	6.613
DC8	9.958	8.921	9.134
DC9	12.244	11.076	11.384
DC10	14.226	12.865	13.054
DC11	16.104	14.508	14.702
DC12	17.495	15.966	16.086
DC13	18.117	16.421	16.613
DC14	18.6	16.859	17.05
DC22	22.558	20.224	20.695
DC26	26.46	23.745	24.286
DC28	28.955	27.177	27.289
DC31	31.761	29.798	29.95
DC32	32.664	30.948	31.07

With the high confidence in the FEM model, proven by the compliance with the laboratory transformer results and behavior (section 7.6), the model was used for tests involving dc injection as elaborated further below:

8.3 Results Discussion

The refined FEM model with the modified mid-limb joints was tested under dc excitation. This section outlines some of the results of this investigation. Comparisons are made with the laboratory results. The nature of the magnetizing current, the generated harmonics, non-active power and the flux density of the core were assessed.

8.3.1 Input magnetizing current

The ac component of the magnetizing current was recorded as the transformer approached its deep saturation stage. The ac component is the ripple that appears on the current waveform after the shift due to part-wave saturation. This ac component appears to be constant at lower values of dc excitation for the FEM model as shown in Figure 8.1. The FEM results were compared with the laboratory results. The Laboratory measured magnetizing current appears to be about 3 times higher than the FEM magnetizing current results. The reason for this is firstly because of the outlined disparities between the laboratory transformer and the FEM model. The laboratory transformer appears to undergo higher levels of saturation than the FEM model. The lab transformer is full of various manufacturing flaws, like some loose laminations and burrs, whose collective effect is increased saturation, which were not accounted for in the FEM model. The FEM model follows mathematical algorithms that are computed based on parameters of the physical transformer's structural design.

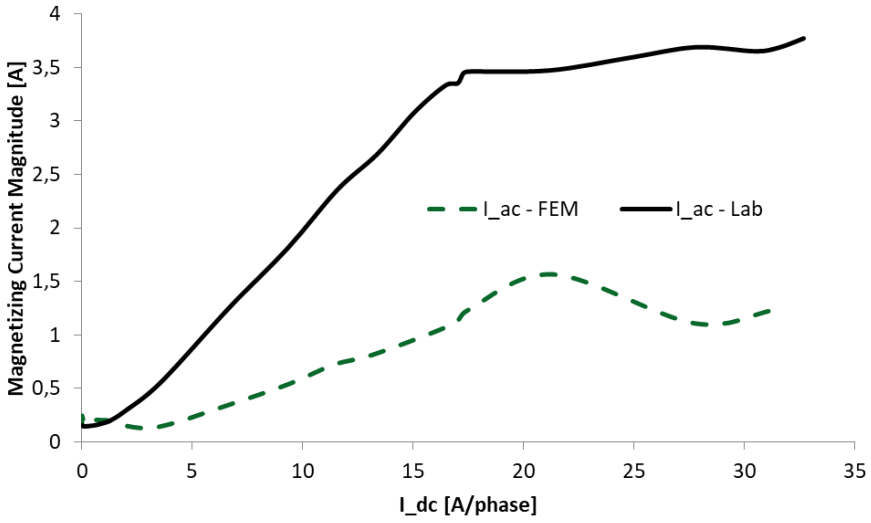

Figure 8.1: AC component of the transformer magnetizing current at different levels of dc excitation.

Figure 8.2 gives a more detailed view of the ac waveform. The ac component seems to grow more in the deep saturation region at a dc excitation of 150 A/phase.

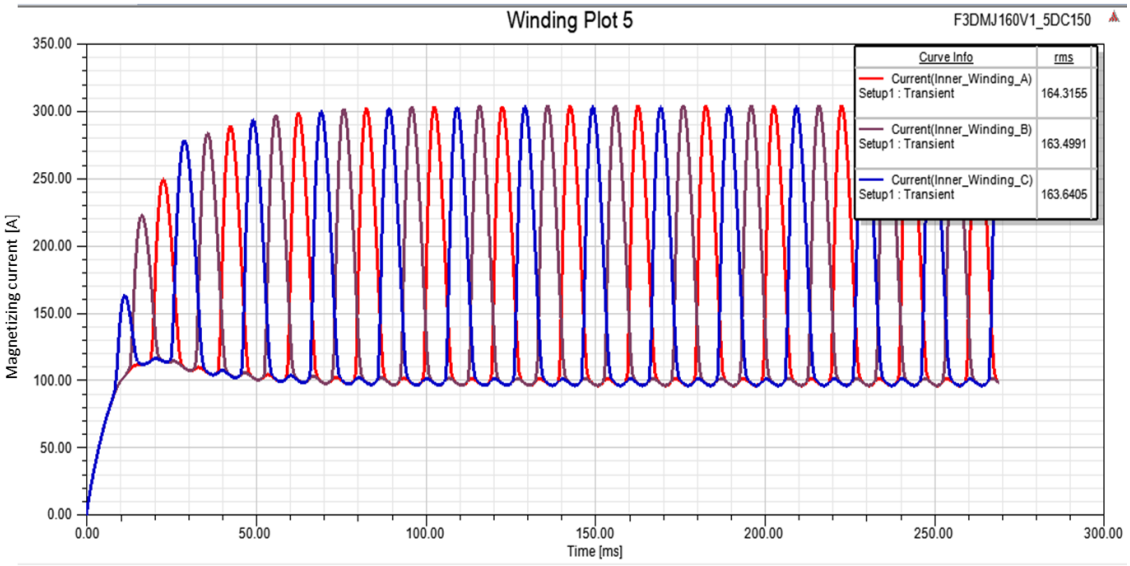

Figure 8.2: ac component of the TuT current waveform Harmonic Component

The magnetizing current of a transformer is usually accompanied by harmonics under dc injection. Figure 8.3 presents the harmonic component results for the final FEM model, injected with varying levels of dc. The widely reported increase in harmonics with increasing dc levels [73] can be noted from the results. Also, the observed trends are very similar to the laboratory results. The main trends are: (1) the drop in harmonic magnitude with increasing dc and (2) the rise of both odd and even harmonics with increasing dc. These trends are explained extensively under the laboratory results discussion (section 6.2.4). In this case, the model seems to have a similar operation as the laboratory transformer. The detailedresults are shown in Appendix C.

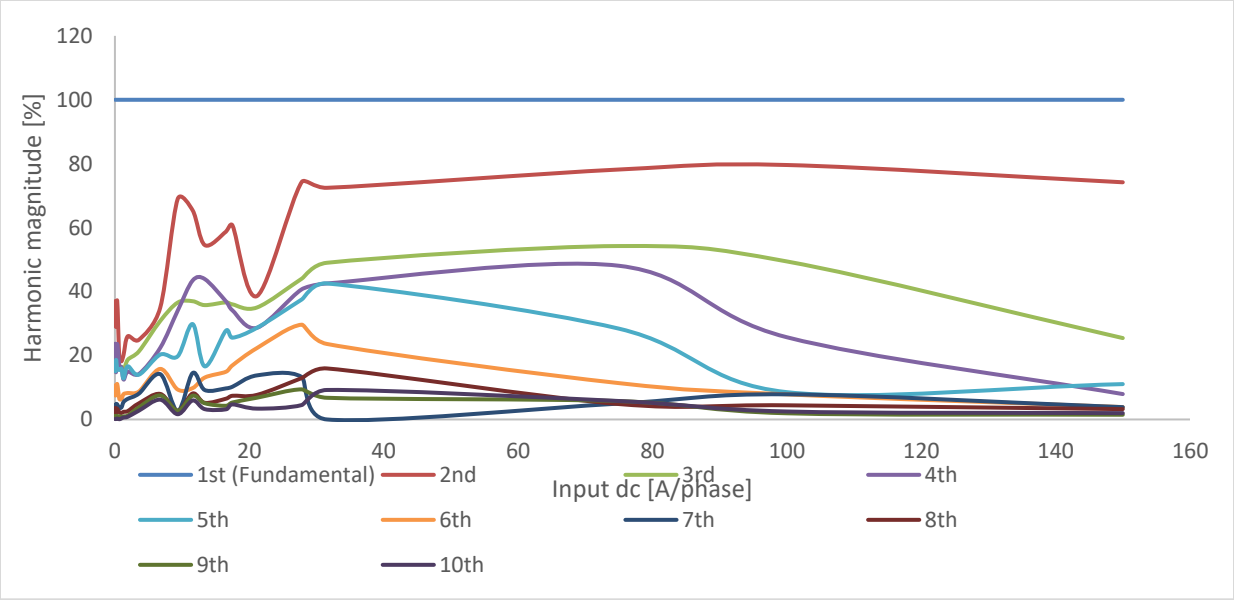

Figure 8.3: 3p3L FEM model harmonic content under dc excitation

Figure 8.4 shows a comparison between the FEM transformer and laboratory transformer harmonic magnitude results. The results largely show similar trends in the drop of harmonic magnitudes with increasing harmonic order. The FEM model appears to over-estimate the harmonics at dc values below 6 A/phase, while it indicates higher harmonic magnitudes for higher dc levels. The FEM harmonic magnitudes also appear to fluctuate with increasing dc. FEM presents the harmonic magnitude results at a range of frequencies, most of which are not exact multiples of the fundamental, from which harmonic magnitude data must be extracted. While this may have provided a bit of uncertainty, it was ensured that data was extracted from the associated frequency as close as possible to the multiple of the fundamental for increased integrity. Future work can assess how this data can be extracted from ANSYS Maxwell effectively.

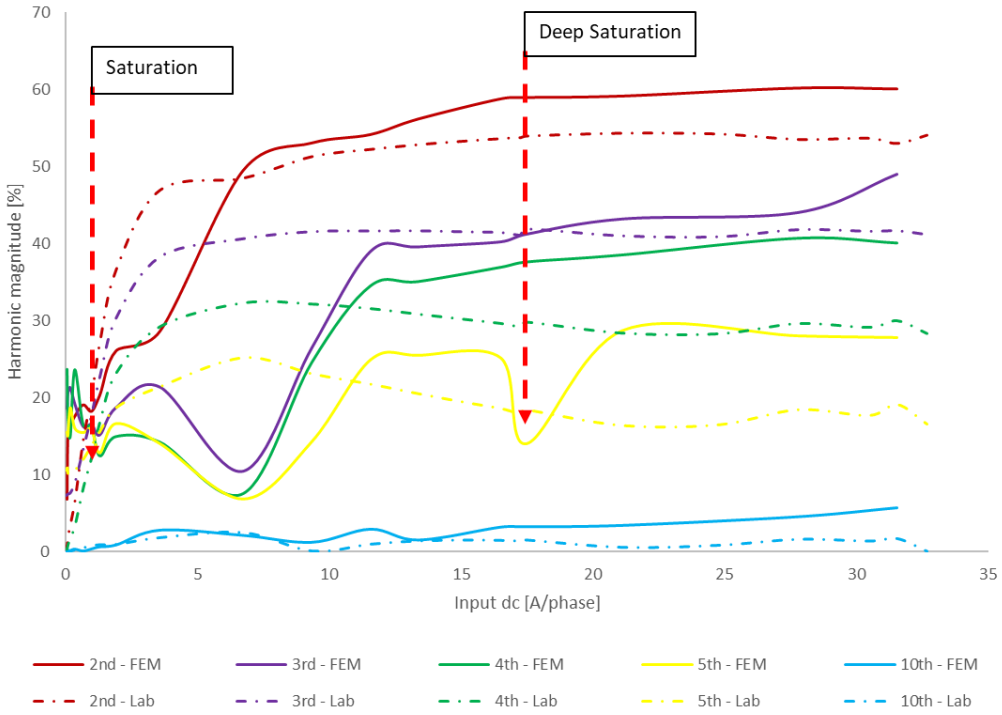

Figure 8.4: Comparison of harmonic data between FEM and Lab results

8.3.2 Input power components

The general power theory was used to investigate the amount of non-active power taken up by the transformer under dc. The results of this investigation are shown in Figure 8.5 where P is the active power component, Q is the non-active power component and S is the apparent power component. The linear relationship between the non-active power taken up by the transformer as discussed in detail previously and the level of dc appears to hold even for the FEM model. This relationship seems to hold even for more extreme levels of dc injection. The active power component increases linearly at lower dc values, while this changes to a much faster linear rate with the injection of 150 A_dc. The transformer is already deeply saturated at this dc current injection, hence the resistors are also heating up the resistors hence increasing the active power taken up.

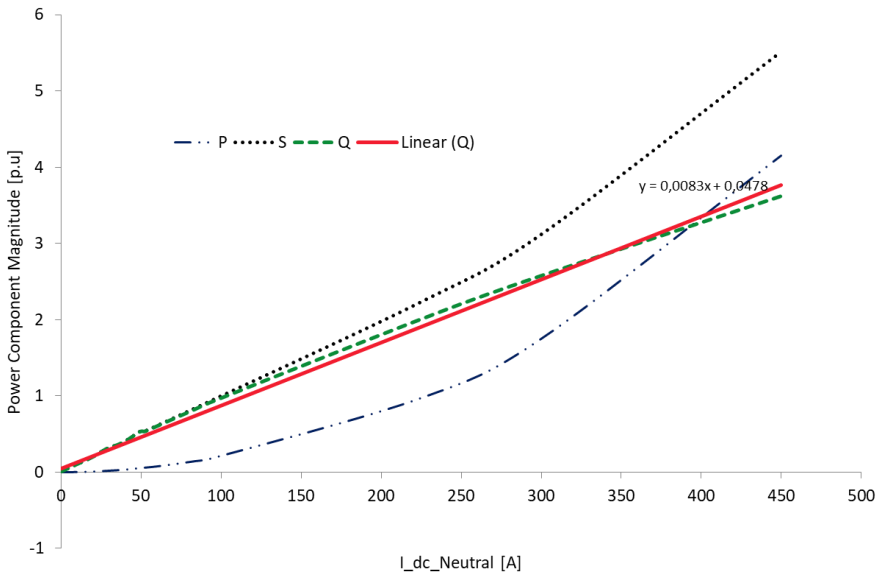

Figure 8.5: Input power components of the FEM transformer model under dc, computed with the GPT

8.3.3 Core search coils

The core search coil data were also captured for the FEM model under dc excitation. The results show a drop in the recorded core flux density (indicated by the search coil voltage). This drop is due to the saturation of the core, further causing flux to seek alternative paths outside of the core due to its saturation.

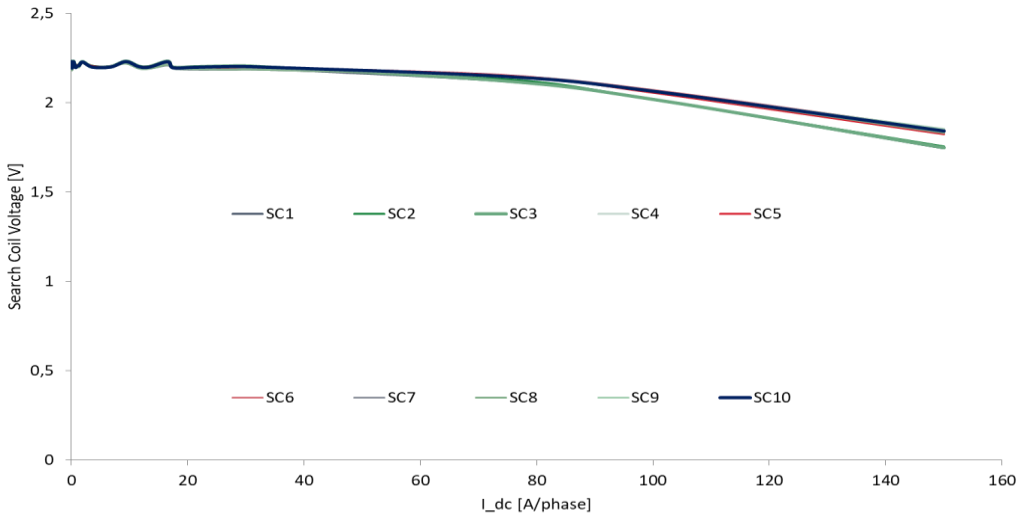

Figure 8.6: TuT FEM model search coil voltages

8.3.4 Air search coils

The voltages induced in the air search coils appeared to be generally different from those of the core search coils. The air search coil voltages appear to increase at dc excitation above 40 A/phase (Figure 8.8). The search coils inserted into the holes had lower voltages, even at extreme values of dc. This

shows that the flux barely goes through the hole, as it finds alternative paths around the holes, leading to saturation around the holes. Most of the search coil flux was measured from the corner of the corner joints (AC1, AC2, AC3 and AC4). The search coils inside the joints recorded even lower voltages. This indicates that as the transformer core saturates, most flux linkage happens around the top parts of the corner joints. The flux is distributed across the entire core in deep saturation, extending to the top parts of the corner joints.

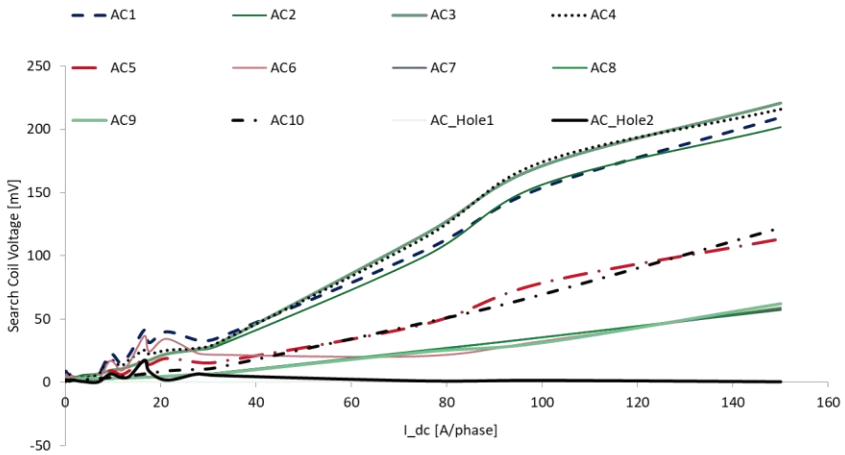

Figure 8.7: TuT FEM model air search coil voltages

8.3.5 Output voltage

During the laboratory testing phase, which included dc excitation up to about 32 A/phase of dc, the transformer output voltage appeared to be barely affected by the presence of dc. The output voltage at dc values lower than 32 A/phase appeared to be barely affected for the FEM model as well. This further validates the accuracy of the developed model.

Extreme levels of dc were explored to study the FEM transformer model response. These dc ranges were deemed impractical for the laboratory testing phase. The drop in the output voltage increases from about 40 A/phase of dc. The voltage drop was around 5% when the dc injection reached about 80 A/phase dc. At about 120 A/phase of dc injection, the voltage drop increased to 10%. The drop in the output voltage of the transformer with increasing dc levels follows a similar trend as the core search coil voltages. This shows the effect that the deep saturation state of the transformer has on the induction process and the transformation ratio of the transformer.

Voltage drop has been reported to be one of the challenges posed by the presence of dc/GICs in power systems, with voltage collapse being one of the dreaded consequences. The developed FEM model can be used for investigating the effects of a wide range of dc injection on the transformer's output voltage, which shows large voltage drops for extreme levels of dc injected.

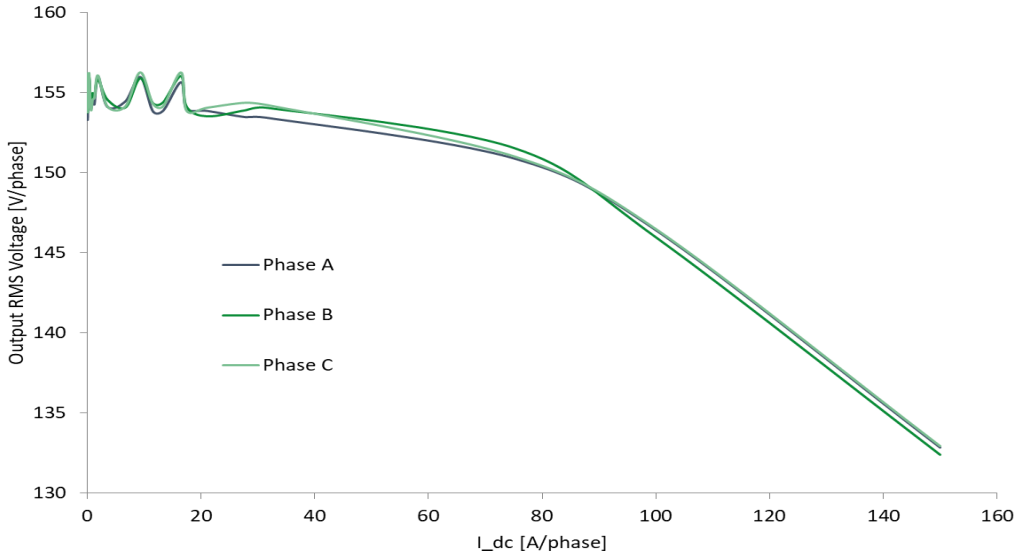

Figure 8.8: Output voltage drop for FEM model at extreme dc

8.4 Chapter Summary

This chapter presented the results of the dc tests ran on the optimal FEM model. These results were benchmarked against the dc test results from the laboratory. The results proved that the trade-offs between model complexity and computational burden affects the consistency of laboratory and simulation results. This was largely evident in the harmonic analysis, where significant differences between the magnitudes of the harmonics from the laboratory and simulation results were observed. The difference in harmonic magnitude is on average, about 50%. Nonetheless, the overall trends in the FEM model harmonics profile were similar with those in the laboratory results.

9. Conclusions and Recommendations

This study involved the development of a 3p3L FEM model for dc/GICs studies in power systems, as an extension to previous studies that focussed on developing a FEM model for single-phase, four-limb (1p4L) transformers with butt lap joints [13, 14, 79, 80, 109]. The FEM model was developed following a laboratory testing exercise that investigated the transformer saturation under dc excitation and identified critical levels of dc associated with transformer saturation. The laboratory results were used as a benchmark for developing the FEM model. Conclusions are presented in this chapter in line with the hypothesis and scope of the study. These conclusions provide further answers to the research questions.

9.1 Laboratory Testing

The 3p3L transformer was tested in a laboratory under a range of dc levels. The following conclusions are made following the laboratory experiments:

- Transformer saturation

  The transformer has two distinct levels of saturation (early saturation and deep saturation). Following different testing methods, the early saturation point for the 3p3L transformer was found to be at around a dc input of 1.8 A/phase (which is about 18% of the rated current). Deep saturation starts at around a dc input of 16 A/phase (72% of rated current)

- Holes on the transformer

  The holes on the transformer were found to impact on the voltage operating point of the transformer. The holes lowered the knee-point voltage by about 26%, hence transformer manufacturers need to avoid drilling holes into the laminations as part of stacking. Alternative methods can be sought.

9.2 FEM Model Development

A FEM model was developed following the laboratory experiments. The FEM model development started off with the development of a 2D model of the transformer, followed by a refined 3D model. The following conclusions were made:

- T-Joints contribution to saturation

  The T-joints were found to have the biggest contribution towards the transformer behaviour. A refinement of the T-Joints alone lowered the difference between the FEM magnetizing current and laboratory magnetizing current from 66% to about 6.4%.

- Laminations

  Phase 2 laminations as discussed in this dissertation have proven to be sufficient for the model to avoid system crash. The phase 2 laminations involve splitting each core step into 2, allocating 4% of the step volume to air gaps. A fully laminated model cannot be modelled in FEM even with the most advanced computational resources that were utilised. Further details can be applied to the joints, which contribute the most towards the transformer saturation.

- 2D Model

  The transformer 2D model is highly inaccurate, and may distort the magnetizing current by over 100% per phase and by about 60% on average. This is thus not advised for GICs studies.

- 3D Model

  The solid 3D model is a good entry level model to be used as a refence point while building a detailed FEM model. This improves magnetizing current result by about 30%.

- Model application for dc

  The developed model behaves similarly to the physical transformer. The transformer harmonic components were compared between the FEM model and the laboratory results, which showed a maximum variance of about 10% at higher dc excitation values of about 5% (which is within an acceptable range). The model can thus be confidently applied in dc or GICs studies.

9.3 Responses to the Research Questions

In Chapter one, research questions were listed to guide the testing of the hypothesis that **"Transformer laboratory test results can be used as a guide for developing suitable Finite Element Matrix (FEM) models for conducting GICs/dc experiments."**

In the following paragraphs, the results of the research are applied to answer each research question.

RQ1: What laboratory testing methods exist for measuring transformer response to GICs and how do current FEM models in literature accommodate for the study of transformer response to dc/GICs?

- The laboratory protocol was developed in alignment with some of the noticeable responses of transformers to GICs. These included the increase in non-active power absorbed by the transformer, increase in harmonics, increase in THD and TDD, part-wave saturation of the magnetizing current, and the increased flux density.
- FEM models in literature emphasize the need for joint inclusion in transformers because of the observed influence of the transformer joints on its saturation.

RQ2: How do the FEM model behaviours differ from laboratory transformers?

- FEM allows users to build any type of transformer, applying a range of equations to provide solutions. The behaviour of the FEM model largely depends on the design of the model and the amount of structural detail applied. Trade-offs between the amount of structural detail included in the model and the associated computational burden are required to guarantee converging solutions and reduced computational times. The 2D FEM model was found to be highly inaccurate and misleading, with magnetizing current difference of about 60% compared to the laboratory results. This is due to the loss of the transformer physical attributes and details in the 2D model. The solid 3D model takes the transformer physical topology into account, hence it reduces the difference from the laboratory transformer results to about 34%. Further structural details application on the 3D model reduce the difference even further.

RQ3: What kind of structural detail needs to be incorporated in FEM models for improved resemblance to the laboratory transformer?

- The core appears to be of paramount importance in developing a FEM model. Most of the detail applied in the FEM model was in the representation of the core. Some of the specific areas that require special attention are the joints and laminations.

RQ4: How can we balance between the amount of detail applied to a FEM transformer model and the computational restrictions without compromising the accuracy of the FEM models?

- One must largely work around the computational resources at their disposal. The best place to start when modelling the core is the solid model. This gives an indication of the proximity to a desired model and gives an indication of the capabilities of the machine required for running that model.

9.4 Recommendations for Future Work

As much as extensive experimentation was carried out as part of this research, the research led to an opportunity for more future work. Future work can particularly focus on the following areas:

- Transformer testing under more extreme dc.

The physical transformers that were tested did not show any signs of temporal or permanent damage during the testing within the range of dc applied. This presents an opportunity for testing of higher ranges of dc with the right equipment and protection mechanisms put in place. This present research was limited by the equipment that was available, which could not cater for much higher levels of dc.

- Identifying thresholds of dc or GICs initiating transformer damage.

This area is of critical importance as it can help power system operators to be able to predict certain dc values that can lead to transformer damage. This can further help transformer designers to identify ways of designing transformers that can withstand such levels of dc.

- FEM Model Scale up

Future research can also look at how the develop FEM model can be scaled up to much larger power transformers. This can offer valid contributions towards the prediction and analysis of transformers in operation, as physical tests are currently not possible.

- Check if lamination application approach holds for other models.

There are various FEM model design principles that were applied in this research. These principles can be taken forward to other transformer models to check if they would still apply.

9.5 Validity of Hypothesis

The results and extensive discussions presented in chapters five (5) to eight (8) validate the hypothesis which states "*Transformer laboratory test results can be used as a guide for developing suitable Finite Element Matrix (FEM) models for conducting GICs/dc experiments*". The laboratory results offered a good guidance towards the development of the model, giving insight on areas of the transformer that required more focus when modelling. Refinement of such particular areas led to improvement in the FEM model behaviour, producing results that were increasingly conforming to the laboratory results. With a maximum variance of about 5% between the laboratory and FEM harmonic results, the FEM model proved to be suitable for conducting dc/GICs experiments.

References

[1] R. Kataoka and A. Pulkkinen, "Geomagnetically induced currents during intense storms driven by coronal mass ejections and corotating interacting regions," *Journal of Geophysical Research: Space Physics,* vol. 113, 2008.

[2] V. S. Efimov, V; Sakharov, Ya;, "Impact of Geomagnetically Induced Currents on transformers in the Kola power grid," presented at the 2019 International Multi-Conference on Industrial Engineering and Modern Technologies (FarEastCon), 2019.

[3] D. Boteler, R. Pirjola, and H. Nevanlinna, "The effects of geomagnetic disturbances on electrical systems at the Earth's surface," *Advances in Space Research,* vol. 22, pp. 17-27, 1998.

[4] J. Kappenman, *Geomagnetic storms and their impacts on the US power grid*: Metatech, 2010.

[5] J. G. Kappenman, "Geomagnetic storms and their impact on power systems," *IEEE Power Engineering Review,* vol. 16, p. 5, 1996.

[6] C. Gaunt and G. Coetzee, "Transformer failures in regions incorrectly considered to have low GIC-risk," in *Power Tech, 2007 IEEE Lausanne*, 2007, pp. 807-812.

[7] J. G. Kappenman, "An overview of the impulsive geomagnetic field disturbances and power grid impacts associated with the violent Sun-Earth connection events of 29–31 October 2003 and a comparative evaluation with other contemporary storms," *Space Weather,* vol. 3, 2005.

[8] J. Ramírez-Niño, C. Haro-Hernández, J. H. Rodriguez-Rodriguez, and R. Mijarez, "Core saturation effects of geomagnetic induced currents in power transformers," *Journal of applied research and technology,* vol. 14, pp. 87-92, 2016.

[9] O. Bíró, G. Koczka, G. Leber, K. Preis, and B. Wagner, "Finite element analysis of three-phase three-limb power transformers under DC bias," *IEEE Transactions on Magnetics,* vol. 50, pp. 565-568, 2014.

[10] NERC Geomagnetic Disturbance Task Force, "Special reliability assessment interim report: effects of Geomagnetic Disturbances on the bulk power system," *North American Electric Reliability Council,* 2012.

[11] L. Marti, A. Rezaei-Zare, and A. Narang, "Simulation of transformer hotspot heating due to geomagnetically induced currents," *IEEE Transactions on Power Delivery,* vol. 28, pp. 320-327, 2013.

[12] S. A. Mousavi, C. Carrander, and G. Engdahl, "Comprehensive study on magnetization current harmonics of power transformers due to GICs," in *International Conference on Power Systems Transients (IPST2013) in Vancouver, Canada July 18-20, 2013.*, 2013.

[13] L. D. Borrill, H. K. Chisepo, and C. T. Gaunt, "Flux measurements with AC and DC components of current present show transformer equivalent circuit models need core joint details," in *Power System Technology (POWERCON), 2016 IEEE International Conference on*, 2016, pp. 1-6.

[14] H. K. Chisepo, L. D. Borrill, and C. T. Gaunt, "Measurements and Finite Element Model of transformer core joints with dc and ac excitation," in *Advanced Research Workshop on Transformers*, La Toja Island, Spain, 2016.

[15] U. C. Office, "National risk register of civil emergencies, 2012 edition," 2010.

[16] C. Office, "National risk register of civil emergencies," ed: Cabinet Office London, UK, 2015.

[17] DHS Office of Risk Management and Analysis, "Geomagnetic storms: an evaluation of risks and risk assessments," 2011.

[18] United States Government Accountability Office, "Protecting the electric grid from geomagnetic disturbances," Department of Energy, Bonneville Power Administration; Department of Energy, Western Area Power Administration2018.

[19] Internal Security (Ministry of Interior), "National risk assessment 2018," Helsinki2018.

[20] South African National Space Agency (SANSA), "Economic impact of space weather," 2017.

[21] D. Albert, T. Halbedl, H. Renner, R. L. Bailey, and G. Achleitner, "Geomagnetically induced currents and space weather-A review of current and future research in Austria," in *2019 54th International Universities Power Engineering Conference (UPEC)*, 2019, pp. 1-6.
[22] E. Camporeale, M. D. Cash, H. J. Singer, C. C. Balch, Z. Huang, and G. Toth, "A gray-box model for a probabilistic estimate of regional ground magnetic perturbations: Enhancing the NOAA operational Geospace model with machine learning," *arXiv preprint arXiv:1912.01038,* 2019.
[23] S. Wang, P. Dehghanian, L. Li, and B. Wang, "A Machine learning approach to detection of Geomagnetically Induced Currents in power grids," in *2019 IEEE Industry Applications Society Annual Meeting*, 2019, pp. 1-7.
[24] T. S. Molinski, "Why utilities respect geomagnetically induced currents," *Journal of atmospheric and solar-terrestrial physics,* vol. 64, pp. 1765-1778, 2002.
[25] L. Marti, J. Berge, and R. K. Varma, "Determination of geomagnetically induced current flow in a transformer from reactive power absorption," *IEEE Transactions on Power Delivery,* vol. 28, pp. 1280-1288, 2013.
[26] T. Hutchins, "Geomagnetically induced currents and their effect on power systems," 2012.
[27] E. J. S. Oughton, A; Horne, R B; Thomson, A W; Gaunt, C T, "Quantifying the daily economic impact of extreme space weather diue to failure in electricity transmission infrastructure," *Space Weather,* vol. 15, 2017.
[28] R. M. Del Vecchio, B. Poulin, M.-E. F. Feeney, P. T. Feghali, D. M. Shah, R. Ahuja*, et al.*, *Transformer design principles: with applications to core-form power transformers*: CRC press, 2001.
[29] H. K. Chisepo, "The response of transformers to geomagnetically induced-like currents," University of Cape Town, 2014.
[30] A. Rezaei-Zare, L. Marti, A. Narang, and A. Yan, "Analysis of three-phase transformer response due to GIC using an advanced duality-based model," *IEEE Transactions on Power Delivery,* vol. 31, pp. 2342-2350, 2016.
[31] B. Røen, "Geomagnetic Induced Current effects on power transformers," NTNU, 2016.
[32] S. Mkhonta, "Designing setups to measure network thevenin equivalent when exposed to GIC-like currents," BSc. Eng in Electrical Engineering Undergraduate Dissertation, Electrical Engineering Department, University of Cape Town, 2016.
[33] J. Berge, R. K. Varma, and L. Marti, "Laboratory validation of the relationship between Geomagnetically Induced Current (GIC) and transformer absorbed reactive power," in *Electrical Power and Energy Conference (EPEC), 2011 IEEE*, 2011, pp. 491-495.
[34] S. Mousavi, "Electromagnetic modelling of power transformers for study and mitigation of effects of GICs," KTH Royal Institute of Technology, 2015.
[35] R. Lv and K. Zhu, "Quantitative Analysis of Saturation of Measurement Current Transformer by Direct Current Bias," in *2019 IEEE 3rd International Conference on Green Energy and Applications (ICGEA)*, 2019, pp. 1-5.
[36] S. Mousavi, G. Engdahl, and E. Agheb, "Investigation of GIC effects on core losses in single phase power transformers," *Archives of Electrical Engineering,* vol. 60, pp. 35-47, 2011.
[37] O. Samuelsson, "Geomagnetic disturbances and their impact on power systems," *Ind. Elec. Eng. Auto., Lund Univ., Lund, Sweden,* pp. 1-18, 2013.
[38] K. R. Vasudevan, Sridhara G; Rao, Sasidhara;. (June 10). *Electrical machines 1: harmonics*. Available: https://www.academia.edu/7513450/Electrical_Machines_I
[39] A. AbuHussein, "Impact of Geomagnetically Induced Current on Distributed Generators," in *2018 IEEE/PES Transmission and Distribution Conference and Exposition (T&D)*, 2018, pp. 1-5.
[40] A. Lotfi, H. K. Høidalen, and N. Chiesa, "Effect of dc biasing in 3-legged 3-phase transformers taking detailed model of off-core path into account," *Electric Power Systems Research,* vol. 138, pp. 18-24, 2016.

[41] R. Siti, S. Hassan, and M. Anuar, "Study the harmonic characteristics of dc bias on the single phase power transformer," in *Power Engineering and Optimization Conference (PEDCO) Melaka, Malaysia, 2012 Ieee International*, 2012, pp. 501-504.
[42] J. Yao, M. Liu, C. Li, and Q. Li, "Harmonics and reactive power of power transformers with DC bias," in *Power and Energy Engineering Conference (APPEEC), 2010 Asia-Pacific*, 2010, pp. 1-4.
[43] A. Rezaei-Zare, "Behavior of single-phase transformers under geomagnetically induced current conditions," *IEEE Transactions on Power Delivery,* vol. 29, pp. 916-925, 2014.
[44] C. Bergsåker, "Impact of transformer core size on the reactive power requirement of power transformers due to GIC," ed, 2014.
[45] C. Gaunt, "Notice of proposed rulemaking on reliability standard for transmission system," ed, 2015.
[46] S. D. Mitchell and J. S. Welsh, "Initial parameter estimates and constraints to support gray box modeling of power transformers," *IEEE Trans. Power Del.,* vol. 28, pp. 2411-2418, 2013.
[47] N. Chiesa, B. A. Mork, and H. K. Høidalen, "Transformer model for inrush current calculations: Simulations, measurements and sensitivity analysis," *IEEE Transactions on Power Delivery,* vol. 25, pp. 2599-2608, 2010.
[48] S. Kohli, S. Mahajan, P. Sanjeevikumar, V. Fedák, and V. Oleschuk, "Impact of dc bias on the magnetic loading of three-phase three-limb transformer based on Finite Element Method," in *Advances in Power Systems and Energy Management*, ed: Springer, 2018, pp. 97-106.
[49] A. M. T. Yagoub, Zheng, "Modelling & mitigation of Geomagnetically Induced Currents (GICs) for single-phase power transformer," presented at the 2018 International Conference on Computer, Control, Electrical, and Electronic Engineering (ICCCEEE), 2018.
[50] A. Kulkarni and V. John, "Mitigation of lower order harmonics in a grid-connected single-phase PV inverter," *IEEE Transactions on Power Electronics,* vol. 28, pp. 5024-5037, 2013.
[51] P. R. Price, "Geomagnetically induced current effects on transformers," *IEEE Transactions on Power Delivery,* vol. 17, pp. 1002-1008, 2002.
[52] S. Lu, Y. Liu, and J. De La Ree, "Harmonics generated from a dc biased transformer," *IEEE Transactions on power Delivery,* vol. 8, pp. 725-731, 1993.
[53] S. Mkhonta, T. Murwira, D. Oyedokun, K. Folly, and C. Gaunt, "Investigation of transformer reactive power and temperature increases under dc," in *2018 IEEE PES/IAS PowerAfrica*, 2018, pp. 595-600.
[54] D. T. O. Oyedokun, "Geomagnetically Induced Currents (GIC) in large power systems including transformer time response," Doctor of Philosophy (PhD) degree in Electrical Engineering, Electrical Engineering, University of Cape Town, Cape Town, 2015.
[55] S. Marsal and J. Torta, "Quantifying the performance of geomagnetically induced current models," *Space Weather,* vol. 17, pp. 941-949, 2019.
[56] C. Liu, D. H. Boteler, and R. J. Pirjola, "Influence of shield wires on geomagnetically induced currents in power systems," *International Journal of Electrical Power & Energy Systems,* vol. 117, p. 105653, 2020.
[57] A. Najafi and I. Iskender, "Comparison of core loss and magnetic flux distribution in amorphous and silicon steel core transformers," *Electrical Engineering,* vol. 100, pp. 1125-1131, 2018.
[58] A. Ahmad, I. Javed, W. Nazar, and M. A. Mukhtar, "Short circuit stress analysis using FEM in power transformer on HV winding displaced vertically & horizontally," *Alexandria engineering journal,* 2016.
[59] X. Liu, Y. Wang, J. Zhu, Y. Guo, G. Lei, and C. Liu, "Calculation of core loss and copper loss in amorphous/nanocrystalline core-based high-frequency transformer," *Aip Advances,* vol. 6, p. 055927, 2016.

[60] G. Bai, C. Gu, and L. Lai, "Electromagnetic Analysis of an Air-Core HTS Transformer," *IEEE Transactions on Applied Superconductivity,* vol. 29, pp. 1-3, 2019.
[61] W. A. Pluta, "Core loss models in electrical steel sheets with different orientation," *Przegląd Elektrotechniczny,* vol. 87, pp. 37-42, 2011.
[62] V. C. Sarac, Goran, "FEM aided design of distribution transformer," *TEM Journal,* vol. 5, pp. 197 - 203, 2016.
[63] G. Loizos, T. D. Kefalas, A. G. Kladas, and A. T. Souflaris, "Flux distribution analysis in three-phase Si-Fe wound transformer cores," *IEEE Transactions on Magnetics,* vol. 46, pp. 594-597, 2010.
[64] T. D. Kefalas, G. Loizos, and A. G. Kladas, "Transformer joints FE analysis using pseudo-source technique," *IEEE Transactions on Magnetics,* vol. 47, pp. 1058-1061, 2011.
[65] T. D. Kefalas, G. Loizos, and A. G. Kladas, "Normal flux distribution at step-lap joints of Si-Fe wound cores," in *Materials Science Forum*, 2011, pp. 284-290.
[66] S. Lu and Y. Liu, "FEM analysis of dc saturation to assess transformer susceptibility to geomagnetically induced currents," *IEEE Transactions on Power Delivery,* vol. 8, pp. 1367-1376, 1993.
[67] X. Zhang, "Stranded core transformer loss analysis," 2008.
[68] H. K. Chisepo, L. D. Borrill, and C. T. Gaunt, "Measurements show need for transformer core joint details in finite element modelling of GIC and DC effects," *COMPEL-The international journal for computation and mathematics in electrical and electronic engineering,* vol. 37, pp. 1011-1028, 2018.
[69] J. Olivares, S. Kulkarni, J. Cañedo, R. Escarela-Perez, J. Driesen, and P. Moreno, "Impact of the joint design parameters on transformer losses," *International Journal of Power and Energy Systems,* vol. 23, pp. 151-157, 2003.
[70] Q. Tang, S. Guo, and Z. Wang, "Magnetic flux distribution in power transformer core with mitred joints," *Journal of Applied Physics,* vol. 117, p. 17D522, 2015.
[71] K. E. Makram, Mohamed, "Improvement of transformer core joints model with finite element method," *Transactions on Systems, Signals & Devices,* vol. 6, pp. 197-211, 2011.
[72] M. Ertl and H. Landes, "Investigation of load noise generation of large power transformer by means of coupled 3D FEM analysis," *COMPEL-The international journal for computation and mathematics in electrical and electronic engineering,* vol. 26, pp. 788-799, 2007.
[73] S. Kohli, S. Mahajan, S. Badave, P. Sanjeevikumar, and A. Iqbal, "Finite Element Method based determination of magnetic loading of three-phase five-limb transformer with impact of dc offset," in *Advances in Power Systems and Energy Management*, ed: Springer, 2018, pp. 241-249.
[74] M. Beltle and S. Tenbohlen, "Power transformer diagnosis based on mechanical oscillations due to AC and DC currents," *IEEE Transactions on Dielectrics and Electrical Insulation,* vol. 23, pp. 1515-1522, 2016.
[75] H. Chisepo, C. Gaunt, and D. Oyedokun, "Testing the response of laboratory bench transformers to Geomagnetically Induced-like currents," in *Southern African Universities' Power Engineering Conference, p37-42, Potchefstroom, January*, 2013.
[76] M. Malengret and C. Gaunt, "General theory of average power for multi-phase systems with distortion, unbalance and direct current components," *Electric Power Systems Research,* vol. 84, pp. 224-230, 2012.
[77] C. Gaunt and M. Malengret, "True power factor metering for m-wire systems with distortion, unbalance and direct current components," *Electric Power Systems Research,* vol. 95, pp. 140-147, 2013.
[78] T. T. Murwira, S. Mkhonta, D. T. Oyedokun, K. A. Folly, and C. Gaunt, "Three-phase five-limb transformer harmonic analysis under dc-bias," in *2019 Southern African Universities Power*

Engineering Conference/Robotics and Mechatronics/Pattern Recognition Association of South Africa (SAUPEC/RobMech/PRASA), 2019, pp. 420-424.
[79] L. D. Borrill, H. K. Chisepo, and C. T. Gaunt, "Determining the terminal saturation inductance of a single-phase four-limb transformer," in *25th Southern African Universities Power Engineering Conference*, Stellenbosch, South Africa, 2017, pp. 120-124.
[80] L. D. Borrill, "Duality derived topological model of single-phase four-limb transformers for GIC and DC bias studies," Doctor of Philosophy in Electrical Engineering, Electrical Engineering, University of Cape Town, Cape Town, South Africa, 2017.
[81] S. Jazebi, F. De Leon, A. Farazmand, and D. Deswal, "Dual reversible transformer model for the calculation of low-frequency transients," *IEEE Transactions on Power Delivery,* vol. 28, pp. 2509-2517, 2013.
[82] F. De Leon, A. Farazmand, and P. Joseph, "Comparing the T and pi equivalent circuits for the calculation of transformer inrush currents," *IEEE Transactions on Power Delivery,* vol. 27, pp. 2390-2398, 2012.
[83] S. Jazebi and F. De León, "Duality-based transformer model including eddy current effects in the windings," *IEEE Transactions on Power Delivery,* vol. 30, pp. 2312-2320, 2015.
[84] Q. Wu, S. Jazebi, and F. De Leon, "Parameter estimation of three-phase transformer models for low-frequency transient studies from terminal measurements," *IEEE Transactions on Magnetics,* vol. 53, pp. 1-8, 2017.
[85] ANSYS Inc, "ANSYS Maxwell V16 training manual lecture 3: static magnetic solvers," May 21, 2013 2013.
[86] S. O. Mkhonta, David, "Title," unpublished|.
[87] H. K. Chisepo, C. Gaunt, and L. D. Borrill, "Measurement and FEM analysis of DC/GIC effects on transformer magnetization parameters," in *2019 IEEE Milan PowerTech*, 2019, pp. 1-6.
[88] M. Malengret and C. Gaunt, "General theory of instantaneous power for multi-phase systems with distortion, unbalance and direct current components," *Electric Power Systems Research,* vol. 81, pp. 1897-1904, 2011.
[89] M. Malengret and C. T. Gaunt, "General theory of average power for multi-phase systems with distortion, unbalance and direct current components," *Electric Power Systems Research,* vol. 84, pp. 224-230, 2012.
[90] W. G. Morsi and M. El-Hawary, "A new fuzzy-based total demand distortion factor for nonsinusoidal situations," *IEEE Transactions on Power Delivery,* vol. 23, pp. 1007-1014, 2008.
[91] A. Norouzi, "Open phase conditions in transformers analysis and protection algorithm," in *Protective Relay Engineers, 2013 66th Annual Conference for*, 2013, pp. 112-125.
[92] S. S. Mahalingan, "Magnetic Flux Distributions in Transformer Core Joints," *Ijltemas,* vol. 3, 2014.
[93] M. Elleuch and M. Poloujadoff, "New transformer model including joint air gaps and lamination anisotropy," *IEEE Transactions on Magnetics,* vol. 34, pp. 3701-3711, 1998.
[94] R. Jez, "Influence of the Distributed Air Gap on the Parameters of an Industrial Inductor," *IEEE Transactions on Magnetics,* vol. 53, pp. 1-5, 2017.
[95] R. Jez and A. Polit, "Influence of air-gap length and cross-section on magnetic circuit parameters," in *Proc. Comsol Conf.*, 2014, pp. 1-6.
[96] G. Mechler and R. S. Girgis, "Magnetic flux distributions in transformer core joints," *IEEE Transactions on Power Delivery,* vol. 15, pp. 198-203, 2000.
[97] L. D. Borrill, "Duality derived topological model of single phase four limb transformers for GIC and DC bias studies," University of Cape Town, 2017.
[98] C. W. T. McLyman, *Transformer and inductor design handbook*: CRC press, 2016.
[99] IEEE Power And Energy Society, "IEEE Std 519-2014," in *IEEE Recommended Practice and Requirements for Harmonic Control in Electric Power Systems*, ed. New York, NY: IEEE, 2014.
[100] F. De La Rosa, *Harmonics and power systems*: CRC press Boca Raton, 2006.

[101] EIC, "Power Transformers - Part 1: General," in *International Standard IEC 60076-1*, ed, 1976.
[102] IEC, "International Standard: IEC 60076-2 second edition: power transformers part 2 - temperature rise," ed, 1993.
[103] R. D. Henderson and P. J. Rose, "Harmonics: the effects on power quality and transformers," *IEEE transactions on industry applications,* vol. 30, pp. 528-532, 1994.
[104] D. Pejovski, K. Najdenkoski, and M. Digalovski, "Impact of different harmonic loads on distribution transformers," *Procedia engineering,* vol. 202, pp. 76-87, 2017.
[105] H. I. Zynal and A. Ala'a, "The effect of harmonic distortion on a three phase transformer losses," *ratio,* vol. 6, p. 7, 2012.
[106] S. Saleh, X. S. Onge, C. Richard, E. Ozkop, K. McDonald, and S. Panetta, "Impacts of grounding and winding configurations on voltage harmonics in 3φ power transformers," in *Industrial and Commercial Power Systems Technical Conference (I&CPS), 2018 IEEE/IAS 54th*, 2018, pp. 1-9.
[107] X. Gong, "Harmonic analysis of transformer excitation currents," 1993.
[108] ANSOFT Corporation, "User's guide: Maxwell 3D V11," Pittsburg, PA 2006.
[109] H. K. Chisepo, L. D. Borrill, and C. T. Gaunt, "An evaluation of learning through research: the journey of two doctoral students in the same field of interest," in *25th Southern African Universities Power Engineering Conference*, Stellenbosch, South Africa, 2017, pp. 796-801.

Appendix A

Laboratory Transformer Under Test (TuT) Specifications, Design, And Compliance Testing

TuT specifications and final design parameters

The first part of the framework aimed at drawing specifications for the transformer that would be tested. The laboratory scale transformer was set to match the capabilities of an actual power transformer. To emulate real power transformers, the TuT was specified to have mitered step-lapped joints. Table A1 gives a summary of some of the most important specifications set for the TuT with some justification.

Table A 1: 3p3L 15 kVA transformer specifications for laboratory testing

PARAMETER	SPECIFICATION [UNITS]	JUSTIFICATION
Power Rating	15 [Kva]	A reasonably priced transformer with a similar rating to a distribution transformer.
Voltage ratio	380/380 [V], (When connected in Yy)	Constrained by lab supply voltage. Transformer rating had to be lower to be able to over-excite it using supply voltage for deep saturation tests. Transformer would saturate at around 380 (+-10) V.
Vector group	Winding 1: Fixed Y Winding 2: Open winding/lose tails	Winding 2 left open for easy reconfiguration when used for other experiments.
Impedance V	5 [%]	A standard value selected to be low enough for a higher fault level and not very high to cause a larger voltage drop, [123].
Tank	Detachable	A small detachable tank will be used to capture the stray flux for thermal response studies. The tank should be detachable for easy access to the windings for installation of temperature sensors and search coils.
Core Cross Section	4 step-lapped	A step-lapped transformer to resemble a power transformer yet not further delaying the manufacturing process. To minimize costs, [124].
T-joints and Corner Joints	45° mitered	For more efficient flux transfer at the joints with lower losses [71]
Core material	CRGO M5	1.39 W/kg at 1.7 T at rated supply voltage. Offers lower losses, 0.95 w/kg at 1.5 T, [125]
Transformer cooling	Air natural	Transformer windings and core will need to be accessed from time to time during the experiment.
Winding insulation	Silicone	Can handle higher thermal loading under DC injection.
Winding material	copper	A standard material used for windings
Lamination plate thickness	0.3 [mm]	Standard lamination thickness for lower losses
Interlayer insulation	Normex 410	Normex is a high standard insulation material with peculiar properties which include high inherent dielectric strength, mechanical toughness, thermal stability, flexibility and resilience, plus a range of thickness variations available [126]

Table A 2: General TuT parameters

Parameter	Value	Units
KVA Rating (S)	15	KVA
$\boldsymbol{Primary\ voltage}\ (V_{Line\_primary})$	380	V
Secondary voltage ($V_{Line\_secondary}$(	380	V
Phase Voltage (Vph)	219	V/ph
Rated current ($I_{rated(pri\ and\ sec)}$(	22.79	A
Frequency (f)	50	Hz
Current Density (Cd)	2600000	$A/m\text{^}2$
Maximum Flux Density (Bmp)	1.72	T

Table A 3: Calculated TuT parameters

CORE LIMB			WINDINGS			YOKE			WINDOW		
Parameter	Value	Units	Parameter	Value	Units	Parameter	Value	Unit	Parameter	Value	Unit
Cross section area (Ai)	2635	mm^2	Conductor size (A_c)	8.765	mm^2	Flux (φ_m)	0.00523	Wb	Window Area (A_w)	33575.6	mm^2
Ai*1.1	2899	mm^2	Diameter (d)	3.34	mm	Length of Yoke (W)	386	mm	Window Height (h_w = L)	366.5	mm
Factor Ki	0.62	-	Rounded up diameter (d_n)	4	mm	Width of Yoke (b_y)	63	mm	Window Length (W_w)	91.6	mm
Circumscribed diameter (d)	68.38	mm	Re-calculated conductor size (A_n)	12.57	mm^2	Height of Yoke (h_y)	48.2	mm	Limb to center distance (D)	161.2	mm
Round-up Circumscribed diameter (d)	70	mm	Re-calculated current density (C_{dn})	1.81	$\frac{A}{mm^2}$						
Re-calculated area (Ai)	3038	mm^2	k factor	0.45	-						
b	64.4	mm	Volt per turn (E_t)	1.006	$V/turn$						
c	54.6	mm	Number of turns (N)	218.034	turns						
d	42	mm	Rounded up number of turns (N_n)	219	turns						
e	25.2	mm									

Transformer open circuit equipment requirement and testing procedure

List of equipment required:

a) Three phase power supply that can deliver about 1.5 pu of the rated transformer input voltage (400 V_{line}).

b) Power Analyzer for terminal measurements.

Testing Procedure

a) Isolate the supply.
b) Isolate transformer.
c) Disconnect any load connected on the secondary side of the TuT.
d) Connect the power analyzer at the primary and secondary side of the TuT.
e) Set the power analyzer to the correct type of measurements to record phase voltages, currents, apparent power, reactive power and active power.
f) Connect the three-phase power supply to the low voltage (LV) side of the TuT; leave the high voltage (HV) side open circuited.
g) Check that all connections are up to standard.
h) Energize the supply.
i) Check if the power analyzer is displaying the correct values.
j) Vary the input voltage from 0 V to above the operating voltage.
k) Record the power analyzer voltage, current and power readings at each p.u step.
l) Once completed, isolate the circuit breaker.
m) Turn the variable supply down to 0 V.
n) Isolate the variable supply.
o) Disconnect the power analyzer.

TuT Load loss test equipment requirement and testing procedure

Equipment required:

a) Three-phase power supply with enough power and current to deliver the transformer rated current on the HV side.
b) Power analyzer for terminal measurement.

Testing Procedure:

a) Isolate the variable supply.
b) Isolate the tested transformer.
c) Disconnect any load connected on the secondary side.
d) Use $6mm^2$ or larger cables to short circuit the low voltage side of the TuT, preferably using three short wire links in a delta-like connection (manufacturer suggestion).
e) Connect the current measuring instrument on the LV side, between the shorting wires.
f) Connect the power analyzer and set it to the correct testing requirements.
g) Set the variable supply voltage to 0 V.
h) Connect the transformer to the variable three phase supply.

i) Energize the variable supply.
j) Check the voltage readings on the power analyzer (should be around 0 V).
k) Slowly raise the primary voltage while monitoring the primary and secondary current (should not exceed the rated currents on both primary and secondary side).
l) Record the power analyzer voltage, current and power readings once the rated current has been reached on either side.
m) Turn the supply voltage back to zero.
n) Isolate the supply breaker.
o) Isolate the three-phase supply.
p) Disconnect the power analyzer.
q) Disconnect the three shorting wires.
r) Replace source transformer 1 with source transformer 2 and repeat steps 1 to 17.
s) Replace source transformer 2 with TuT and repeat steps 1 to 17.

Base test system set up procedure

a) Ensure that the three-phase socket is switched off.
b) Connect 6 mm^2 phase cables between the variac output and the primary side of source transformer 1.
c) Connect 11 kV cables between Source transformer 1 and source transformer 2.
d) Connect 6 mm^2 phase cables between source transformer 2 and power analyzer input (channels 1 to 3).
e) Connect 6 mm^2 phase cables between power analyzer output (channels 1 to 3) and TuT input (inner winding).
f) Connect 6 mm^2 phase cables between TuT output (outer winding) and power analyzer input (channels 4 to 6).
g) Connect 60 A cable between the 3-phase socket and Variac input.
h) Record the voltage and current total harmonic distortion (THD) appearing at the input of the TuT as measured by the power analyzer.
i) The system is now ready for further tests.

DC circuit preparation

The dc circuit was prepared with the use of 12 V 100 Ah batteries and a range of resistor banks (1 ohm, 2 ohms and 10 ohms). Each of these resistors were rated at 50 W, hence much care was taken to ensure that the overall dc current flowing in the neutral does not lead to the total power exceeding

the resistor power rating. Two batteries were connected in parallel at a time to avoid a faster discharge while conducting the experiments. The dc circuit comprised of the batteries, resistor combinations and a 100 A three-phase switch as shown in Figure A1.

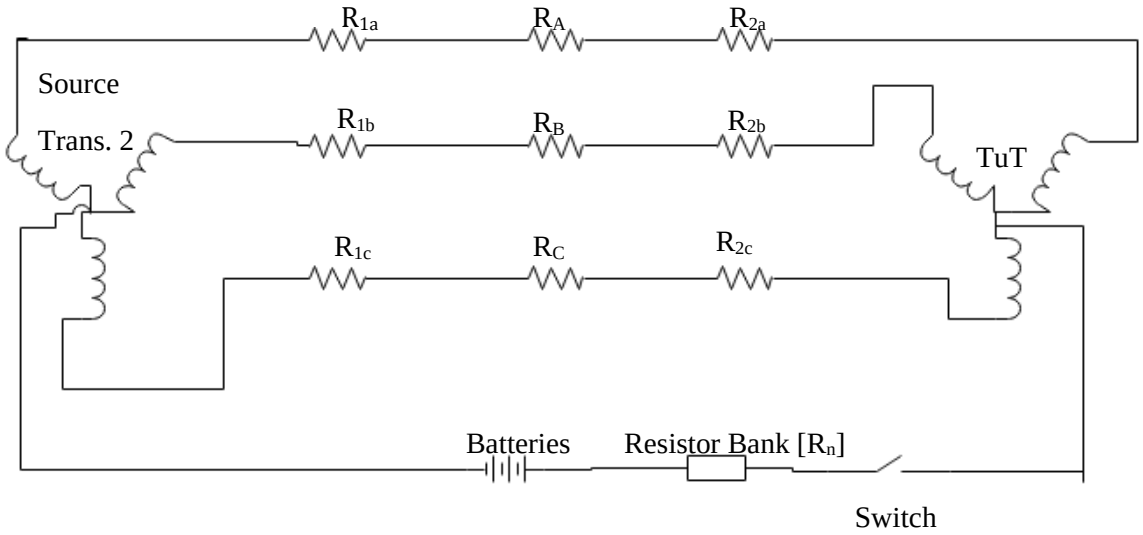

Figure A 1: DC current injection resistance circuit

Where:

R_{1a}, R_{1b} and R_{1c}: Source Transformer 2 winding resistances

R_A, R_B and R_C: Line resistances

R_{2a}, R_{2b} and R_{2c}: Transformer under test winding resistances along the dc path

R_n: equivalent resistance formed by the resistor banks, which includes the neutral wire resistance of 0.19 Ω.

$$R_{dc} = R_n + \frac{1}{\frac{1}{R1_a+R_A+R2_a}+\frac{1}{R1_b+R_B+R2_b}+\frac{1}{R1_c+R_C+R2_c}} \qquad \text{(A1)}$$

Table A 4: DC circuit resistance values

R#	R1_a	R1_b	R1_c	R_A	R_B	R_C	R2_a (in)	R2_b (in)	R2_c (in)	R2_a (out)	R2_b (out)	R2_c (out)
R [ohm]	0.16	0.16	0.15	0.22	0.21	0.21	0.176	0176	0.176	0.225	0.205	0.215

The expected dc values and resistor combinations are shown in Table A5, at a dc voltage of about 12.5 V. The use of one resistor at a time was avoided as much as possible to avoid exceeding its power limitation.

Table A 5: Expected dc values

DC#	Resistor combinations	R_n [Ω]	Total R_dc_in [Ω]	Total R_dc_in [Ω]	Expected neutral dc current, In_dc [A] - Inner	Expected neutral dc current, In_dc [A] - Outer
DC0.125	8*10 Ω resistors in series	80.19	80.3707	80.379	0.16	0.16
DC0.25	5*10 Ω resistors in series	50.19	50.3707	50.379	0.25	0.25
DC0.5	2*2 Ω in series with 2*10 Ω in series	24.19	24.3707	24.379	0.51	0.51
DC1	10 Ω and 2 Ω in series	12.19	12.3707	12.379	1.01	1.01
DC2	2*2 Ω series with 2*1 Ω	6.19	6.3707	6.379	1.96	1.96
DC3	2*2 Ω series	4.19	4.3707	4.379	2.86	2.85
DC4	2 Ω in series with 1 Ω	3.19	3.3707	3.379	3.71	3.70
DC5	2*1 Ω in series	2.19	2.3707	2.379	5.27	5.25
DC6	2*2 Ω in parallel	1.19	1.3707	1.379	9.12	9.06
DC7	2*1 Ω in parallel	0.69	0.8707	0.879	14.36	14.22
DC8	3*1 Ω in parallel	0.52	0.7007	0.709	17.84	17.63
DC9	4*1 Ω in parallel	0.44	0.6207	0.629	20.14	19.87
DC10	7*1 Ω in parallel	0.39	0.5707	0.579	21.90	21.59
DC11	8*1 Ω in parallel	0.2	0.3807	0.389	32.83	32.13
DC12	9*1 Ω in parallel	0.15	0.3307	0.339	37.80	36.87
DC13	10*1 Ω in parallel	0.1	0.2807	0.289	44.53	43.25

Procedure for testing dc sources

The following protocol was used:

a) Set up for the experiment as shown in **Error! Reference source not found.**.
b) Start by connecting a battery for the dc supply circuit as shown in **Error! Reference source not found.**.
c) Measure the equivalent neutral impedance (including dc source impedance).
d) Measure the equivalent dc resistance of the phases.
e) Measure dc flowing in the neutral at the start of the experiment (t = 0).
f) Measure the amount of dc flowing through the three phases.
g) Check balance between phases
h) Measure dc flowing through the neutral at different time intervals (t = 0.5 min, 1 min, 1.5 min…., 4 min) until t = 4.
i) Plot the profile of dc versus time.
j) Capture current and voltage waveforms using a Yokogawa WT1800 power analyzer.
k) Measure the THD and individual harmonics introduced by the dc source.

Detailed reactive power tests

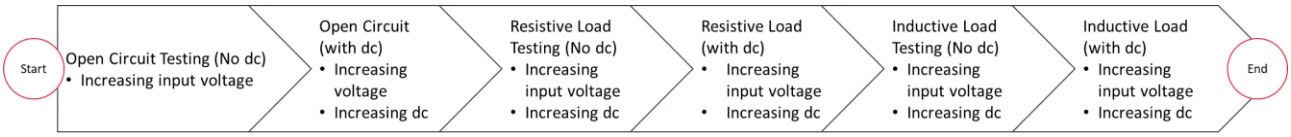

Figure A 2: Overall reactive power tests workflow

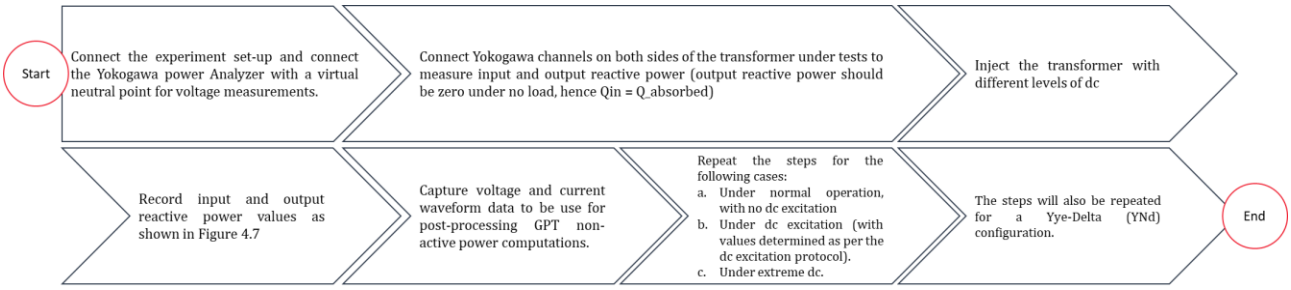

Figure A 3: Reactive power measurement using the GPT

Load preparation

Different load types were prepared for use in the dc studies. As part of the initial specifications, the transformer was to be able to handle a load up to about 6 kVA continuously. Due to the limited availability of load types and load ranges, a few load points were used for the experiment, with a selection of two loads for three different load cases (Table A6 – Table A8).

Table A 6: Resistive load values

Load Label	KVA at 160 V/ph	KVA at 219 V/ph
RL1	0.038	0.062
RL2	0.47	0.91
RL3	0.69	1.30
RL4	1.34	2.46
RL5	1.71	2.88
RL6	2.94	5.30
RL7	4.27	7.86
RL8	5.54	10.35

Table A 7: Inductive load values

Load Label	KVA at 160 V/ph	KVA at 219 V/ph
IL1	4.35	7.97
IL2	5.17	9.90

Table A 8: Resistive and inductive load combination values

Load Label	KVA at 160 V/ph	KVA at 219 V/ph
IRL1	1.24	2.31
IRL2	2.19	3.97
IRL3	2.54	4.63

Appendix B

Extra Results from Laboratory Tests on the TuT

Transformer time response

The following data show the computation of the time response values of the TuT under dc excitation. The results were taken from the moment the dc source was switched on to the moment the excitation current waveform average was equal to the dc value injected in each phase.

Table B 1: TuT time response data

I_dc [A]	T2 [s]	T1 [s]	T2-t1 [s]	Delta_T [ms]
0.1522	0.88625	0.80625	0.08	8
0.2416	0.18688	0.11375	0.07313	7.3125
0.5064	0.50188	0.44625	0.05563	5.5625
1.0059	0.8325	0.77938	0.05313	5.3125
1.9821	0.61625	0.56938	0.04688	4.6875
2.9322	0.33063	0.295	0.03563	3.5625
5.7214	0.2856	0.25125	0.03435	3.435
10.7472	0.2894	0.255	0.0344	3.44
20.225	0.49938	0.46688	0.0325	3.2499
34.704	0.41125	0.3944	0.01685	1.685
45.314	0.81125	0.795	0.01625	1.625
51.151	0.8106	0.7956	0.015	1.5

No load test results at rated voltage (219 V/ph)

The energization of windings was classified as follows:

IWNT – inner winding, no tank.

IWWT – inner winding, with tank.

OWNT – outer winding, no tank.

OWWT – outer winding, with tank.

Table B 2: No load test result for IWNT case

Parameter	Phase A	Phase B	Phase C
V_{oc} **[V]**	218.62	219.29	218.77
I_{oc} **[A]**	1.22	0.98	1.14
P_{oc} **[W]**	56.82	20.26	-1.30
Q_{oc} **[Var]**	261.56	212.50	269.34

Table B 3: No load test result for IWWT case

Parameter	Phase A	Phase B	Phase C
V_{oc} [V]	217.30	217.10	217.90
I_{oc} [A]	1.1589	0.93	1.09
P_{oc} [W]	54.49	19.94	0.82
Q_{oc} [Var]	246.08	201.26	254.18

Table B 4: No load test result for OWNT case

Parameter	Phase A	Phase B	Phase C
V_{oc} [V]	218.67	218.38	219.38
I_{oc} [A]	1.28	1.02	1.29
P_{oc} [W]	59.22	19.84	-2.8
Q_{oc} [Var]	273.95	221.97	283.02

Table B 5: No load test result for OWWT case

Parameter	Phase A	Phase B	Phase C
V_{oc} [V]	217.75	217.23	218.05
I_{oc} [A]	1.23	0.90	1.13
P_{oc} [W]	54.29	20.20	0.37
Q_{oc} [Var]	240.25	194.29	246.93

Load loss test results at rated current (22 A)

Table B 6: Load loss test results at 22 A

Parameter	Phase A	Phase B	Phase C
V_{sc} [V]	9.45	9.52	9.68
I_{sc} [A]	22.11	22.81	22.83
P_{sc} [W]	116.9	122.1	127.5
Q_{sc} [Var]	173	179.4	180.5

Further flux density analysis

Following an analysis of the non-active power, the saturation of the transformer due to the presence of dc can be further analysed by looking at the flux density distribution. Even though this was covered in detail at no load earlier, this section seeks to solidify the argument of where the saturation starts (at what dc level). The specific locations of the search coils analyzed are shown in Figure B1 for the top part of the transformer.

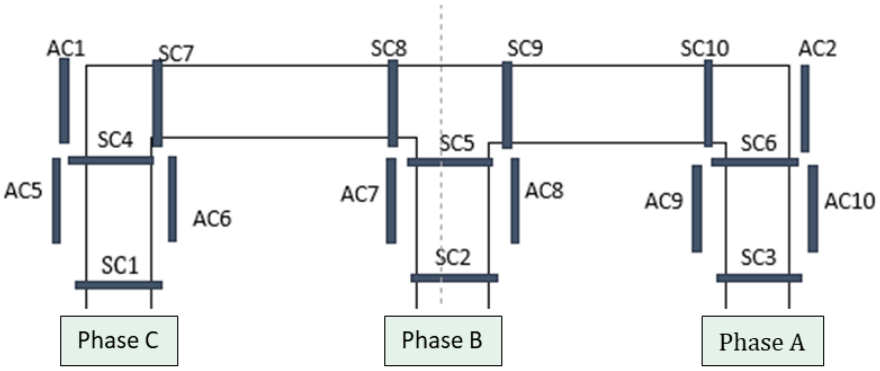

Figure B1: 3p3L Search coil location for measurement of flux density distribution and stray flux around the transformer T and Corner joints

The input voltage was varied at no load while recording the voltage on the search coils. The results are shown on Figure B2. The voltages induced in the search coils are similar at lower input voltages. It can be noted that as the transformer becomes over-excited (at higher input voltages i.e. at about 0.9 p.u input voltage), the readings start to differ. The per-unit voltage values are a function of the transformer rated voltage of 1 p.u (219 V/phase rms). Hence, the search coil readings start showing disparities at about 0.91 p.u (200 V/phase rms). The maximum difference in flux was about 0.052 T (2.2 % of SC1 maximum), i.e. between SC1 and SC8.

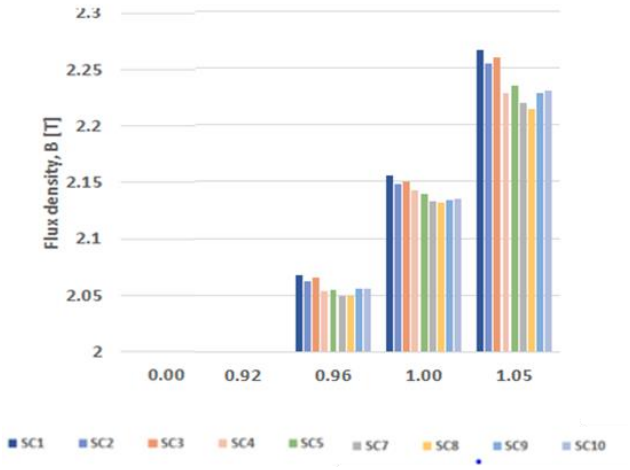

Figure B2: Core search coil flux density values at no load and varying input Voltage

A higher amount of flux density was recorded at the mid-point of the wound limbs (results from SC1, SC2 and SC3) shown in Figure B1. This is where the bulk of the induction process takes place, within the windings. Hence, this is where the maximum flux would be induced. In a non-saturated state, the flux would be expected to spread evenly around the core, hence the similar readings at lower input voltage values (Figure 6.9). The slightly lower values on SC4 and SC5 also located on the wound limbs indicate a loss of flux somewhere along the limb. With the 10 mm diameter hole located further down

the limb, this is an indication of an early saturation of the upper joints (T-joint and the corner joints). To further support this claim, SC9 and SC10 on the top right yoke record similar values even at over-excitation, indicating that there is no sign of flux loss along the limb. Alternatively, stray flux around the holes would eventually make its way back into the limb, hence the readings from SC9 and SC10 would remain the same. Thus, the lower readings on SC4 and SC5 are due to stray flux from the wound limbs linking directly to the adjacent yokes. To further investigate this claim, air search coil readings were recorded in accordance with Figure B2, with the results shown in Figure B3.

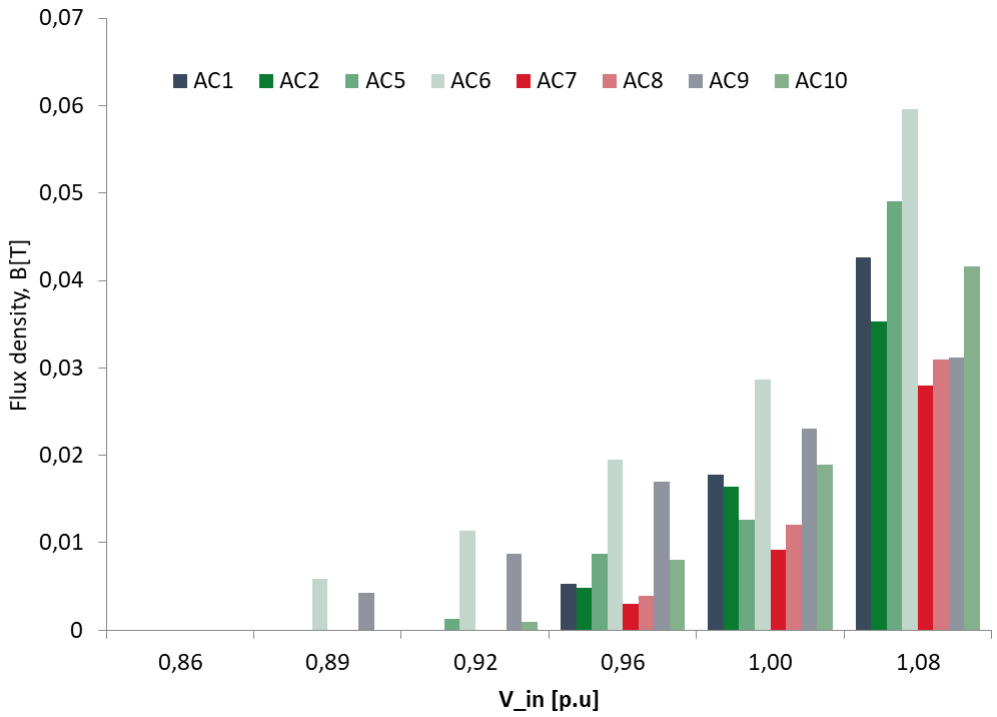

Figure B3: Mid limb air search coil flux density at increasing input voltage with no dc

The air search coil values appear to start capturing flux shortly after the disparities in core search coil values started showing. Air search coil AC6 appears to record the highest amount of stray flux. This explains the large difference between the readings from SC1 and SC4, indicating a higher amount of stray flux. Thus, there is a direct link between the core flux loss and the amount of flux recorded by the air search coils. This is an indication of saturation of the joints. It can be concluded following the above investigation that the transformer joints saturate at about 200 V/phase rms. With this conclusion in mind, the transformer was then injected with dc under load conditions to assess its response as discussed in the following section.

Appendix C

FEM Solid 3D Model Design Data and Harmonics Profile Under DC

Table C 1: FEM 2D model

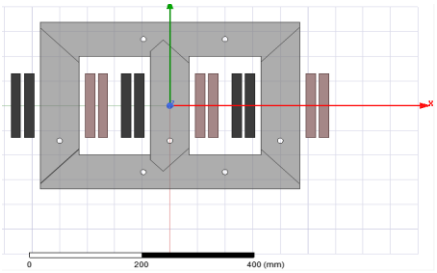

Table C 2: FEM solid 3D model design data

Feature	Volume [m^3]	Area [m^2]
Core	0.0066	N/A
Region	45.27	N/A
Phase A Inner Winding	0.0008	N/A
Phase A Outer Winding	0.0011	N/A
Phase B Inner Winding	0.0008	N/A
Phase B Outer Winding	0.0011	N/A
Phase C Inner Winding	0.0008	N/A
Phase C Outer Winding	0.0011	N/A
Phase A Inner Winding Terminal	N/A	0.0023
Phase A Outer Winding Terminal	N/A	0.0022
Phase B Inner Winding Terminal	N/A	0.0023
Phase B Outer Winding Terminal	N/A	0.0022
Phase C Inner Winding Terminal	N/A	0.0023
Phase C Outer Winding Terminal	N/A	0.0022

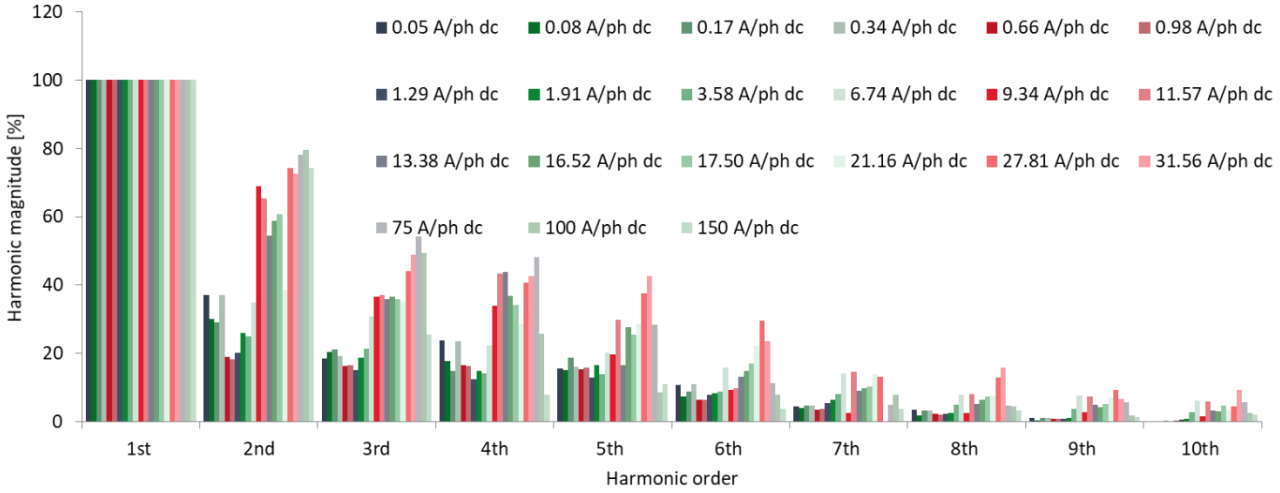

Figure C 1: Detailed FEM TuT harmonics under dc